

**Joint Regeneration**  
**Mechanisms in Red-spotted Newts**  
**(*Notophthalmus viridescens viridescens*)**

**Dissertation**

zur Erlangung des

Doktorgrades der Naturwissenschaften (Dr. rer. nat.) des  
Fachbereichs Biologie und Chemie der Justus-Liebig-Universität Gießen

vorgelegt von

Sony Adhi Susanto M.Sc. (Chemie)

geboren am 07.10.1979 in Jakarta (Indonesien)

Bad Nauheim 2014



Diese Arbeit wurde am Lehrstuhl für Innere Medizin mit Schwerpunkt Rheumatologie der Justus-Liebig-Universität Gießen angefertigt.

Dekan: Prof. Dr. Holger Zorn  
Heinrich-Buff-Ring 58, 35392 Gießen

1. Gutachter: Prof. Dr. Adriaan Dorrestein  
Lehrstuhl für Allgemeine Zoologie und Entwicklungsbiologie des  
Fachbereichs Biologie  
Justus-Liebig-Universität Gießen

2. Gutachter: Prof. Dr. Ulf Müller-Ladner  
Lehrstuhl für Innere Medizin mit Schwerpunkt Rheumatologie des  
Fachbereichs Medizin  
Justus-Liebig-Universität Gießen

Tag der Disputation: 24.07.2014

For my wife Nungki Susanto  
My son Pio Yeremia Susanto  
My Family, my Lord Jesus

*For my lovely daughter Rafka Liora Susanto<sup>†</sup>*  
*My respected Mentor Prof. Robert M Dinser<sup>†</sup>*

## Table of Contents

1	Introduction.....	1
1.1	Regeneration.....	1
1.1.1	Epimorphic regeneration .....	1
1.2	Eastern newt.....	3
1.3	Osteoarthritis .....	4
1.3.1	Pathological changes in articular cartilage during OA.....	6
1.3.1.1	Healthy articular cartilage .....	6
1.3.1.2	Articular cartilage in OA.....	8
1.3.2	Properties, development, and remodeling of healthy and OA bone .....	9
1.3.2.1	Healthy bone .....	9
1.3.2.2	Development and remodeling of healthy long bone .....	10
1.3.2.3	Bone remodeling in OA .....	11
1.3.2.3.1	Subchondral bone remodeling .....	11
1.3.2.3.2	Osteophyte development .....	12
1.4	Newt as model organism to study regeneration of the knee joint .....	12
1.5	cDNA Microarray .....	13
1.6	Matricellular proteins and their role on repair and regeneration.....	15
1.6.1	SPARC .....	15
1.6.2	Tenascins.....	17
1.6.2.1	Tenascin-cytotactin .....	18
1.6.3	Periostin.....	20
1.6.4	Decorin .....	21
1.7	Innate immune system and its role in regeneration .....	21
1.8	Vitamin A and its role in regeneration .....	22
1.9	Aim of this thesis .....	24
2	Materials.....	25
2.1	Animals.....	25
2.2	Chemicals and materials.....	25
2.3	Media and solutions.....	27
2.4	Enzymes.....	29
2.5	Antibodies.....	29
2.6	Molecular biological kits.....	30
2.7	PCR primers .....	31
2.8	Softwares .....	33
2.9	Instruments.....	33
2.10	Organs and tissues.....	34

2.11	List of cells and cell lines .....	36
3	Methods .....	37
3.1	Animal models of OA and differential expression analysis with cDNA microarray ...	37
3.2	Preparation of newt knee joint paraffin tissue.....	37
3.3	Cell biological methods.....	38
3.3.1	Pre-coating of culture plates/flasks with gelatin .....	38
3.3.2	Quantification of cells .....	38
3.3.3	Isolation of primary newt chondrocytes .....	38
3.3.4	Culture of newt cell lines .....	39
3.4	Molecular biological methods.....	39
3.4.1	RNA isolation .....	39
3.4.2	Reverse transcription .....	39
3.4.3	Real-time PCR .....	39
3.5	Histological and immunological methods .....	42
3.5.1	Tissue section preparation .....	42
3.5.2	Pappenheim staining.....	42
3.5.3	Safranin-O staining .....	42
3.5.4	Hematoxylin and Eosin staining .....	43
3.5.5	Immunohistochemistry .....	43
3.5.5.1	IHC using paraffin-embedded tissue sections.....	44
3.5.5.2	IHC stainings to evaluate TN-C expression during newt knee joint regeneration in the collagenase and surgery model .....	44
3.6	Knockdown experiments using endoribonuclease-prepared small interfering RNAs .....	45
3.6.1	Generating TN-C and negative control <i>lacZ</i> esiRNA .....	47
3.6.2	Purification of esiRNA product.....	50
3.6.3	Evaluation of esiRNA quality .....	50
3.6.4	Knockdown of TN-C expression in primary newt chondrocytes .....	51
3.6.4.1	Introduction of esiRNA into primary newt chondrocytes.....	51
3.6.5	Scrape motility assay .....	52
3.6.6	Adhesion assay.....	53
4	Results .....	54
4.1	Relative quantification of selected candidate genes.....	54
4.1.1	Relative quantification of selected candidate genes of matricellular proteins .....	54
4.1.1.1	Relative quantification of TN-C .....	54
4.1.1.2	Relative quantification of SPARC .....	55
4.1.1.3	Relative quantification of POSTN .....	56
4.1.1.4	Relative quantification of DCN.....	57

4.1.2	Relative quantification of candidate genes from innate immune system .....	58
4.1.2.1	Relative quantification of CFB .....	58
4.1.2.2	Relative quantification of TLR2.....	59
4.1.3	Relative quantification of genes of the vitamin A pathway .....	60
4.1.3.1	Relative quantification of RARRES1 .....	60
4.2	Spatial expression of dysregulated proteins.....	62
4.2.1	Expression of TN-C and physiological appearance of a healthy newt knee joint.....	62
4.2.2	Spatiotemporal TN-C expression during newt knee joint regeneration in the collagenase model .....	63
4.2.3	Spatiotemporal TN-C expression during newt knee joint regeneration in the surgery model .....	68
4.3	Summary of spatiotemporal TN-C expression of the collagenase and surgery model .....	72
4.4	Evaluation of TN-C contribution to the regenerative process .....	74
4.4.1	TN-C expression levels in different newt cell populations .....	74
4.4.2	TN-C knockdown in primary newt chondrocytes.....	75
4.4.3	Effect of TN-C knockdown on adhesion and motility of the primary newt chondrocytes.....	76
4.4.4	Effect of TN-C knockdown on expression level of SPARC and DCN .....	78
4.5	Expression of SPARC during newt knee joint regeneration.....	80
4.5.1	Optimization of newt non-specific SPARC antibody in human RA bone tissue ...	80
4.5.2	SPARC expression in healthy newt knee joint.....	81
4.5.3	SPARC expression in regenerating newt knee joints after 20 and 40 days of surgery treatment .....	83
5	Discussion.....	86
5.1	Molecular mechanisms during knee joint regeneration in newt .....	86
5.1.1	Role of the innate immune system during knee joint regeneration in the newt....	86
5.1.2	Role of the retinoic acid pathway during knee joint regeneration in the newt .....	87
5.1.3	Role of matricellular proteins during knee joint regeneration in newt .....	88
5.1.3.1	SPARC expression: Analysis, predicted function, and role in knee joint regeneration .....	88
5.1.3.1.1	SPARC expression in healthy knee joint.....	88
5.1.3.1.2	SPARC expression in the regenerating newt knee joint .....	89
5.1.3.2	TN-C and its role in knee joint regeneration in newt .....	91
5.1.3.2.1	TN-C expression in both OA models.....	91
5.1.3.2.2	Relative quantification versus spatiotemporal analysis of TN-C expression during newt knee joint regeneration .....	95

5.1.3.2.3	Establishing expression knockdown in newt and its implication in functional analysis of TN-C .....	95
5.2	Analysis of obstacles during investigation of knee joint regeneration in newt .....	98
5.2.1	The newt as animal model for research .....	98
5.2.2	Problem during transcriptome analysis .....	98
5.2.3	Problem during establishment of spatial expression analysis .....	99
6	Summary .....	101
7	Zusammenfassung .....	103
8	References .....	105
9	Appendix .....	121
9.1	List of figures .....	121
9.2	List of tables .....	122
9.3	List of abbreviations .....	122
9.4	Result of relative quantification of candidate genes with real-time PCR .....	125



# 1 Introduction

Knee joint damage is associated with degenerative joint diseases such as osteoarthritis. Lesions in the articular cartilage are the main reason for this degeneration. Humans do not have the endogenous capacity to repair these lesions, but, in contrast, adult newts such as *Notophthalmus viridescens* are able to reconstitute the damaged tissue and finally restore the knee joint function (Geyer et al., 2010). Therefore, the detailed investigation of the regeneration process in the newt is essential in order to be able to transfer the healing process to humans in the future.

## 1.1 Regeneration

Some amphibians (e.g. axolotl and newts) are able to repair various damaged organs including the heart, eye lenses, and nerves, and to replace lost tissues due to their remarkable capability to perform regeneration (Gilbert, 2000).

There are three major types of regeneration: The first type is morphallaxis. It occurs by reorganization of remaining cells after an injury to form new functional tissues. Hydras regenerate by this mechanism. If a hydra is bisected midway through the body stalk, the remaining cells at the cut surface will be reorganized, which will result in the formation of a new head or foot (Gilbert, 2000; Carlson, 2007). The second type is compensatory regeneration. In this process, cells divide to fill the lost structure without losing their differentiated phenotype (Gilbert, 2000). An example of this type is mammalian liver regeneration. After partial hepatectomy, the remaining hepatocytes at the injury site proliferate to fill the damaged area (Ledda-Columbano et al., 1993). The third type is epimorphosis. In this regeneration type, predominantly after injury, cells dedifferentiate to form a collection of undifferentiated cells. Afterward these cells proliferate and then they redifferentiate to form functional tissue (Gilbert, 2000; Stocum, 2006).

### 1.1.1 Epimorphic regeneration

Salamander limb restoration is an example for epimorphic regeneration. Upon dissection or autotomy (Figure 1, step 1), a wound healing process takes place (Figure 1, step 2). After 6 – 12 hr, epidermal cells migrate from the stump to the wound surface form an epidermis. Afterwards, the cells from the epidermis proliferate to form the apical ectodermal cap (AEC) (Figure 1, step 3) (Chernoff et al., 1995). During the next 4 days, the cells beneath the AEC such as bone cells, chondrocytes, fibroblasts, myocytes and neural cells lose their differentiated character and detach from one another to form an undifferentiated cell mass. This process is called dedifferentiation (Figure 1, step 4). Afterwards, the AEC induces the undifferentiated cells to proliferate to form a mesenchymal mass, called the blastema

(Figure 1, step 5) (Globus et al., 1960). In addition to the undifferentiated cells, resident stem cells, which reside in the wound area, also contribute to the mesenchymal cell population in the blastema (Odelberg, 2005; Morrison et al., 2006). Afterwards, the blastema tissue grows and expands its size from a small bud into an elongated cone. In the next regeneration stage, it undergoes a redifferentiation process, which starts from the proximal side of the blastema towards its distal tip (Figure 1, step 6). Afterwards, cartilage condensation and myogenesis initiate the morphogenesis event. They are followed by differentiation of connective tissue, vascular system, and establishment of nervous connections (Chaar et al., 2006). The morphogenesis takes place until a functional limb is restored. At the end of the regeneration process, the newly-developed limb cannot be distinguished from its uninjured contralateral counterpart (Figure 1, step 6) (Gilbert, 2000; Chaar et al., 2006).

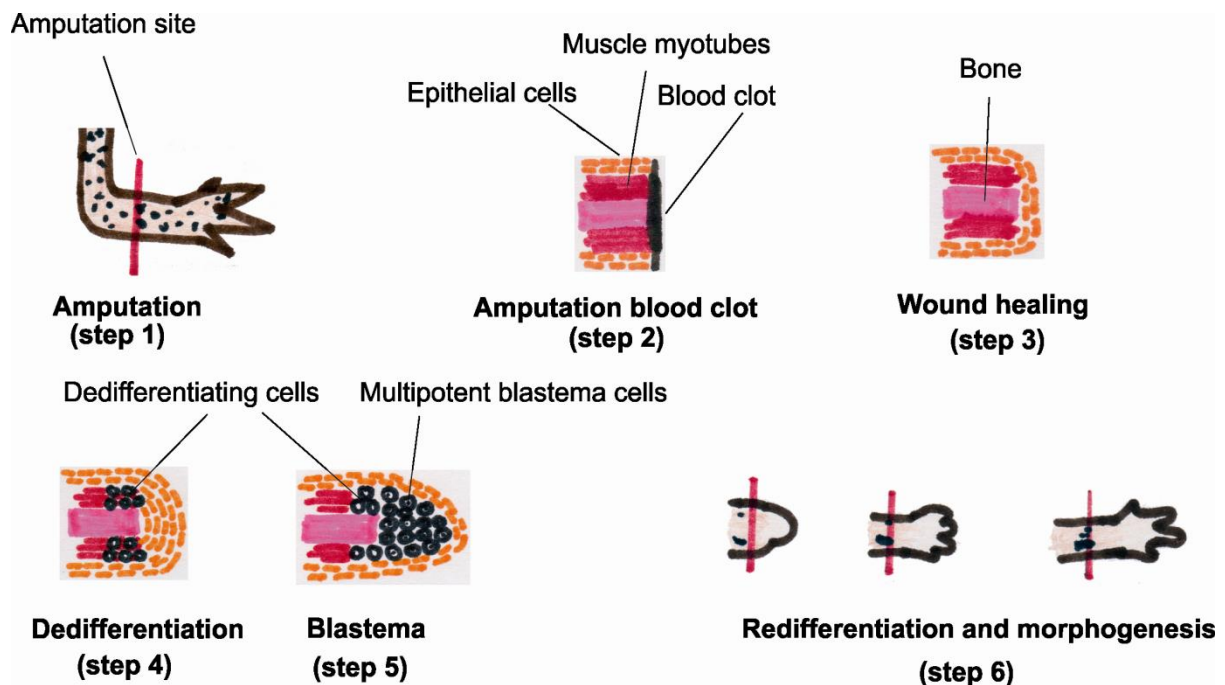


Figure 1: **Stages of limb regeneration in an adult newt (*Notophthalmus viridescens*)** (adapted from Chaar et al., 2006).

The main characteristic in this epimorphic regeneration is the formation of blastema (Brockes, 1997). Some researchers have tried for many years to reveal the cellular origin and potency of this unique tissue. Cells in blastema have been thought to have a high cellular plasticity, as they, after regeneration process, differentiate into various cells types, such as bone, muscle, skin, and cartilage cells. Therefore, some investigators have suggested that the blastema cells are pluripotent (Stocum, 1968; Pietsch, 1961; Holtzer, 1969; Steen, 1970), when performing their experiments in larvae of *Ambystoma maculatum*, *Ambystoma opacum*, and *punctatum*. The method they used was grafting limb blastema to

ectopic sites such as the fin which supported the blastema growth and differentiation process (Pietsch, 1969; Stocum, 1968).

A recent study from Kragl and coworkers in an axolotl limb regeneration model system contrasted the pluripotency of the blastema cells (Kragl et al., 2009). They employed a more precise technique by using integrated green fluorescent protein (GFP) transgene to track the major limb tissue development during limb regeneration in the axolotl. With this technique, they demonstrated that GFP<sup>+</sup>-labeled cartilage cells did not form myogenic cells in the regenerating limb. They also noticed that after GFP-labeled transgenic myotubes were grafted in the regenerating blastema, thereafter the green fluorescence signal was detected only in the regenerating muscle but not in the cartilaginous skeleton and epidermis. Based on these results, they concluded that blastema was a heterogeneous collection of restricted progenitor cells, with the cells in the blastema retaining a strong memory of their tissue or embryonic origin (Kragl et al., 2009).

In contrast to the salamander, adult amniotes including lizards, birds, and mammals, cannot regenerate their limb (Yokoyama, 2008). Upon amputation, the limb stump only undergoes wound healing (Yokoyama, 2008). However, this process usually results in scar or keloid formation, which is composed mostly of collagen type I. The flexibility and the strength of these tissues are inferior in comparison to the original tissue (Hardy, 1989).

Different assumptions have been proposed to explain why amniotes including mammals cannot perform this type of regeneration (Chaar et al., 2006). First, the wound healing process, which results in scar formation, is more efficient and faster than epimorphic regeneration (Brockes et al., 2001; Carlson, 1974). Second, the involvement of immune cells and cytokines such as tumor necrosis factor  $\alpha$  during wound healing interferes with the regeneration response, finally leading to scar formation (Harty, 2003).

Of note, some epimorphic regeneration can also be realized in mammals (Chaar et al., 2006). McGann and coworkers showed that treatment of murine C2C12 myogenic cell lines with protein extract from newt limb regeneration tissue induced a dedifferentiation process (McGann et al., 2001). In their experiment, they further observed that 18% of murine C2C12 cells were re-entered the cell cycle and lost their differentiated character after treatment with the regeneration extract. They could also show that hitherto unknown protein factors in the extract promoted this event (McGann et al., 2001).

## 1.2 Eastern newt

The Eastern newts (*Notophthalmus viridescens*) belong to the *Salamandridae* family which is endemic in North America. There are four known subspecies of the Eastern newt: The red-spotted newt (*Notophthalmus viridescens viridescens*), which lives in the Eastern and North East of the United States (Figure 2), the Central newt (*Notophthalmus viridescens*

*louisianensis*), which lives in the central area of the United States, the Peninsula newt (*Notophthalmus viridescens piaropicola*), which lives in Florida (Riemland, 2000).



Figure 2: **The adult red spotted newt (*Notophthalmus viridescens viridescens*)**. Image source: The image is kindly provided by Carina Schreyäck from our research laboratory.

The life cycle of the *Notophthalmus viridescens* consists of four distinct stages i.e. egg, aquatic larva, red eft (terrestrial juvenile) and adult (Petranka, 1998). The breeding season starts from late winter and lasts to early spring (Behler and King, 1996). Eggs are laid by female newts on submerged vegetation with a hatching period of 3 – 8 weeks (Behler and King, 1996). They can reach adulthood by three different ways: First, metamorphosis via a terrestrial juvenile (eft) stage to an aquatic lunged adult; Second, direct transformation into aquatic lunged adult; Third, paedomorphosis, maturation directly into an aquatic gilled adult without metamorphosis. Paedomorphosis exists only in few newt populations in certain areas such as coastal Massachusetts and Long Island (Mecham, 1967; Healy, 1974; Takahashi, 2009; Takahashi and Parris, 2008). Terrestrial red efts leave their home ponds, spending their lives for three to seven years as terrestrial red efts in the wet forest or wet open land (Forester et al., 1991; Roe et al., 2008). After at least three years, the red efts return to aquatic habitats and become sexually mature. They undergo a second metamorphosis into the aquatic adult form during breeding season.

*Notophthalmus viridescens viridescens* has a green skin color, smooth and mucous skin and a large tail (Gage, 1891; Gill, 1978).

### 1.3 Osteoarthritis

Osteoarthritis (OA) is the most common joint disorder in the world and characterized by pathological changes including localized loss of articular cartilage and formation of outgrowths at the joint margins (osteophytes) (Conaghan et al., 2008; Lark, 1995). In an aging community like in developed countries and athletes, OA has become a major healthcare issue. In Sweden, 8% of those aged between 50 to 70 years suffer from clinically relevant OA (Jacobsson et al., 1989).

OA usually shows distinct symptoms. Pain in the affected joint is the prominent sequelae of this disease. The intensity of the ache gets worse when the affected joint is used for physical activity. If the disease is severe, the pain still persists even after the joint rests (Manek et al., 2000). The second main symptom is stiffness. The affected joint is difficult to move or rotate, especially after a prolonged resting period such as sleeping and sitting. The third symptom of OA is muscle weakness. It is derived from the pain-induced reluctance to use the affected joint (Slemenda et al., 1997).

There are several factors that contribute to the development of OA: The first factor is age. As the joints are getting older, the articular cartilage, which serves as smooth interaction surface of the mobile parts of the joint, is worn-out (Felson et al., 1995; Lawrence et al., 1996). The next factor is obesity: Excessive body weight can cause overloading in the affected joints, which further increases the lesions in the articular cartilage (Zhang et al., 2010). The last factor is injury: Especially rupture of the anterior cruciate ligament (tissue that connects and stabilizes knee joints) increases the risk of OA development substantially. The subsequent tear induces joint-instability and eventually leads to further lesions in the articular cartilage (Lohmander et al., 2004).

Humans do not have an endogenous capacity to heal OA. This problem has been recognized as early as 1743 by Hunter. He noted that lesions of articular cartilage in OA cannot repair themselves, resulting in degenerative arthritis of the affected joint (Hunter, 1743). There are distinct factors contributing to the limited regenerative capacity of articular cartilage. First, cartilage is not supported by a regenerative cell population. It is a collection of progenitor cells that have differentiated into a specialized cell type upon local tissue defect or loss (Matsiko et al., 2013; Buckwalter et al., 2005). Second, articular cartilage lacks vascularization. Therefore, cells from perivascular mesenchymal pools (progenitor cells which reside in the periphery of the blood vessel) cannot usually enter the lesion (Lindahl et al., 2003; Hunziker and Rosenberg, 1996).

Severe articular cartilage damage in OA causes pain in the affected joint. This leads to restriction of patient mobility, which ultimately reduces their quality of life. To overcome this problem and in order to restore the function of the damaged tissue, joint replacement surgery is performed (Kasper et al., 2005). Other efforts to repair damaged articular cartilage have still failed to produce satisfying results, especially for extended cartilaginous lesions. One of the methods to “repair” small lesions is autologous chondrocyte implantation (Steinert et al., 2007). This technique uses - as one example - chondrocytes, which have been isolated from a cartilage tissue derived from a minor load-bearing area on the upper medial femoral condyle of the damage knee. After several weeks of *in vitro* cultivation, the cells are then transplanted into the lesional site (Brittberg et al., 1994). As mentioned, this method is not suitable for treatment of bigger cartilage lesions, which are normally present in OA

patients. At present, this technique is limited to repair small defects ranging from 2 to 10 cm<sup>2</sup>, partially based on the limited number of chondrocytes, which have to be taken from the donor tissue (Steinert et al., 2007).

### 1.3.1 Pathological changes in articular cartilage during OA

#### 1.3.1.1 Healthy articular cartilage

Articular cartilage is located at the ends of bones of a diarthroidal joint. It provides a low friction bearing surface for movement and a high capacity to bear load as impact of locomotion. The thickness of this tissue in adult humans is only 1 - 2 mm, it forms a very thin layer at the distal end of an epiphyseal bone (Stockwell, 1971). In newt knee joint, the articular cartilage is not arranged as thin layer, but it covers major parts of the joint cap as shown in Figure 3.

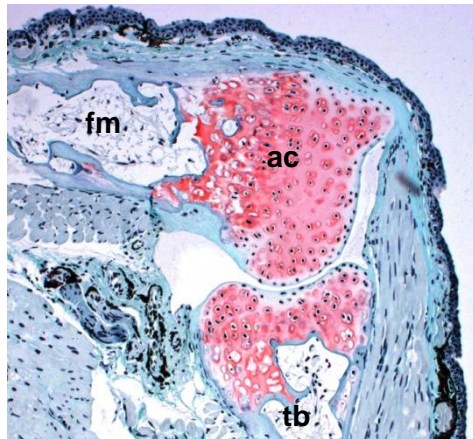


Figure 3: **Healthy newt knee joint.** Safranin-O staining was conducted in sagittal section of healthy newt knee joint. Due to high proteoglycan content in the articular cartilage, this tissue stains red. The Safranin-O staining shows thick articular cartilage in the femoral and the tibial joint cap. Original magnification x 50. fm, femur; ac, articular cartilage; tb, tibia. Image source: The image was provided by Carina Schreyäck of our research group.

Articular cartilage is composed of 65 – 80% water, 10 – 20% collagen type II, 5% aggrecan and less than 5% of other components (proteoglycans, biglycans, decorin, collagen type V, VI, IX, X, XI; hyaluronate, fibronectin and lipids) (Athanasίου et al., 2013).

In comparison to other tissues, articular cartilage is sparsely populated with cells. The only cells residing in this tissue are the chondrocytes. However, they occupy only less than 10% of the total volume of articular cartilage. These cells are located in small cavities (lacunae) and are scattered individually within the cartilage. They receive their nutrition via diffusion of substances from synovial fluid in the joint gap (Athanasίου et al., 2013; Cole et al., 2009). Mature chondrocytes in healthy cartilage do not proliferate, but they are metabolically active and responsive to soluble mediators such as growth factors, and

interleukins (Athanasίου et al., 2013; Cole et al., 2009). Chondrocytes are important for the maintenance of the cartilage because they synthesize components of the extracellular matrix such as proteoglycans and collagens (Buckwalter et al., 2005).

Based on the alignment of collagen fibers, biomechanical function and cellular morphology, the articular cartilage can be subdivided into four horizontal zones: Superficial zone, intermediate or middle zone, deep zone and calcified cartilage (Figure 4) (Matsiko et al., 2013; Cole et al., 2009).

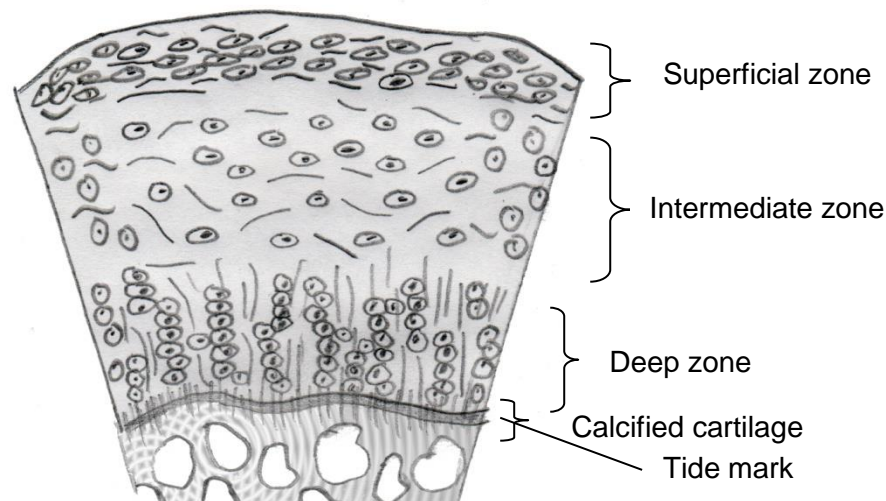


Figure 4: **Structural organization of articular cartilage.** The structural organization of articular cartilage from the superficial zone, the intermediate zone, the deep zone and the calcified cartilage (adapted from Matsiko et al., 2013).

The superficial zone is the thinnest zone of the articular cartilage which accounts for 10 – 20% of the total cartilage volume. It is recognizable by its high number of flattened chondrocytes. This zone has the highest water content, a relatively low proteoglycan density, densely packed collagen fibers (Weiss et al., 1968), and high tensile strength (Cole et al., 2009).

The intermediate zone accounts for 40 – 60% of total cartilage volume. The chondrocytes in this zone are usually spherical in shape and the cells are scattered in the matrix. The collagen fibers are thicker and the proteoglycan content is elevated. This zone provides the necessary resistance to compression (Cole et al., 2009).

The deep zone constitutes 30% of the total cartilage volume. The chondrocytes are spherical in shape and they are arranged in columns. The proteoglycan content is also the highest as compared to the other zones (Cole et al., 2009).

The calcified zone and the tidemark serve as barrier to vascular penetration and as transitional zone between cartilage and subchondral bone. Nutrition from subchondral bone cannot penetrate the calcified zone. Chondrocytes are still found in this zone and are randomly distributed in a matrix filled with apatitic salts (Cole et al., 2009).



### 1.3.1.2 Articular cartilage in OA

Articular cartilage of OA patients undergoes significant structural degenerations. It starts with localized disruptions and fibrillations of the collagen network in the superficial zone in articular cartilage (Buckwalter et al., 2005). The fibrillation of the collagen network is caused by denaturation of collagen type II network (Bennet et al., 1942; Stoop et al., 2001). In the late stadium of OA, the surface of articular cartilage becomes roughened. Fibrillations of the collagen network extend from superficial zone into deeper layer of articular cartilage. Afterwards, the superficial tips of the fibrillated cartilage tears release free fragment in the joint space. It causes reduction of the cartilage thickness until finally reaching the necrotic subchondral bone layer (Buckwalter et al., 2005).

The articular cartilage degeneration process results in substantial reduction of proteoglycan content in this tissue. Matthews showed that the proteoglycan content was higher in healthy than in OA knee joint tissue (Matthews, 1953). This finding is supported by Bollet and coworkers, who investigated articular cartilage from different OA disease grades. They found that the proteoglycan content was getting lower as OA becomes more severe (Bollet et al., 1963).

The articular cartilage degeneration process results also in the reduction of collagen type II content in this tissue (Venn and Maroudas, 1977). It was noticed by Venn and Maroudas, who found that the content of collagen type II in the osteoarthritic femoral head cartilage was lower than the one found in healthy tissue (Venn and Maroudas, 1977).

Chondrocytes in the articular cartilage of OA patients show an unusual activity. As the disease worsens, they undergo programmed cell-death or apoptosis, which decreases their cell number dramatically (Meachim and Collins, 1962; Rothwell and Bentley, 1973). The proliferative activity causes also cell clustering, a unique chondrocyte phenotype in OA cartilage (Meachim and Collins, 1962; Rothwell and Bentley, 1973; Sandell and Aigner, 2001).

As the disease proceeds, the composition and structural alterations of the ECM stimulate chondrocytes to produce proteases including matrix metalloproteinases (MMPs) that further promote cartilage degeneration (Samuels et al., 2008). MMPs degrade important components of cartilage such as collagen type II and proteoglycans (Troeborg and Nagase, 2012). MMP-1,-8,-13, and -14 are proteases that responsible for the degradation of collagen type II (Billinghurst et al., 1997; Reboul et al., 1996; Mitchell et al., 1996; Bau et al., 2002; Kevorkian et al., 2004). In addition, MMP-3 is the proteolytic enzyme which degrades the proteoglycans (Fosang et al., 1991).



### 1.3.2 Properties, development, and remodeling of healthy and OA bone

#### 1.3.2.1 Healthy bone

Long bone can be subdivided into distinct parts (Figure 5). The subchondral bone is located next to the articular cartilage (Figure 5, inset). The epiphysis is located next to the subchondral bone. Adjacent to the epiphysis is the epiphyseal line. This tissue is a cartilaginous structure, which exists only during the growth phase and it disappears in adulthood. The metaphysis is located adjacent to the epiphyseal line (Figure 5). The epiphysis and the metaphysis are composed of trabecular bone. Another part of the long bone is the diaphysis. This bone is composed of cortical bone or the compact bone. Unlike the trabecular bone, cortical bone is dense and solid. The adult human skeleton is composed of 80% cortical bone and 20% trabecular bone (Clarke, 2008).

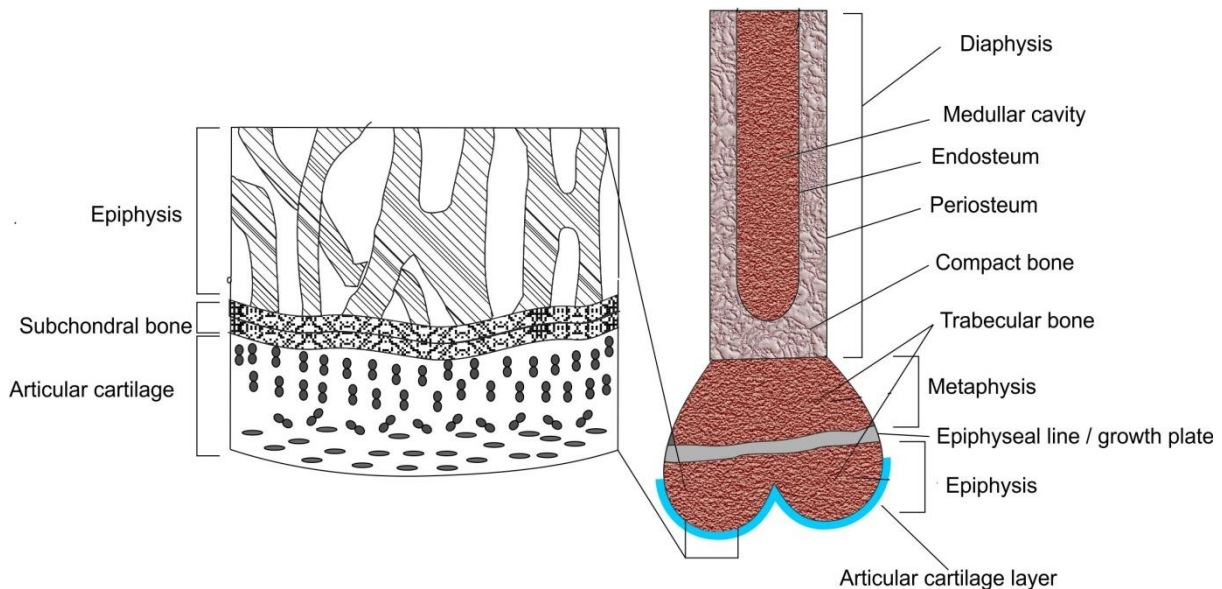


Figure 5: **Anatomy of an adult human long bone**

The periosteum is a fibrous connective tissue sheath that surrounds the outer cortical surface of bone (Figure 5), exception the joints. It contains blood vessels, nerve fibers, osteoblasts and osteoclasts (Clarke, 2008). The periosteum plays an important role in bone development and regeneration (Bourne, 1944; Colnot et al., 2012). Upon fracture, it can release progenitor cells, which can differentiate into osteoblasts. These cells then synthesize new bone matrix to heal the damage (Colnot et al., 2012).

Endosteum is a membraneous structure surrounding the inner surface of cortical bone, trabecular bone and the central canal (Figure 5). It consists of simple flattened layers of osteoblasts, osteoclasts and osteoprogenitor cells (mesenchymal stem cells that can differentiate into osteoblasts) (Clark, 2005; Martini and Frederich, 2005). Endosteum plays

roles in regeneration and bone remodeling (Epker et al., 1965; Stoker and Epker, 1971; Martini and Frederich, 2005). The osteoclasts in this tissue perform bone resorption and the osteoblasts synthesize new bone matrix (Clarke, 2008).

### 1.3.2.2 Development and remodeling of healthy long bone

Long bone develops by endochondral ossification (Mackie et al., 2011). In this process, embryonic mesenchymal cells condense and differentiate into chondrocytes that form a cartilage template (Figure 6A). Then these cells proliferate, which expands the cartilage “model” in size. Afterwards, the chondrocytes in the mid-shaft of the model undergo a phenotypic conversion to hypertrophy (terminal stage of chondrocyte differentiation, which is characterized by enlargement of the cellular volume and the occurrence of gene expression markers such as collagen type X and alkaline phosphatase) (Sharma et al., 2007). This event initiates the formation of primary ossification. In this stage, the hypertrophic chondrocytes express vascular endothelial growth factor (VEGF) (Zelzer et al., 2002). This growth factor promotes blood vessels to invade the cartilage template. Then, osteoblasts, which are surrounding the mid-shaft of the model, deposit a periosteal bone collar (Figure 6B). Subsequently, the ossification process expands toward each end side of the cartilage model. During this process, osteoclasts remove the cartilage ECM, then osteoblasts deposit new bone matrix on the remnant (Figure 6C). A secondary center of ossification forms at each end of the cartilage model, which creates a growth plate between both centers of ossification (Figure 6D). The bone development process is finished, when the expanding primary center of ossification meets the secondary center of ossification (Figure 6E). The endochondral ossification starts during fetal life until growth is terminated in adulthood (Mackie et al., 2011).

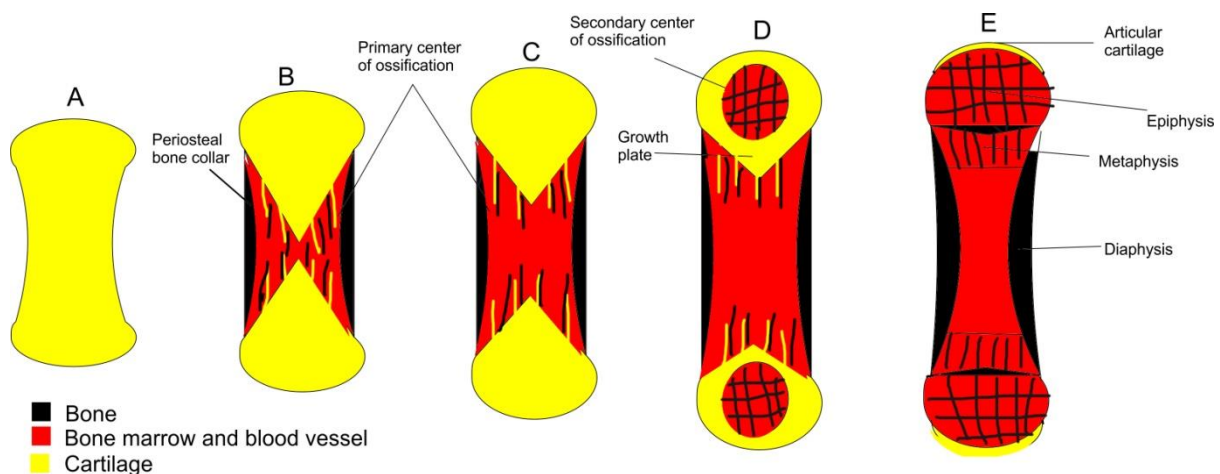


Figure 6: **Illustration of long bone development by endochondral ossification.** (A) The cartilage model of the future mature bone. (B) Formation of a periosteal bone collar and initiation of primary center of ossification. (C) Expansion of the primary center of ossification towards the end side of the

cartilage model of the future bone. **(D)** Formation of a secondary center of ossification at each end of the cartilage model and a cartilaginous growth plate between the primary and secondary center of ossification. **(E)** Formation of adult bone. The cartilaginous growth plate exists only in the actively developing bone (juvenile bone), and has disappeared in the adult bone. The only remaining cartilage is the articular cartilage at the ends of the bone (adapted from Mackie et al., 2011).

In contrast to bone development, remodeling of bone takes place during the complete lifetime of a human organism. It is a continuing process by which bone is renewed to maintain its strength and mineral homeostasis (Clarke, 2008; Eriksen, 2010).

If required, the remodeling process starts with bone resorption, which is performed by osteoclasts. Afterwards, osteoblasts start to synthesize new collagenous organic matrix (osteoid) to fill the resorption area. The osteoid is composed of unmineralized organic compounds, which predominantly consist of collagen type II. Then, mineralization of the osteoid takes place together with collagen deposition. In the final stage, the rate of collagen synthesis dramatically decreases while mineralization activity still continues until the osteoid matrix becomes fully mineralized to form a new bone. Thereafter, the osteoblasts are trapped within the newly mineralized bone in the bone lacunae and their volume shrinks. Then, they are called osteocytes. These osteocytes produce matrix proteins that regulate the exchange of minerals in the fluid within the lacunae (Hadjidakis, 2006; Clarke, 2008; Eriksen, 2010).

### **1.3.2.3 Bone remodeling in OA**

In OA patients pathological changes also involve the subchondral bone and the development of osteophytes at the joint margins.

#### **1.3.2.3.1 Subchondral bone remodeling**

The important manifestation of subchondral bone remodeling in OA is sclerosis. It is characterized by a decrease in mechanical stability, trabecular thickening, and an increase of bone stiffness (Lajeunesse et al., 1999). Some researchers suggested that sclerosis was caused by adaptive response of the tissue due to increase of mechanical stress on the subchondral bone (Chiba et al., 2011). Here, the increase of the mechanical stress originates from the mechanical loading that cannot be absorbed by damaged articular cartilage (Lajeunesse et al., 1999; Chiba et al., 2011).

Osteoblasts are known to play important role in the development of subchondral bone sclerosis in OA. Researchers reported that this pathological phenotype was derived from abnormal osteoblast activity. They overproduced homotrimeric  $\alpha 1$  of collagen type I that caused abnormal mineralization of the subchondral bone (Mansell et al., 1998; Bailey et al., 2002).

### 1.3.2.3.2 Osteophyte development

An osteophyte is a fibrocartilage-capped bony outgrowth, which can be detected at the margins of a diarthroidal (joints that connect long bone), apophyseal (joints that connect bone in the spine) joint, and vertebral bodies (van der Kraan, 2007).

Osteophytes form in the early development of OA and contribute to significant clinical symptoms such as joint pain and loss of function. The pain is probably caused by nerve compression (Matsumoto et al., 2002). Matsumoto and coworkers investigated the source of the pain in patients with osteophytes in vertebral bodies. They found that it originated from an entrapment of spinal nerves which was caused by the osteophytes (Matsumoto et al., 2002).

The mechanism of development of this bony outgrowth has been exclusively investigated in experimental murine OA (Van der Kraan, 2007). The osteophyte growth is initiated by induction of mesenchymal stem cell proliferation, which takes place in the periosteum covering the subchondral bone and cartilage boundary (van der Kraan, 2007). Afterwards, the mesenchymal cells undergo chondrogenesis to form cartilage cells and deposit matrix molecules such as proteoglycans in the tissue. Chondrocytes, which reside in the center of this newly-formed cartilage, further differentiate into a hypertrophic phenotype. This phenotype is characterized by volume enlargement and gene expression markers such as collagen type X and alkaline phosphatase (Sharma et al., 2007; van der Kraan, 2007). Afterwards, endochondral ossification takes place producing bone and bone marrow cavities. The fully developed osteophyte is integrated with the subchondral bone. It composes of bony structure which is covered by a cartilage layer (van der Kraan, 2007).

## 1.4 Newt as model organism to study regeneration of the knee joint

Some vertebrates, such as axolotl and *Xenopus*, are able to regenerate body parts such as limb and tail (Hazard, 1959; Tanaka and Reddien, 2011). However, axolotls are not adult animals, because they retain their larval phenotype throughout their live. Therefore, they do not represent adult animals, which can still perform regeneration (Tompkins, 1978). The larvae of *Xenopus laevis* can restore their lost limb. However, they lose their regenerative capacity after metamorphosis (Muneoka et al., 1986).

In contrast, adult newts still retain the exceptional ability to regenerate some of their body parts including appendages (Brockes et al., 1997), lenses (Henry et al., 2010), the heart (Borchardt and Braun, 2007), and some parts of the central nervous system (Berg et al., 2010). In addition, our group was successful to show that adult newts are able to heal knee joint defects after artificially induced OA. This was shown by using two different models: Collagenase- and surgically-induced OA. The first method (Figure 7A) is already reported elsewhere (Geyer et al., 2010). The second model was performed as shown in Figure 7B-D

(unpublished work of Dr. med. Matthias Geyer and Prof. Dr. med. Robert M. Dinser<sup>‡</sup>): The right limb knee joint was opened (Figure 7B), and the femoral cartilage was removed (Figure 7C), thereafter, the wound was sealed with tissue glue (Figure 7D).

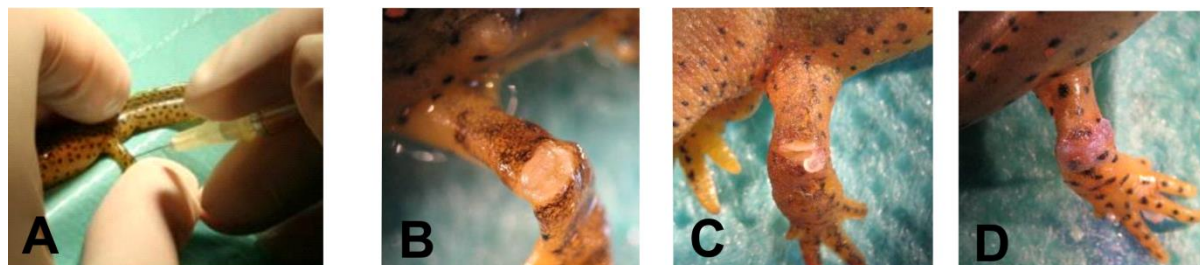


Figure 7: **Collagenase- and surgically-induced knee joint defect in newt. (A) Collagenase-induced knee joint defect.** Collagenase is injected intra-articularly in the knee joint to induce a knee joint defect. **(B), (C), (D) Surgically-induced knee joint defect.** The surgery method is performed by (B) opening the knee joint by transverse section, (C) removing the femoral cartilage, and (D) sealing the knee with tissue glue (Histoacryl®). Images source: Kindly provided by Prof. Dr. med. Robert M. Dinser<sup>1</sup> of our group.

In order to describe the severity of OA, a scoring system was developed using both clinical evaluation and histology (Geyer et al., 2010). The clinical assessment was conducted by investigating the defective position of the treated limb, atypical movements of the animals, loss of stretchability, and incident instability of the limb. Evaluation of the disease level with histology was performed with Giemsa, Safranin-O staining and immunohistochemistry (IHC) for collagen type II. The first two methods visualize the proteoglycan content and the last detects collagen components in the articular cartilage.

Clinical evaluation of the collagenase treated knee joints showed an increment of the score, which peaked on day 6 after treatment. At this time point, the clinical examination demonstrated that the knee joint was inflamed and the animals did not tend to use it. After day 6 post treatment, the clinical score attenuated until it became indistinguishable from the respective buffer-injected knee joint. During this phase, the histological evaluation revealed a temporary loss of collagen type II and proteoglycan content, which also peaked on day 6 after treatment. After this time point, the content of these components increased when the knee joint function restored (Geyer et al., 2010).

## 1.5 cDNA Microarray

To study the underlying mechanisms driving regeneration, cDNA microarray was performed using the regenerating newt knee joint after artificially induced damage

<sup>1</sup> Prof. Dr. med. Robert M. Dinser<sup>‡</sup> was killed by a drunken car driver during the experimental period of this dissertation.

(unpublished work from Dr. med. Matthias Geyer, Dr. rer. nat. Thilo Borchardt, and Prof. Dr. med. Robert M. Dinser<sup>‡</sup>). cDNA microarray is a powerful method to perform rapid expression profiling of thousands of genes during a unique biological process like knee joint regeneration in newts (Schena et al., 1995). This technique is based on selective hybridization of fluorescence-labeled cDNA from treated and control newt knee joint utilizing 100.000 cDNA spots from custom-made newt cDNA library (Bruckskotten et al., 2012).

cDNA microarray allows the characterization of genes, which play an important role in the regenerative process. Genes, which are involved in regeneration, will be differentially up- (or down-) regulated only in the treated knee joint but not in the control tissue. In order to characterize the genes, which play an important role in regeneration, a careful sample preparation for the cDNA microarray should be performed. It consists of common molecular biological techniques. It starts with RNA isolation from treated and control tissue. Afterwards, the transcribed segments are converted to fluorescence-labeled cDNA using reverse transcription reaction with dye-attached deoxynucleotides. The product is then hybridized with the DNA spots on the microarray chip (Hegde, et al., 2000; Leung and Cavalieri, 2003).

cDNA microarray analysis of the regenerating newt knee joint, which preceded this doctoral work, resulted in 290 genes which were differentially regulated in both OA models. Among them, 172 genes could not be characterized because there was no known homology with the public DNA database. The rest of them (88 genes) were homolog to the public database and they were classified based on their predicted function into 13 groups (Figure 8): Cytoskeleton (7 genes), matricellular proteins (12 genes), matrix degradation (10 genes), energy generation in mitochondria (8 genes), signal transduction (17 genes), structural proteins (4 genes), metabolic pathways (4 genes), cytokines (2 genes), cell adhesion (3 genes), intracellular protein metabolism (7 genes), transcription/cell cycle (6 genes), unknown function (8 genes) and uncertain classification (30 genes) (see Figure 8) (unpublished work from Prof. Dr. med. Robert Dinser<sup>‡</sup>). For this doctoral study, 10 genes were selected from this selection for further investigation with real-time PCR and IHC experiments. They were secreted protein acidic and rich in cysteine (SPARC), periostin (POSTN), tenascin-C (TN-C), decorin (DCN), complement factor B (CFB), gamma  $\beta$  crystalline (CRYGB), retinol saturase (RETSAT), olfactomedin-like 3 (OLFML-3), thymosin beta 4 (TMSB4), complement factor B (CFB).

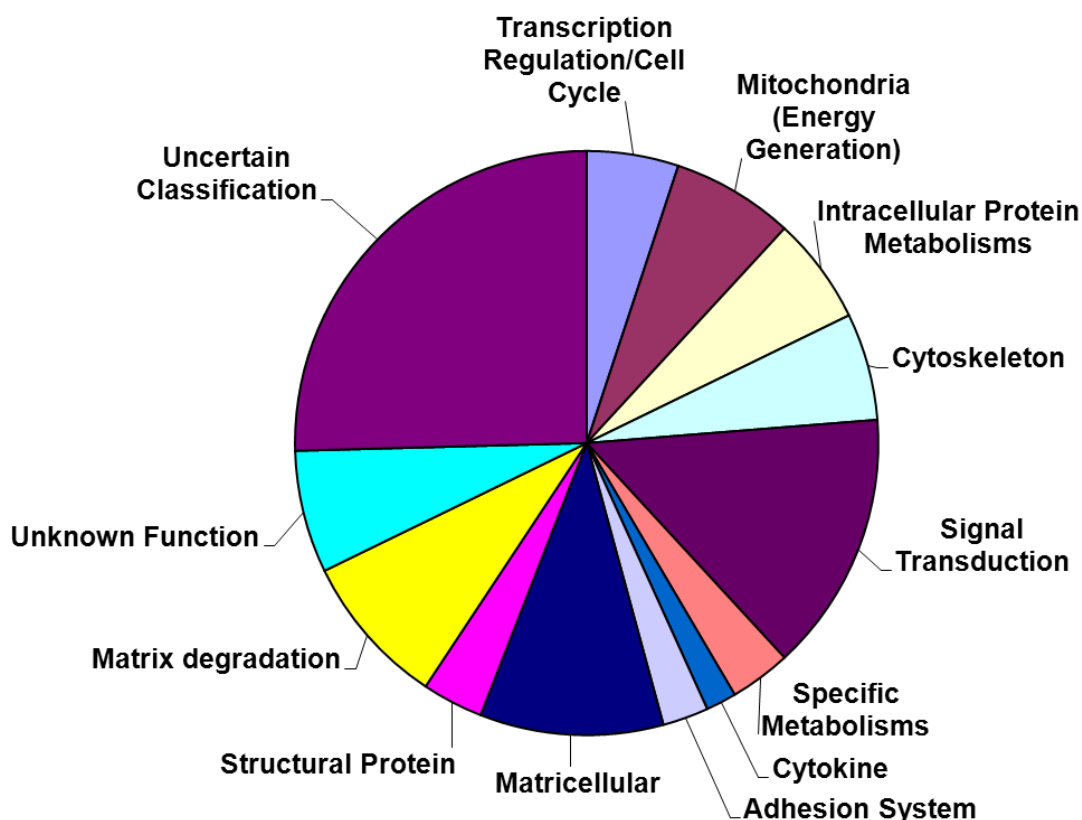


Figure 8: **Classification of 88 differentially deregulated genes from the cDNA microarray of regenerating newt knee joint.** Eighty-eight deregulated genes from the cDNA microarray were classified according to their predicted function based on their DNA sequence homology to the public database. Image source: Kindly provided by Prof. Dr. med. Robert M. Dinser<sup>®</sup> of our group.

## 1.6 Matricellular proteins and their role on repair and regeneration

Extracellular matrix (ECM) proteins contribute directly to the organization and physical properties of the ECM. For example, collagen I serves as adhesive protein within bones, tendons and ligaments (Carragher et al., 1999). There are also groups of proteins in the ECM, which do not directly contribute to the formation of the structural elements. They serve as modulator of cell-matrix interactions and cell function. This group of proteins is called matricellular proteins. Some well-known examples of these proteins are secreted protein acidic and rich in cysteine (SPARC), which is also known as osteonectin or BM40, periostin (POSTN), tenascin-C (TN-C), and decorin (DCN) (Bornstein and Sage, 2002).

### 1.6.1 SPARC

SPARC is a 43 kDa glycoprotein. It was first described by three independent groups as a major constituent of bovine and human bone and as a protein secreted by proliferating calvarial cells (osteoblasts from skullcap bone) *in vitro* (Termine et al., 1981; Sage et al., 1984; Sage et al., 1981; Otsuka et al., 1984). SPARC is a highly conserved protein among



different species such as *C. elegans*, *Drosophila*, chicken and mammals (Bradshaw et al., 2001).

SPARC consists of 3 modular domains (Figure 9): The acidic domain enables SPARC to bind hydroxyapatite which is a major component of bone matrix (Lane and Sage, 1994). The second domain is homologous to the repeated domain in follistatin, which binds to activin and inhibin, members of transforming growth factor- $\beta$  superfamily (Lane and Sage, 1994). The last domain is an extracellular  $\text{Ca}^{2+}$ -binding domain. This domain is responsible for its affinity to different collagen types including I, III, and V, in a  $\text{Ca}^{2+}$ -dependent fashion (Sasaki et al., 1997; Sasaki et al., 1998).

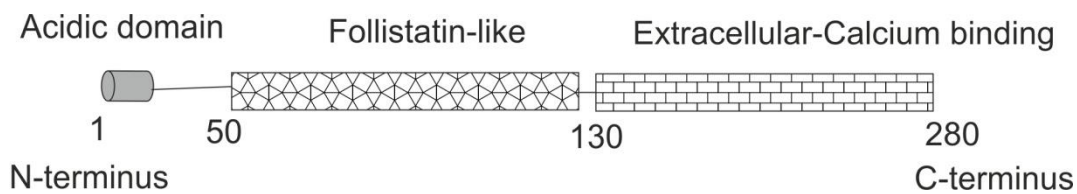


Figure 9: **Modular structure of human SPARC.** Three structural modules of SPARC are the acidic, follistatin-like, and extracellular  $\text{Ca}^{2+}$ - binding domain (adapted from Hohenester et al., 1997).

During human embryonic development, SPARC is essential for skeletal muscle development. In fetuses 15 weeks of age, SPARC is found in the newly forming myotubes. In neonatal muscle, SPARC expression can still be detected in a few mononuclear cells (progenitor cells of myotubes). In adult human muscle, SPARC was detected in satellite cells. They are a collection of progenitor cells that have ability to generate new muscle fibres or to provide new myonuclei during postnatal growth (Jorgensen et al., 2009; Kadi et al., 2005).

SPARC is one of the most abundant non-collagenous matrix proteins. SPARC is expressed in the ECM especially in osteoids of trabecular bone (Termine et al., 1981), osteoblasts (Kelm et al., 1994), hypertrophic chondrocytes in the normal human tibial growth plate (Hecht and Sage, 2006), fibroblasts, smooth muscle and endothelial cells in the dermis of adult human skin (Hunzelmann et al., 1998).

SPARC regulates cell growth by interaction with other ECM molecules such as various collagen types (Sage et al., 1984). The binding of SPARC to collagen type I, II, III, IV, V is the best characterized interaction and these interactions are facilitated by the extracellular  $\text{Ca}^{2+}$ -binding domain (Sasaki et al., 1998). SPARC has different affinities to the different collagen types. This is due to the tissue-specific glycosylation pattern of SPARC (Kaufmann et al., 2004). For example, SPARC expressed in bone is undergoing post-translational glycosylation with mannose. Therefore, it has a high affinity to collagen I, which is abundant in bone. SPARC from blood platelets does not possess post-transcriptional



modification with mannose, so that it has a lower affinity to collagen I (Kaufmann et al., 2004).

SPARC is also known as counter-adhesive protein. SPARC, which is purified from parietal yolk sac cells, interferes the interaction of endothelial cells to ECM by binding to collagen type I. It causes rounding and apoptosis of endothelial cells (Sage et al., 1989). However, the mode of action of SPARC to modulate collagen interactions is still unknown. This matricellular protein may act exclusively in the extracellular space to modulate collagen interactions with cell-surface receptors or intracellularly in collagen trafficking and post-translational modifications (Bradshaw, 2009).

SPARC-null mice showed abnormal collagen fibril morphology and substantial collagen decrease in adult tissues including skin (Bradshaw et al., 2002), and in epididymal fat pads (Bradshaw et al., 2003). SPARC-null mice developed cataractogenesis because these animals do not express collagen type IV, which is important for lens transparency (Gilmour et al., 1998; Norose et al., 1998).

Under pathological conditions including OA and RA, chondrocytes in the superficial and middle zones of articular cartilage express SPARC, while it is absent in these zones of normal/healthy cartilage (Nakamura et al., 1996). In healthy cartilage, weak SPARC signals emerge from a few chondrocytes in the deep zone. SPARC expression levels in chondrocytes can be induced by growth factors such as TGF- $\beta$ 1 (Nakamura et al., 1996). However, proinflammatory cytokines such as IL-1 $\beta$  and IL-1 $\alpha$  decrease SPARC expression levels (Nakamura et al., 1996).

SPARC involvement in regeneration has been shown for skin and bone tissue (Lane et al., 1994; Alford and Hankenson, 2006). In adult dermal repair, expression of this protein appears to promote blood vessel formation as it is expressed in high levels during the process (Lane et al., 1994). Angiogenesis is induced by plasmin, a serine protease which dissolves fibrin blood clots, cleaves SPARC within the follistatin-like region resulting in the production of peptides that stimulate angiogenesis (Iruela-Arispe et al., 1995). As angiogenesis is required for the dermal repair, SPARC is suggested to promote skin regeneration (Lane et al., 1994). In bone fracture healing, expression of this protein is detected in proliferating osteoblasts in the periosteum (Hirakawa et al., 1994). In addition, Alford and Hankenson suggested a role for SPARC in the fracture healing as a modulator of new bone formation, based on its upregulation throughout the healing process (Alford and Hankenson, 2006).

### 1.6.2 Tenascins

Tenascins are a highly conserved family of large oligomeric glycoproteins in the ECM and can be found only in vertebrates (Hsia and Schwarzbauer, 2005). There are currently

four tenascin paralogues that have been identified in mammals: C, R, X and W. Expression of these proteins is tightly regulated during development and throughout the life span of an organism. Upregulation of these proteins is also being observed during pathological states such as cancer and tissue injury (Hsia and Schwarzbauer, 2005).

### 1.6.2.1 Tenascin-cytotactin

Tenascin-cytotactin or tenascin-C (TN-C) was the first member identified and is, thus, the best characterized family member of tenascins. TN-C is an oligomeric protein and forms a hexameric structure by linking its monomer with a disulfide bridge. It has a molecular weight of 190 to 240 kDa depending on its glycosylation pattern (Pearson et al., 1988).

TN-C has four domains: The TA domain functions as a bridge to form hexabrachions (Figure 10A). The various epidermal growth factor-like (EGFL) domains consist of 31 amino acids and contains 6 cysteine residues that participate in intrachain disulfide bonds (Jones and Jones, 2000). The fibronectin-III (FN-III) domains consist of two types: The conserved and spliced FN-III domains (see Figure 10B). The conserved domain shows homology with other tenascin members, and the spliced domain is a unique TN-C motif. It can only be found in TN-C and TN-X (Erickson, 1993). At the C terminus, the fibrinogen globe is located. It contains an EF-hand calcium binding site (Aukhil, 1993).

TN-C is involved in tissue development including chondrogenesis (Mackie et al., 1987). TN-C appears in the condensing mesenchyme of immature cartilage during chick's bone development. The function of TN-C during chondrogenesis is modulating fibronectin interaction with mesenchymal cells that promote their differentiation to chondrocytes (Mackie et al., 1987). TN-C also appears in the cerebral cortex during rat brain development (Götz et al., 1997). This matricellular protein plays also a role in neuronal migration and axon pathfinding during brain development. These functions are mediated specifically by the EGFL domain (Fischer et al., 1997; Götz et al., 1997). TN-C knockout mice demonstrate an altered neuronal development, resulting in aberrant behavior like hyperactivity and poor sensorimotor coordination (Mackie and Tucker, 1999).

TN-C is expressed in normal/healthy tissue, which is subjected to mechanical forces including osteotendinous junctions (OTJ) (Jarvinen et al., 1999). In adult rats, TN-C appears in this tissue when it is actively used for normal muscle construction. If OTJ is immobilized, then the TN-C expression disappears (Jarvinen et al., 1999). TN-C plays also an important role in normal hematopoietic system (Ohta et al., 1998). Deficiency of this matricellular protein leads to reduction of hematopoietic cells (such as stromal cells) and bone marrow cell proliferation (Ohta et al., 1998).

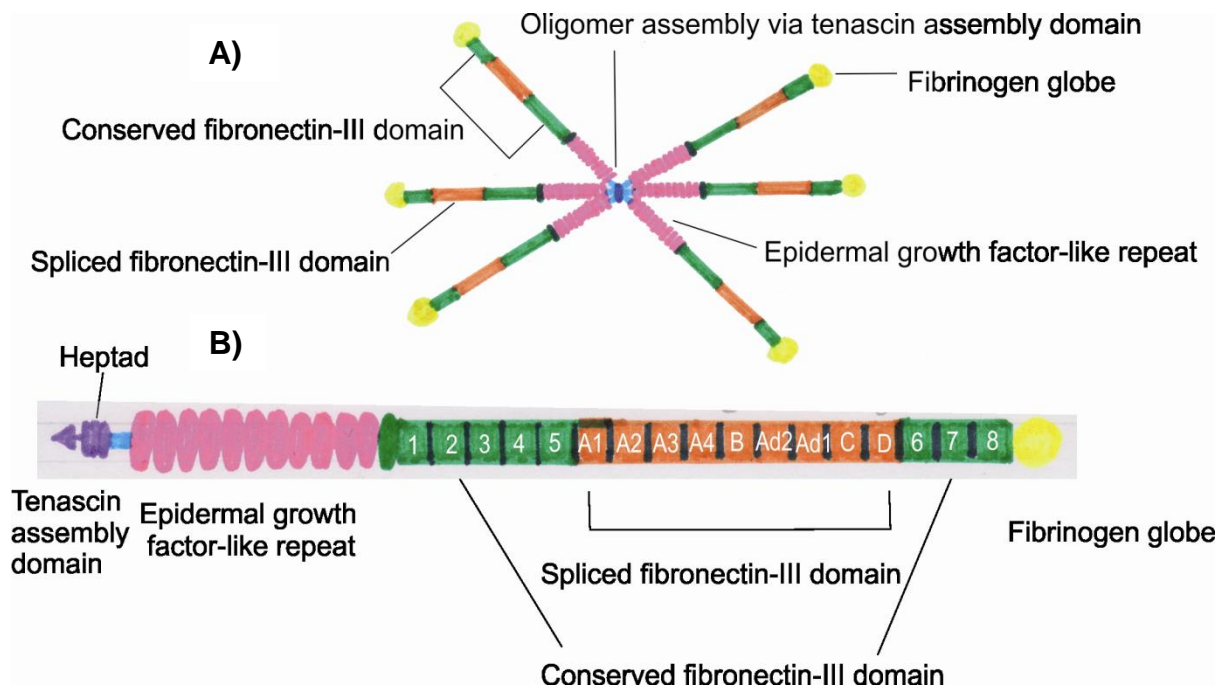


Figure 10: **Molecular structure of TN-C.** (A) **Illustration of TN-C hexabrachions.** The TN-C assembly (TA) domain connects six TN-C monomers. (B) **Schematic representation of TN-C.** TN-C consists of tenascin assembly (TA) domain, epidermal growth factor-like (EGFL) repeats, fibronectin-III (FN-III) domains and fibrinogen globe (FG) (adapted from Jones and Jones, 2000).

Onda and colleagues reported that TN-C is expressed in regenerating newt limbs after amputation (Onda et al., 1990). By employing a monoclonal antibody specific for urodele TN-C (mAb MT1) in IHC experiments, they identified TN-C in the blastema of regenerating newt and axolotl limbs. It appeared as early as 5 days after amputation in the dedifferentiation area. Afterwards, it increased in the distal stump during preblastema stages. Some TN-C also appeared within cells in the wound epithelium. During blastema formation, high expression of TN-C emerged in the blastemal matrix and in a thick layer underlying the wound epithelium. In addition, they observed that TN-C reactivities were also found in the tendon, i.e. the myotendinous junction (site of connection between tendon and muscle) and periosteum in untreated limbs.

In subsequent *in-situ* hybridization experiments, they used RNA probes, which specifically detect newt TN-C RNA transcripts. They were able to show that TN-C expression in wound epithelium, which they observed previously in IHC, originated from epithelial cells (Onda et al., 1991). They also detected other similarities with IHC as TN-C was expressed in all of the mesenchymal cells in the blastema tissue. During redifferentiation of these cells, TN-C expression was reduced and was restricted only to the condensing but not to differentiated tissue (Onda et al., 1991).

Calve and coworkers found an involvement of TN-C during newt muscle regeneration (Calve et al., 2010). They used two methods: *in vivo* 3-dimensional spatiotemporal matrix

map and *in vitro* functional time-lapse imaging to observe the expression behavior of three ECM proteins: TN-C, hyaluronic acid and fibronectin. They showed that TN-C together with the other two ECM components created an environment that supported blastema development and thus, regeneration. Additionally, they demonstrated that TN-C promoted myoblast migration and myofiber fragmentation, which also facilitated blastema formation (Calve et al., 2010).

TN-C is expressed in the OA cartilage. TN-C is re-expressed when the articular cartilage undergoes degeneration, whereas TN-C does not appear in normal cartilage. Treatment of primary human articular chondrocytes with TN-C accelerates the cellular proliferation rate followed by an increase in proteoglycan content in culture and upregulation of aggrecan expression (Nakoshi et al., 2010).

### 1.6.3 Periostin

Periostin (POSTN) was originally described as an osteoblast specific factor. It was first identified in a mouse osteoblastic cell line as a putative cell adhesion protein for preosteoblasts (Takeshita et al., 1993). The name derives from its preferential expression in the periosteum (Takeshita et al., 1993).

In adult tissues, POSTN is expressed in the periodontal ligament of the dental pulp in murine and human organisms (Horiuchi et al., 1999). POSTN is secreted by fibroblasts and osteoblasts in the periodontal ligament (Horiuchi et al., 1999). In bone, POSTN is expressed only during embryonic development and to a lesser extent in neonates, young and adult rodents (Horiuchi et al., 1999; Litvin et al., 2004; Kii et al., 2010), in osteoblasts lining the trabecular bone (Horiuchi et al., 1999; Zhu et al., 2009; Ogita et al., 2008), and abundantly in the periosteum during embryogenesis and bone growth. However in bone, POSTN expression is absent in terminally differentiated mineralized tissues (Afanador et al., 2005; Wen et al., 2010).

POSTN is expressed during development of collagen-rich, fibrous connective tissues subjected to mechanical stress such as heart valves (Rios et al., 2005; Kruzynska-Frejtag et al., 2004) and tendons (Yoshida et al., 2007). Under pathological conditions, POSTN appears in adult tissues after myocardial, vascular and skeletal muscle injuries as well as during bone fracture healing (Wang et al., 2003; Nakazawa et al., 2004).

There is evidence that POSTN is involved in tissue regeneration. POSTN promotes periodontal ligament repair by stimulating the proliferative and migratory capacity of human periodontal ligament cells (Padial-Molina et al., 2013). POSTN is also important in cutaneous wound healing (Nishiyama et al., 2011). POSTN knockout mice show a delay in re-epithelization and in the reduction of keratinocyte proliferation which causes decreasing of wound healing capacity in comparison to wild-type mice (Nishiyama et al., 2011).

#### 1.6.4 Decorin

Decorin (DCN) is a small leucine-rich proteoglycan which is found to be associated with collagen fibrils in all connective tissues (Hocking et al., 1998). This proteoglycan has a molecular weight of approximately 90 kDa. In the skeletal system, it is located in the ECM of articular cartilage (Bock et al., 2001).

DCN knockout mice have unusually lax and fragile skin, alterations in tendon structure, and abnormal periodontal ligaments. These alterations are all caused by an abnormal fibrillar organization of collagen type I, IV, VII, and IX in these tissues (Häkkinen et al., 2000; Reed and Iozzo, 2003). This is due to the fact that binding of DCN to collagen is required for proper fibrillogenesis (Danielson et al., 1997).

DCN is an important protein for tissue repair and regeneration (Li et al., 2007). Gene transfer of this protein can promote skeletal muscle regeneration by stimulating myoblast differentiation, reducing fibrous scar formation, regulating expression and activity of several factors including TGF- $\beta$ , and follistatin (Li et al., 2007). The capacity of DCN to regulate the activity of TGF- $\beta$  is also present in skin wound healing (Zhang et al., 2012). When this proteoglycan is downregulated, the activity of TGF- $\beta$  is increased, which then promotes scar formation that ultimately influences skin healing (Honardoust et al., 2012).

### 1.7 Innate immune system and its role in regeneration

Innate immunity protects organisms against invasion of infectious agents. It consists of cells and proteins, such as NK cells (Haller et al., 1977), eosinophils (Janeway et al., 2002), and the complement system (Janeway et al., 2002), which are always present to defend against a wide range of distinct pathogens such as viruses, bacteria, fungi and eukaryotic parasites (Müller et al., 2008).

Innate immunity is not only essential for the defense against pathogen invasion, some experiments showed also its importance in tissue repair and regeneration in mammals (mice) and urodele amphibians (axolotls and newts) (Jiang et al., 2005; Godwin et al., 2013; Kimura et al., 2003). Jiang and coworkers demonstrated that macrophage chemokine production was required to promote this tissue repair after bleomycin-induced acute mice lung injury. The respective inflammatory response required activation of toll-like receptors (TLR) 2 and 4 as well as the adaptor protein myeloid differentiation primary response protein 88 (MyD88). They also showed that TLR2 and 4 knockout mice displayed impaired lung regeneration capacity after acute lung injury (Jiang et al., 2005). In addition, Godwin and coworkers showed that axolotls (*Ambystoma mexicanum*) required the immune system for proper regeneration activity including limb restoration after amputation (Godwin et al., 2013). In addition, macrophage infiltration was required for blastema formation during axolotl limb regeneration. Therefore, systemic macrophage depletion in amputated axolotls resulted in

sole wound closure. In treated animals, a blastema was formed and the subsequent reconstitution of a new limb structure was hindered (Godwin et al., 2013). Kimura and coworkers showed that complement components 3 (C3) and 5 (C5) are involved in newt limb and eye regeneration. By using ISH, C3 and C5 RNA transcripts can be detected in the blastema, regenerating lens vesicle and in the cornea. In contrast, in intact newt limb and a completely restored newt eye, the RNA of C3 and C5 cannot be detected with ISH. The differential expression of C3 and C5 in this process demonstrates their importance in newt limb and eye regeneration (Kimura et al., 2003). This collection of evidence demonstrates the significance of the innate immune system in regeneration. Based on these functions, some additional genes including TLR2, TLR5, and MyD88, which were absent in cDNA microarray, were included in the experiments of the thesis to elucidate role in knee joint regeneration.

## 1.8 Vitamin A and its role in regeneration

Vitamin A is the name of a group of fat-soluble retinoids (Ross, 2010). These compounds cannot be synthesized by any animal species and are only obtained from nutrition in the form of retinol, retinyl ester, and  $\beta$ -carotene. They are then oxidized to retinal and finally to retinoic acid in liver. The first compound is important for normal vision, while the final product has more diverse biological functions in repair, regeneration, development, and apoptosis (Bushue and Wan, 2010). In order to perform these roles, retinoic acid relies on binding to specific molecules. These receptors are retinoic acid (RAR) and retinoid X receptor (RXR). Each of them has three subtypes;  $\alpha$ ,  $\beta$ , and  $\delta$ . They are all located in the transcription regulation sites of DNA in the nucleus. When the retinoids bind to these receptors, they activate gene expression, which is important for diverse biological function including the activation of aldehyde dehydrogenase (ALDH1), which is required for differentiation and development of human fetal islet cell (Bushue and Wan, 2010; Li et al., 2014).

The role of vitamin A in regulating tissue repair and regeneration has been described in amphibians including axolotl (Maden et al., 1982). Vitamin A regulates pattern formation during limb regeneration in this animal (Maden et al., 1982). Addition of external vitamin A into the regenerating limb resulted in proximodistal duplication. It stimulated also the growth of additional skeletal elements that were already present in the developing tissue (Maden, 1983). The proximodistal regulation of vitamin A was also mediated by activation of retinoic acid receptors (RARs) (Pecorino et al., 1996).

These functions of vitamin A stimulated also to investigate, whether these receptors are involved and play a role in newt knee joint regeneration. Thus, RAR $\alpha$ ,  $\beta$ , and  $\delta$  as well as RXR were selected for real-time PCR experiments to quantify their expression level in regenerating newt knee joint.

Vitamin A derivatives may also have potential roles in regeneration (Maden, 1982). An example is a synthetic pharmaceutical compound called tazarotene. This drug induces the expression of retinoic acid receptor responder 1 (RARRES1) after binding to other retinoic acid receptor, RAR- $\beta/\delta$  (Nagpal et al., 1996). It was firstly identified by Nagpal and coworkers who observed that RARRES1 was upregulated when applying tazarotene in the skin raft (Nagpal et al., 1996).

RARRES1 is known as inhibitor of tumor growth (Zhang et al., 2004). In cancer cells including nasopharyngeal carcinoma, its expression is downregulated through promoter hypermethylation (Shutoh et al., 2005). Ectopic expression of A and B isoforms of RARRES1 in human colon cells suppress also the growth of cancer cells (Zhang et al., 2004).

RARRES1 seems to have role in newt knee joint regeneration based on its differential upregulation in cDNA microarray (Unpublished work from Prof. Dr. med. Robert Dinser<sup>†</sup>). Therefore, this expression of this gene was also quantified with real-time PCR analysis to confirm its upregulation value during knee joint regeneration.

## **1.9 Aim of this thesis**

As mammals cannot restore the function of tissue damage, especially upon severe damage of a diarthrodial joint, it is of utmost interest to elucidate repair processes in animals that have this ability to be able to develop future strategies for the human beings. In contrast, adult newts are able to reconstitute damaged tissue, and to finally restore specifically knee joint function (Geyer et al., 2010). In order to elucidate the molecular mechanisms underlying the regenerative process, cDNA microarrays of reconstituting tissue were performed. Of the several candidate genes, which were found to be differentially regulated, those known for a role in regeneration, were selected for further investigation addressing the following research questions in this doctoral work:

1. Evaluation and confirmation of the candidate genes with real-time PCR.
2. Spatiotemporal analysis of expression pattern of selected gene candidates.
3. Functional analysis of the selected candidate genes using siRNA-mediated knock-down analysis.



## 2 Materials

### 2.1 Animals

All animals were obtained from the Charles Sullivan newt farm (Nashville, Tennessee, USA). The animals used in this study had undergone complete metamorphosis and were sexually mature, having ages ranging from 3 to 4 years. The maintenance of the animals was done by the animal care staff of the Max Planck Institute for Heart and Lung Research, Bad Nauheim, Germany, under supervision of Prof. Dr. med. Robert Dinser<sup>‡</sup>, Dr. med. Matthias Geyer and Dr. rer. nat. Thilo Borchardt. The newly incoming animals were kept in a disinfection solution containing 0.5% sulfamerazine for 2-3 hr. Afterwards they were maintained in aerated aquaria in the aquarium facility in groups of maximally 15 animals. The water temperature in the aquaria was set to 18–20°C. They were fed with gnat larvae and artemia twice a week. Animal care was conducted in accordance with the Guide for the Care and Use of Laboratory Animals published by the US National Institutes of Health (NIH Publication No. 85-23, revised 1996). Animal experiments were conducted according to the animal welfare act and approved by the Darmstadt regional administrative council. All animal experiments and surgery approaches were performed by Prof. Dr. med. Robert Dinser<sup>‡</sup> and Dr. med. Matthias Geyer. Tissues used as described in this thesis were provided for the realization of this work.

### 2.2 Chemicals and materials

Table 1: List of chemicals and materials

Description	Manufacturer
6-well plates	Corning, Wiesbaden
12-well plates	Corning, Wiesbaden
24-well plates	Corning, Wiesbaden
Basal medium eagle (BME) with Earle's salts and 2.2 mg/ml NaHCO <sub>3</sub>	Biochrom AG, Berlin
β-mercaptoethanol	Merck, Darmstadt
Bromophenol blue	Sigma-Aldrich, Taufkirchen
Bovine serum albumin (BSA)	Carl-Roth, Karlsruhe
3-(Cyclohexylamino)-1-propanesulfonic acid (CAPS)	Carl-Roth, Karlsruhe
Cell culture flask (25 cm <sup>2</sup> /75 cm <sup>2</sup> )	Corning, Wiesbaden
Cell strainer, 100 μm	BD Falcon, BD Biosciences, Heidelberg

<b>Description</b>	<b>Manufacturer</b>
Cell strainer, 70 µm	BD Falcon, BD Biosciences, Heidelberg
Coverslips for microscope slides (20x20 cm), (20x50 cm)	Carl-Roth, Karlsruhe
Crystal violet	Carl-Roth, Karlsruhe
Diethylpyrocarbonate (DEPC)	Carl-Roth, Karlsruhe
Dithiothreitol (DTT) (10 mM)	Life Technologies, Darmstadt
Dulbecco's Modified Eagle Medium (DMEM), 1 g/l glucose	PAN Biotech, Aidenbach
DMEM/Ham's F12	PAA Laboratories, Cölbe
Dimethylsulfoxide (DMSO)	Sigma-Aldrich, Taufkirchen
Ethylenediaminetetraacetic acid (EDTA)	Carl-Roth, Karlsruhe
Entellan® (microscope slide mounting medium)	Merck, Darmstadt
Fast green FCF	Fluka Biochemika, Steinheim
Fetal calf serum (FCS)	Sigma-Aldrich, Taufkirchen
Gelatin (cell culture tested)	Merck, Darmstadt
Giemsa's azur eosin methylene blue solution	Merck, Darmstadt
Glycine	Carl-Roth, Karlsruhe
Hematoxylin	Carl-Roth, Karlsruhe
4-(2-hydroxyethyl)-1-piperazineethane-sulfonic acid (HEPES)	PAA Laboratories, Cölbe
Histoacryl® (tissue glue)	B. Braun, Melsungen
Insulin transferrin selenium, 100x, (ITS)	Biochrom AG, Berlin
Kaiser's glycerol gelatine (microscope slide mounting medium)	Merck, Darmstadt
L-ascorbic acid (vitamin C)	Sigma-Aldrich, Taufkirchen
L-glutamine	PAA Laboratories, Cölbe
LightCycler capillaries (20 µl)	Roche, Mannheim
May-Gruenwald solution	Carl-Roth, Karlsruhe
Methanol	Carl-Roth, Karlsruhe
Microfilter (non protein binding, SCAA/PF, 0.2 µm)	Corning, Berlin
Microscope slides for paraffin sections; Super Frost Plus	R. Langenbrinck, Emmendingen

Description	Manufacturer
Minimum essential medium (MEM), supplemented with GlutaMAX™	Life Technologies, Darmstadt
Neubauer-improved chamber	Marienfeld, Lauda-Königshofen
Nonidet P40 Substitute	Sigma-Aldrich, Taufkirchen
Phosphate buffered saline, 10x, 1x, and 0.7x (PBS)	PAA Laboratories, Cölbe
Penicillin/Streptomycin	PAA Laboratories, Cölbe
Proteinase-K	PeqLab Laboratories, Erlangen
RNase-free dH <sub>2</sub> O	Applied Biosystems, Darmstadt
Safranin-O	Carl-Roth, Karlsruhe
Sulfamerazine	Sigma-Aldrich, Taufkirchen
TissueTek® OCT™ Compound (Embedding medium)	Sakura, Staufen
TransblotSD semi dry transfer cell	Biorad laboratories, Munich
Tricaine	Sigma-Aldrich, Taufkirchen
2-Amino-2-hydroxymethyl-propane-1,3-diol (Tris)	Carl-Roth, Karlsruhe
Trypan blue	Aldrich, Steinheim
Xylene	Carl-Roth, Karlsruhe
Xylene cyanol	Sigma-Aldrich, Taufkirchen

All other reagents and solutions were obtained from Sigma-Aldrich (Taufkirchen), Merck (Darmstadt) or Carl-Roth (Karlsruhe).

## 2.3 Media and solutions

Table 2: List of media and solutions

Name	Composition
4% Paraformaldehyde (PFA)	4 g/100 ml PFA, 3 ml of 1 M NaOH, the mixture was stirred gently until the powder was dissolved, 1xPBS was added and pH was adjusted to 7.4 with HCl
aDMEM/Ham's F12 (70% DMEM/Ham's F12)	0.7x DMEM/Ham's F12 in sterile ddH <sub>2</sub> O

Name	Composition
Anesthetic solution	0.1% (w/v) tricaine
aPBS (70% PBS)	0.7x PBS in sterile ddH <sub>2</sub> O (The PBS concentration was reduced to amphibian osmolarity)
Crystal violet	1% (w/v) crystal violet was dissolved in methanol
Diethylpyrocarbonate-treated (DEPC) ddH <sub>2</sub> O	0.1% (v/v) DEPC in ddH <sub>2</sub> O
Lysis buffer	50 mM Tris, 1% (v/v) Nonidet P40 substitute, 1x complete protease inhibitor
A1 cells medium	70% BME supplemented with Earle's salts (Biochrom), 10% (v/v) FCS, 100 U/ml penicillin, 10 µg/ml streptomycin, 2 mM L-glutamine, 1x ITS, 10 mM NaHCO <sub>3</sub> , 25 mM HEPES
B1H1 cells medium	70% MEM supplemented with GlutaMAX™, Earle's salts; 10% (v/v) FCS, 100 U/ml penicillin, 10 µg/ml streptomycin, 1x ITS, 10 mM NaHCO <sub>3</sub> , 25 mM HEPES
Primary newt chondrocytes medium	70% DMEM/Ham's F12, 5% FCS / 10% FCS, 25mM HEPES, 100mM NaHCO <sub>3</sub> , 100 U/ml penicillin, 10 µg/ml streptomycin, 2 mM l-glutamine, 1x ITS, and 17.5 µg/ml vitamin C
PCR loading buffer (6x)	0.25% (w/v) bromophenol blue, 0.25% (w/v) xylene cyanol, 30% (v/v) glycerine diluted in ddH <sub>2</sub> O
Proteinase K for IHC	10 µg/ml proteinase K, 50 mM Tris pH 8.0, 5 mM Na <sub>2</sub> EDTA
RNA gel-loading buffer (1.5x)	95% (v/v) formamide, 0.025% (w/v) bromophenol blue, 0.025% (w/v) xylene cyanol, 5 mM EDTA
Tris borate EDTA (TBE), (10x)	0.9 M Tris, 0.9 M boric acid, 20 mM EDTA, pH 8.0
Tris acetic acid EDTA (TAE) electrophoresis buffer (50x)	2 M Tris, 1 M acetic acid, 50 mM EDTA
Weigert's solution	Solution A: 1% (w/v) haematoxylin, 95% (v/v) ethanol; Solution B: 1.16% FeCl <sub>3</sub> .6H <sub>2</sub> O, 0.32% (v/v) HCl. Equal volumes of solution A and B were mixed and used within 4 weeks.

## 2.4 Enzymes

Table 3: List of enzymes

Description	Manufacturer
ABSOLUTE™ QPCR SYBR® Green	Thermo Fischer Scientific, Schwerte
Accutase	PAA Laboratories, Cölbe
Collagenase P	Roche, Mannheim
Collagenase type VII	Sigma-Aldrich, Taufkirchen
Pronase	Sigma-Aldrich, Taufkirchen
Proteinase K	PeqLab, Erlangen
Quantitect™ SYBR® Green PCR Kit	Qiagen, Hilden
ShortCut® RNase III	New England Biolabs, Frankfurt am Main
SuperScript™ II Reverse Transcriptase	Life Technologies, Darmstadt
Taq DNA polymerase master mix	Qiagen, Hilden
Trypsin/EDTA	PAA Laboratories, Cölbe
Hyaluronidase	Sigma-Aldrich, Taufkirchen

## 2.5 Antibodies

Table 4: List of primary antibodies

Name	Application (working conc./ incubation duration /temperature)	Application (blocking so- lution/dura- tion/wash)	Manufactu- rer	Secondary antibody
Rabbit anti- human TN-C	IHC (10 µg/ml/ 1 hr/RT)	5% BSA/ 30 min/PBS	Millipore, Darmstadt	Simple Stain MAX PO (Multi) anti- mouse,- rabbit (Histofine)
Goat polyclonal anti-mouse SPARC (M-15)	IHC (4 µg/ml/1 hr/ RT)	IHC (2% BSA/ 1 hr/PBS)	Santa Cruz Biotechnolo- gy, Dallas, USA	Simple Stain MAX PO anti-goat (Histofine)

Name	Application (working conc./ incubation duration /temperature)	Application (blocking so- lution/dura- tion/wash)	Manufactu- rer	Secondary antibody
Mouse anti- newt tenascin antibody (MT1)	IHC (1:100/overnight /4°C)	IHC (5% BSA + 0.5% (v/v) Triton™X-100/ 30 min/PBS+ 0.5% Triton™X-100	Development Studies Hybridoma Bank, Iowa City, USA	SimpleStain MAX PO anti-mouse (Histofine)

Table 5: List of isotype control antibodies

Isotype control	Manufacturer
Rabbit polyclonal IgG	Abcam, Cambridge, UK
Goat polyclonal IgG	Santa Cruz Biotechnology, Heidelberg

Table 6: List of secondary antibodies

Name	Working conc.	Blocking solution/duration	Manufacturer
Histofine Simple Stain MAX PO (Multi) anti- mouse, -rabbit	Undiluted	Included/30 min	Nichirei Biosciences Inc., Tokyo, Japan
Histofine Simple Stain MAX PO anti-goat	Undiluted	Included/30 min	Nichirei Biosciences Inc., Tokyo, Japan

## 2.6 Molecular biological kits

Table 7: List of molecular biological kits

Name	Manufacturer
3-amino-9-ethylcarbazole (AEC)	Vector Laboratories, Burlingame, CA, USA
Nucleofector Kits for Human Chondrocytes	Lonza, Cologne
BLOCK-iT™RNAi TOPO® Transcription Kit	Life Technologies, Darmstadt
RNeasy Easy Plus Micro Kit	Qiagen, Hilden

Name	Manufacturer
RNeasy Mini Kit	Qiagen, Hilden
Superscript® II Reverse Transcriptase	Life Technologies, Darmstadt
QIAquick Gel Extraction Kit	Qiagen, Hilden
TRIzol® Reagent	Life Technologies, Darmstadt

## 2.7 PCR primers

All of the primers (except siTN-C-F and siTN-C-R) were designed by Dr. med. Matthias Geyer using the Primer3 software (<http://biotools.umassmed.edu/bioapps/primer3-www.cgi>) and the quality of the selected primers was analyzed (oligoanalyzer software, <http://eu.idtdna.com/analyzer/applications/oligoanalyzer/>). The primers were ordered from Sigma-Aldrich. The target genes of the primers were: complement factor B (CFB-1), decorin (DCN-1), gamma  $\beta$  crystalline (CRYGB), myeloid differentiation primary response gene 88 (MyD88), retinoic acid receptor- $\alpha$  (RAR- $\alpha$ ), retinoic acid receptor- $\beta$  (RAR- $\beta$ ), retinoic acid receptor- $\delta$  (RAR- $\delta$ ), retinoid x receptor (RXR), olfactomedin-like 3 (OLFML-3), secreted protein, acidic cysteine-rich or osteonectin (SPARC), periostin (POSTN), retinoic acid receptor responder 1 or tazarotene-induced gene 1 (RARRES1), retinol saturase (RETSAT), toll-like receptor 2 (TLR2), toll-like receptor 5 (TLR5), thymosin  $\beta$ 4 (TMSB4), tenascin-C (TN-C), and tenascin-C for siRNA generation (siTN-C). Primer sequences and used PCR conditions are listed in Table 8

Table 8: List of real-time PCR primers

Name	Sequence (5'→3')	MgCl <sub>2</sub> (mM)	Ta (°C)
CFB-1-f	CACTGAAAGCCTCCCTCTATG	2.5	54
CFB-1-r	CAAGGGAGCACTTTGAATAGG		
DCN-1-f	TGCAGTTCCTGGAATAAAAG	3.5	56
DCN-1-r	TGGCACAAGAGGAGGAAATAC		
CRYGB-1-f	GTCTACGAACACTCGGGATTC	3.0	58
CRYGB-1-r	TCATCAGTGATCAGCTTCAGG		
MyD88-2-f	TGCTTCTTTGAACCCAGAGAG	3.0	58
MyD88-2-r	TCACTGGGTCAGGGTCATTAG		
NvRAR- $\alpha$ -f	AGTACGCAAGGCTCATCAGG	3.0	60
NvRAR- $\alpha$ -r	CGATGGTGAGTGTGGTGAAG		
NvRAR- $\beta$ -f	GCCTTACACTCAACCGAACC	2.5	56
NvRAR- $\beta$ -r	GTGGCTCTTGGAGTTTGTCC		

Name	Sequence (5'→3')	MgCl <sub>2</sub> (mM)	Ta (°C)
NvRAR $\delta$ -f	TCAACAAGGTGACACGGAAC	3.0	60
NvRAR $\delta$ -r	TCCTGATGTGCTTTGCTGAC		
NvRXR-f	AGTGGTGTGAACGAGGAAATG	4.0	60
NvRXR-r	GAAGTGAGGGATACGCTTGG		
NvS21_f	ATCATGCGTCAATCCAGATG	2.5	54
		3.0	56
NvS21_r	CATGTTCCAGTGCCACAAAG	3.5	58
		4.0	60
OLF-1-f	GGAAGTCGACGAGAAGTTGAC	3.5	58
OLF-1-r	TTCTGAAGTTCCCATCAGGTC		
OSN-1-f	CAGCGTCAGTGAGTTTGAGAG	4.0	58
OSN-1-r	TGTGACAAGGACGTTCTTCAG		
POSTN-1-f	TCGTGGGGAATCTATAAGCTG	2.5	54
POSTN-1-r	TCATTTCCATGCAGACAGAAC		
RARR-1-f	AAAAAGTTGGAACGTGCTCTG	3.0	60
RARR-1-r	ACTTTTCCCACATCACCAAAC		
Retsat-1-f	TCATAATGGACCAGCTGACTG	3.0	58
Retsat-1-r	CAACAACGTGTGATACGCTTC		
TLR2-1-f	AGCAAGACTTGTCTGCCTACC	4.0	54
TLR2-1-r	CTCAGAAGGCTTGTTGACTCC		
TLR5-2-f	CGCTTGTGAAGAATACCATTG	3.0	60
TLR5-2-r	GGCTTTGTCATGGAGCTTTAG		
TMSB4-1-f	TGCAAAGATGTCTGACAAACC	2.5	54
TMSB4-1-r	ATAAGAAGGCAATGCTTGTGG		
TN-C-1-f	GGTGACTCCATGACCTACCAC	2.5	56
TN-C-1-r	CCAATGGAACCAGTTTACACC		

Table 9: List of primer to generate esiRNA tenascin-C

Name	Sequence (5'- 3')	Amplicon length
siTN-C-F	GCGGGTTGACCTCAAATGT	560 bp
siTN-C-R	GTCGTCAGGGCAAGTGACT	



## 2.8 Softwares

Table 10: **Softwares**

<b>Name</b>	<b>Manufacturer</b>
ND-1000 V3.5.2	PeqLab Biotechnology, Erlangen
Leica Application Suite (LAS) Ver. 4.0.0.	Leica Microsystems, Wetzlar
GraphPad Prism	GraphPad Software Inc., San Diego, California
Oligoanalyzer	Integrated DNA Technologies, Inc, Iowa, USA

## 2.9 Instruments

Table 11: **List of instruments**

<b>Name</b>	<b>Manufacturer</b>
Cryostat microtome (Leica CM 3050S)	Leica Microsystems, Wetzlar
Gel documentation (Genius I)	Syngene, Cambridge, UK
Incubator (C150)	Binder GmbH, Tuttlingen
LightCycler <sup>®</sup> 1.5 Instrument	Roche, Mannheim
Microscope (Leica DMI 6000D)	Leica Microsystems, Wetzlar
PCR instrument (GeneAMP PCR system 9700)	Life Technologies, Darmstadt
Photometer (Nanodrop <sup>®</sup> )	PeqLab, Erlangen
Rotation instrument (Cat RM5)	Cat RM Zipperer, Staufen
Swing Mill MM 301	Retsch, Haan
UV Transilluminator (BTS-20.M)	Progen Scientific, London, UK
LightCycler <sup>®</sup> Carousel Centrifuge	Roche, Mannheim,
Microscope camera (Leica DFC 295)	Leica Microsystems, Wetzlar
Microscope Axiovert 2s	Zeiss, Jena
Milli-Q Biocell	Millipore, Darmstadt
Paraffin microtome (Microm HM 340 E Coolcut)	Thermo Fisher Scientific, Schwerte
Centrifuge (Multifuge 3SR)	Thermo Fisher Scientific, Schwerte
Centrifuge 5417C	Eppendorf, Hamburg
Centrifuge (Biofuge <sup>®</sup> , Primo <sup>®</sup> R)	Thermo Fisher Scientific, Schwerte

## 2.10 Organs and tissues

Newt knee joint tissues were available from previous experiments which were performed by Dr. med. Matthias Geyer, Prof. Dr. med. Robert Dinser<sup>‡</sup>, and Carina Schreiyäck (Section 2.1).

Paraffin embedded human tissues (RA bone tissue) were available from joint replacement surgery at the Orthopedic Department of the University of Gießen. The paraffin embedded tissues were available and used to evaluate the specificity of the SPARC antibody. All of the human tissues were taken with the approval of the ethics committee of the Justus-Liebig-University of Giessen, Germany. All patients gave informed consent and fulfilled the criteria of the American College of Rheumatology.

Table 12: List of organs and tissues

Tissue	Name	Storage	Description
Leg, newt	OP5-3R12	Paraffin-embedded	Surgically-treated newt leg, 10 days after injury
Leg, newt	OP5-3L12	Paraffin-embedded	Sham-operated control newt leg, 10 days after injury
Leg, newt	OP5-6R12	Paraffin-embedded	Surgically-treated newt leg, 10 days after injury
Leg, newt	OP5-6L12	Paraffin-embedded	Sham-operated control newt leg, 10 days after injury
Leg, newt	OP2-6L20	Paraffin-embedded	Sham-operated control newt leg, 20 days after injury
Leg, newt	OP2-4L20	Paraffin-embedded	Sham-operated control newt leg, 20 days after injury
Leg, newt	OP2-4R20	Paraffin-embedded	Surgically-treated newt knee leg, 20 days after injury
Leg, newt	OP2-4L20	Paraffin-embedded	Sham-operated control newt leg, 20 days after injury
Leg, newt	OP1-23R47	Paraffin-embedded	Surgically-treated newt leg, 40 days after injury
Leg, newt	OP1-23L47	Paraffin-embedded	Sham-operated control newt leg, 40 days after injury
Leg, newt	OP1-24R47	Paraffin-embedded	Surgically-treated newt leg, 40 days after injury
Leg, newt	OP1-24L47	Paraffin-embedded	Sham-operated control newt leg, 40 days after injury

<b>Tissue</b>	<b>Name</b>	<b>Storage</b>	<b>Description</b>
Leg, newt	OP1- 12R47	Paraffin- embedded	Surgically-treated newt leg, 40 days after injury
Leg, newt	OP1- 12L47	Paraffin- embedded	Sham-operated control newt leg, 40 days after injury
Leg, newt	901JL09	Paraffin- embedded	Buffer-injected control newt leg, 10 days after injury
Leg, newt	901MR12	Paraffin- embedded	Collagenase-injected newt leg, 10 days after injury
Leg, newt	Col6- 7R11	Paraffin- embedded	Collagenase-injected newt leg, 10 days after injury
Leg, newt	Col6- 7L11	Paraffin- embedded	Buffer-injected control newt leg, 10 days after injury
Leg, newt	Col6- 16L19	Paraffin- embedded	Buffer-injected control newt leg, 20 days after injury
Leg, newt	901HR22	Paraffin- embedded	Collagenase-injected newt leg, 20 days after injury
Leg, newt	Col6- 8R19	Paraffin- embedded	Collagenase-injected newt leg, 20 days after injury
Leg, newt	Col6- 8L19	Paraffin- embedded	Buffer-injected control newt leg, 20 days after injury
Leg, newt	OP2- 1L20	Paraffin- embedded	Sham-operated control newt leg, 20 days after injury
Leg, newt	Col6- 3L40	Paraffin- embedded	Buffer-injected control newt leg, 40 days after injury
Leg, newt	Col6- 3R40	Paraffin- embedded	Collagenase-injected newt leg, 40 days after injury
Leg, newt	Coltest2- 2R35	Paraffin- embedded	Collagenase-injected newt leg, 40 days after injury
Leg, newt	ColTest2- 2L35	Paraffin- embedded	Buffer-injected control newt leg, 40 days after injury
Bone, human	RA348	Paraffin- embedded	Bone tissue derived from RA patients during joint replacement surgery

## 2.11 List of cells and cell lines

Table 13: List of cells and cell lines

Name	Species	Source
B1H1	<i>N. viridescens</i> <i>viridescens</i>	Kindly provided by Prof. Jeremy Brockes from University College London, UK
Chondrocytes	<i>N. viridescens</i> <i>viridescens</i>	Isolated by Carina Schreiyäck during this doctoral work
A1	<i>N. viridescens</i> <i>viridescens</i>	Kindly provided by Prof. Jeremy Brockes from University College London, UK

### 3 Methods

#### 3.1 Animal models of OA and differential expression analysis with cDNA microarray

Experiments established for this section were performed by Dr. med. Matthias Geyer, Carina Schreyäck, Dr. rer. nat. Thilo Borchardt, Dr. rer. nat. Mario Looso and Prof. Dr. med. Robert Dinser<sup>‡</sup>. In these experiments, two OA models were used in newts. The first was an intra-articular injection of collagenase into the newt right knee joint which caused knee joint instability leading to artificial OA (Geyer et al., 2010). The second model was surgically induced OA. In this model, the right knee of the newt was opened by transverse section in the skin. Afterwards, femoral cartilage was removed with a scalpel. Finally, the lesion was sealed with tissue glue (Histoacryl®). The left knees of the animals were slightly opened and closed with tissue glue to serve as control. The newts were sacrificed at 9–47 days after knee surgery or collagenase injection. The treated as well as the control legs were removed after sacrificing the animals. The tissues were embedded in paraffin and were used for the present study.

The initial microarray analysis was performed by Dr. med. Matthias Geyer and Prof. Dr. med. Robert Dinser<sup>‡</sup>. For this study, 5 animals from each of the OA models were sacrificed. Their knees, treated as well as the control, were removed and pooled into two groups. The first group consisted of treated or untreated knees from two animals (pool A), respectively. The second group consisted of treated or untreated knees from three animals (pool B), respectively. The RNA was isolated from those knees and cDNA was generated. The cDNA was labeled and cDNA microarray was performed in the Max Planck Institute for Heart and Lung Research, Bad Nauheim, Germany. Dr. med. Matthias Geyer and Prof. Dr. med. Robert Dinser<sup>‡</sup> performed the evaluation of the cDNA microarray generated data which were used for the present study.

#### 3.2 Preparation of newt knee joint paraffin tissue

Preparation of newt knee joint paraffin tissues was performed in order to provide samples for histological analysis including IHC and H&E, Pappenheim, and Safranin-O staining. The preparation of paraffin tissues used in this doctoral work, were performed by Carina Schreyäck (technical assistant).

The preparation of the newt knee joint paraffin tissues was performed according to the following method: The animals were anesthetized. Then, they were sacrificed and the legs were cut with scalpel. Afterwards, the legs were preserved by incubation in 4% paraformaldehyde or formaldehyde overnight at RT. On the following day, the knee joints

were washed twice with 1xPBS, at RT, each for 5 min. Because the tissues contained bony components, decalcification was performed by incubation in 20% (w/v) Na<sub>2</sub>EDTA for 2 weeks at RT. Then, the tissues were washed two times with 1xPBS at RT for 5 min. Thereafter, dewatering of the sample was performed by incubating them in ascending dilution series of ethanol, which was dissolved in 1xPBS (e.g. 50% for 30 min, 75% for 60 min, 96% for 90 min, 100% for 90 min, and 100% overnight) at RT. Afterwards, the knee joints were rinsed two times with xylene for 45 min at RT. Afterwards, the knee joint tissues were incubated in a solution containing 50% (v/v) of ethanol and paraffin for 1 hr at 60°C. Thereafter, they were incubated another three times in paraffin for 1 hr. Then, the tissues were incubated in a paraffin solution for 12 hr at 60°C. Finally, the casting of paraffin block for the tissues was performed, and then kept at RT or 4°C for further use.

### **3.3 Cell biological methods**

#### **3.3.1 Pre-coating of culture plates/flasks with gelatin**

In order to culture newt cells, the cultured plates/flasks were pre-coated with gelatin to allow adhesion of newt-derived cells. Two percent (w/v) gelatin was diluted in aPBS and then sterile-filtered. The gelatin solution was incubated in a cell culture flask/plate for at least 5 min and discarded before using the container for cultivating newt-derived cells.

#### **3.3.2 Quantification of cells**

To determine the cell numbers, the cells were resuspended in PBS, mixed with trypan blue and incubated for 2 min. The unstained cells were counted in a Neubauer-improved chamber. The cell concentration (cells/ml) was determined using the formula: average counted cell number  $\times 10^4$ .

#### **3.3.3 Isolation of primary newt chondrocytes**

The isolation of the primary newt chondrocytes was performed by Carina Schreyäck for this doctoral work. In order to obtain these cells, first, the newts were submerged in disinfection solution containing 0.5% sulfamerazine overnight at RT in order to prevent bacterial contamination. Afterwards, the animals were anesthetized. Thereafter, by means of surgery, cartilage tissues from several joints such as thigh, hip, and shoulder were isolated and collected in aDMEM/Ham's F12 culture medium. Subsequently, in order to release the cartilage cells from their ECM, the tissue was incubated with 0.5% (w/v) pronase diluted in primary newt chondrocytes medium + 5% (v/v) FCS for 1.5 hr at 25°C. Later on, the cells were washed with aPBS. The rest of the ECM component was digested with 1 ml of 0.5% (w/v) collagenase P diluted in primary newt chondrocytes medium + 5% (v/v) FCS overnight

at 25°C. Thereafter, the cells were separated from the degraded ECM component product by filtration using a cell strainer (100 µm), and then the filtrate was purified again with another cell strainer (70 µm). Afterwards, the primary newt chondrocytes were washed 2-3 times in the culture medium. Later, the number of the viable cells was counted in a Naubauer chamber with trypan blue staining (see Section 3.3.2). Then, the chondrocytes were cultivated in several wells of a gelatin pre-coated 96 well-plate at 25°C.

### **3.3.4 Culture of newt cell lines**

Primary newt chondrocytes, A1 cells and B1H1 newt cells were cultivated in monolayers with their respective culture medium as described in Section 2.3. in the gelatin pre-coated cell culture flasks and incubated at 25°C without CO<sub>2</sub> supplementation. After achieving confluency, cells were detached with 0.5 mg/ml trypsin, 0.22 mg/ml EDTA in aPBS and then seeded into two flasks (1:2) and further cultured.

## **3.4 Molecular biological methods**

### **3.4.1 RNA isolation**

RNA isolation from newt cell lines was done with the RNeasyPlus Micro Kit due to the low amount of the available cells. RNA was isolated according to the manufacturer's instructions. The RNA concentration was determined with a Nanodrop<sup>®</sup> photometer. The RNA was stored at -80°C until further use.

RNA isolation from newt organs/tissues was done with the TRIzol<sup>®</sup> reagent. Frozen newt organs/tissues were put on ice. RNase-free small metal balls and 1 ml TRIzol<sup>®</sup> reagent were added in the newt organ/tissue. Afterwards, the tissue was grinded by rigorous shaking in a swing mill MM 301 at 30 cycles/sec for 5 min. Then, the RNA was extracted according to manufacturer's instructions. The RNA was quantified with Nanodrop<sup>®</sup> photometer and then stored at -80°C until further use.

### **3.4.2 Reverse transcription**

500 or 1000 ng of purified RNA samples were transcribed to cDNA using the reverse transcriptase kit (Superscript<sup>®</sup> II Reverse Transcriptase) according to the manufacturer's instructions. The cDNA was stored at -20°C until further use.

### **3.4.3 Real-time PCR**

The relative quantification of gene expression was done with real-time PCR. The list of the genes and primers can be found in Section 2.7. The RNAs used were kindly provided

by Dr. med. Matthias Geyer and corresponded to the RNA used for the microarray experiment as described in Section 3.1. The RNA was transcribed to cDNA with method described in Section 3.4.2. Real-time PCR quantification was done with the QuantiTect SYBR® Green PCR kit or ABSOLUTE™ QPCR SYBR® Green mix kit with reaction mixture as follows:

### ***Real-time PCR mixture***

SYBR Green mix	1x
cDNA	2 µl
Forward primer	0.5 µM
Reverse primer	0.5 µM
MgCl <sub>2</sub>	(2.5 mM – 4.0 mM) for Quantitect™ SYBR® Green PCR Kit (3.0 mM – 5.0 mM) for ABSOLUTE™ QPCR SYBR® Green Mixes
Final volume	20 µl

The PCR reactions were centrifuged with a LightCycler® 1.5 Carousel centrifuge. Afterwards, the samples were transferred to the LightCycler® Instrument and the following program was applied:

95°C	15 min	Initial denaturation	
95°C	15 sec	Denaturation	} 40-50 cycles
X °C <sup>2</sup>	35 sec	Annealing	
72°C	30 sec	Elongation and fluorescence acquisition	

During the amplification, SYBR® Green dye intercalated into the newly generated double-stranded DNA (dsDNA). The fluorescence signal was measured at the end of the elongation phase. As the amplification proceeded, the number of the dsDNA product increased. The increase of the PCR product was reflected by the increase of the fluorescence signal. In conclusion, the amount of PCR product was proportional to the intensity of the fluorescence signal which was measured at the end of the elongation phase. Cycle threshold (Ct) was defined as the number of amplification cycles required for the fluorescence signal intensity exceeding the background level. The lower the concentration of the starting DNA template, the longer the fluorescence signal exceeded the background levels hence the higher the Ct value. Amplification using a constant ratio of serial DNA dilutions yielded a constant increment of the Ct value and a linear standard curve was formed. The gradient/slope of the standard curve was available for the calculation of the efficiency of the PCR. The Ct value, the standard curve and the slope value were determined

<sup>2</sup> The annealing temperatures of each primer set are listed in Section 2.7.



using the LightCycler® software. Afterwards, the amplification efficiency was deducted from the slope by the following formula: Amplification efficiency (E) =  $10^{(-1/\text{slope})}$ . In order to perform a valid relative quantification using real-time PCR, the amplification efficiency had to be  $2 \pm 0.05$ . Real-time PCR conditions (annealing temperature and magnesium chloride (MgCl<sub>2</sub>) concentration) for each primer pair were optimized to perform a valid and reproducible relative quantification of the selected candidate genes.

### ***Real-time PCR optimization***

For each primer pair, two real-time PCR parameters were optimized: the annealing temperature and the MgCl<sub>2</sub> concentration. To determine the optimal MgCl<sub>2</sub> concentration, serial DNA dilutions as template were prepared (e.g. 1:5, 1:15, 1:45, and 1:135), then the PCR using the serial DNA dilutions for each MgCl<sub>2</sub> concentration (e.g. 2.5 mM, 3.0 mM, 3.5 mM, 4.0 mM and 4.5 mM) for different annealing temperatures (e.g. 54°C, 56°C, 58°C, and 60°C) were performed to achieve the above mentioned PCR efficiencies of  $E = 2 \pm 0.05$ .

### ***Evaluation of amplification specificity***

The specificity of the primer pairs was analyzed with a melting curve analysis. This melting curve analysis was done directly after the DNA amplification. In the melting curve analysis, the dsDNA was denatured by increasing the temperature continuously from 50°C to 99°C. As the dsDNA denatured, the intercalated SYBR Green dye was released, and the fluorescence signal decreased. The PCR product has a specific melting temperature, which can be differentiated from unspecific PCR products or primer dimer formation. If the melting curve analysis showed two or more peaks, the relative quantification could not be evaluated.

### ***Relative quantification real-time PCR ( $\Delta\Delta C_t$ )***

Real-time PCR experiments were performed with their optimized MgCl<sub>2</sub> concentration and annealing temperature. Each primer pair was amplified in parallel to a primer pair of a reference gene (newt ribosomal protein S21). Each PCR was performed in triplicates and the average C<sub>t</sub> values were generated.  $\Delta C_t$  was calculated by subtracting the average C<sub>t</sub> values of candidate genes with the average C<sub>t</sub> values of reference gene. The standard deviation of  $\Delta C_t$  was calculated according to the following formula:

$$\text{Std. deviation } \Delta C_T = ((\text{Std. deviation } C_T \text{ sample})^2 + (\text{Std. deviation } C_T \text{ reference gene})^2)^{1/2}$$

Standard deviation of  $\Delta C_t$  is a measure of dispersion the  $\Delta C_t$  values around the average  $\Delta C_t$  value.

$\Delta\Delta C_t$ s were calculated by subtracting  $\Delta C_t$  of the sample with  $\Delta C_t$  of the reference sample (e.g. untreated control). The standard deviation values of  $\Delta\Delta C_t$  (S) were the same

as the standard deviation of the  $\Delta CT$  of the sample. The difference between the samples was evaluated using the following formula:

$$\text{Fold change} = 2^{-\Delta\Delta CT \pm S}$$

### **3.5 Histological and immunological methods**

#### **3.5.1 Tissue section preparation**

Five  $\mu\text{m}$  thick paraffin tissue sections were prepared from paraffin-embedded tissues using a microtome (Microm HM 340 E Cool-Cut). The tissue sections were mounted on microscope slides, and dried in a  $37^\circ\text{C}$  incubator overnight. They were stored at RT until further use.

#### **3.5.2 Pappenheim staining**

Pappenheim staining was used to visualize articular cartilage content in the newt knee joint specimen. The staining process was based on combination of a May-Gruenwald and a Giemsa staining solution. With the Pappenheim staining, the cartilage area was stained violet.

Paraffin-embedded tissues were incubated in xylene for 10 min twice to dissolve the paraffin component. Afterwards, the tissues were hydrated by incubating the tissues with a serial incubation of 100% and 96% ethanol each for 10 min. The hydration process was continued by incubating the tissues with 80%, 70%, and 50% ethanol each for 5 min. After washing the ethanol remnant by incubating the tissues in PBS for 5 min, the tissues were incubated with May-Gruenwald solution for 5 min. The May-Gruenwald remnant was washed with PBS for 2 min. Afterwards, the tissues were incubated with Giemsa staining solution for 15 min. The Giemsa staining solution was prepared by diluting the Giemsa stock solution with PBS (1:10). Then, the remaining staining solution in the tissues was washed with PBS for 5 min. Thereafter, the tissues were acidified with 1% (v/v) acetic acid for 30 sec. In order to stabilize the tissues for microscopy observation, the tissues were dehydrated and mounted. Dehydration of the tissues was performed by incubation with serial dilution of ethanol (e.g. 96% and 100%) each for 2 min. The tissues were incubated with xylene twice each for 2 min. Finally, they were mounted with Entellan®.

#### **3.5.3 Safranin-O staining**

Safranin-O staining was used to visualize articular cartilage content in newt knee joint specimen. The staining process was based on a combination of Weigert solution, Fast Green

(FCF) solution, and Safranin-O. With the Safranin-O staining, the cartilage area was stained red/pink.

Paraffin-embedded tissues were incubated in xylene for 10 min twice to dissolve the paraffin component. Thereafter, the tissues were hydrated by incubating the tissues with descending ethanol series of 100% and 96% ethanol each for 10 min. The hydration process was continued by incubation the tissues with descending ethanol series of 80%, 70%, and 50% ethanol each for 5 min. After washing the tissues in PBS for 5 min, they were incubated in Weigert solution for 10 min. Thereafter, the tissues were washed with tap water for 10 min. Then, the tissues were stained with 0.05% (w/v) Fast Green (FCF) solution for 5 min. Thereafter, the tissues were stained with 1% (v/v) acetic acid for 10 sec. Subsequently, the tissues were stained with 0.1% (w/v) Safranin-O solution for 5 min. In order to stabilize the tissues for microscopic examination, the tissues were dehydrated in an ascending ethanol series and xylene. Finally, the tissues were mounted in Entellan®.

#### **3.5.4 Hematoxylin and Eosin staining**

Hematoxylin and eosin staining was used for tissue overview. Nuclei were stained blue (hematoxylin), cytoplasm and extracellular matrix pink (based on the affinity to the eosin dye). Deparaffinization of paraffin-embedded sections was done by incubating the sections twice in xylene for 10 min. To restore the water saturation, the tissue sections were incubated in decreasing ethanol concentrations (100%, 96%, and 70% in distilled water) each for 5 min each. Afterwards, the sections were incubated in PBS for 5 min. Then, the sections were incubated in hematoxylin solution (described in Section 2.3) for 7 min and then washed with tap water for 1 min. Subsequently, the sections were incubated in eosin solution (described in Section 2.3) for 7 min, then washed again with tap water. To dehydrate the tissue sections, they were incubated in an ascending series of different ethanol dilutions (50%, 70%, 96% and 100%) for 5 min each. At the end, the tissue sections were mounted in Entellan®.

#### **3.5.5 Immunohistochemistry**

Immunohistochemistry (IHC) is an immunological technique to identify and visualize target antigens in a tissue section. A given target molecule antigen is visualized by using a specific primary antibody and an appropriate secondary antibody tagged with either a fluorescent label or an enzymatic tag (Coons et al., 1942). Used primary antibodies are listed in Section 2.5.

### **3.5.5.1 IHC using paraffin-embedded tissue sections**

Five  $\mu\text{m}$  thick paraffin-embedded joint sections (described in Section 2.10) were deparaffinized by incubating them in xylene and a descending ethanol series (100%, 96%, and 70% ethanol). The pH and isotonic level of the sections were adjusted and equilibrated with PBS for 5 min. Due to fixation with formaldehyde or paraformaldehyde prior to embedding the tissue in paraffin, the antigen/epitope as binding site for the primary antibody is often blocked. Antigen/epitope retrieval is required in order to give access for the antibody reaction with the antigen. Here, antigen retrieval was conducted with 10  $\mu\text{g}/\text{ml}$  proteinase K diluted in TE buffer pH 8.0 (see Section 2.3) for 5 min at 37°C. To increase the proteolytic capacity of the enzyme, a pre-incubation of the proteinase K solution at 37°C was carried out for at least 30 min before it was applied to the slides. The proteolytic activity of proteinase K was then stopped by incubating the sections in PBS for 5 min. 3-amino-9-ethylcarbazole (AEC) was used as chemiluminescent detection reagent. Thus, endogenous peroxidase activity within the tissue sample needed to be inhibited by incubating the section in 3%  $\text{H}_2\text{O}_2$  in methanol for 10 min at 4°C. Afterwards, the sections were washed twice with PBS for 5 min. Unspecific binding of the antibody was blocked by incubating the tissue sections with 40  $\mu\text{l}$  to 200  $\mu\text{l}$  (based on the size of the tissue on the slide) of blocking reagent (see Section 2.5). Incubation with the primary antibody (see Section 2.5) was either performed at RT for 1 hr or overnight at 4°C (conditions depending on the primary antibody as described in Section 2.5). Afterwards, the unbound antibody was removed by incubating the tissue section three times for 5 min each in washing buffer composed of PBS or PBS supplemented with 0.5% Triton X-100 (see Section 2.5). Afterwards, the secondary antibody (as described in Section 2.5) was added to the section followed by an incubation for at least 10 or 30 min (see Section 2.5). The non-bound secondary antibody was removed by washing three times with PBS for 5 min each. Afterwards, the immunoreaction of the antibody was developed by adding 3-amino-9-ethylcarbazole (AEC kit) to the tissue section. The emerging pink or red signal was observed under a transmitted-light microscope. When the signal intensity was clearly visible without background staining, the chemoluminescent reaction was stopped by incubating the slides in PBS. Finally, the sections were mounted with Kaiser's glycerol gelatine.

### **3.5.5.2 IHC stainings to evaluate TN-C expression during newt knee joint regeneration in the collagenase and surgery model**

IHC stainings of regenerating newt knee joints after 10, 20, and 40 days of collagenase- and surgically-induced OA are performed using protocol as mentioned in Section 3.5.5.1. For each time point of the collagenase model, IHCs were performed with knee joint sections from two animals ( $n=2$ ) and for each time point of the surgery model, the

experiments were performed with knee joint sections of three animals (n=3). For illustration, only one representative picture for each time point in both OA models is presented in Section 4.2.2 for collagenase model and Section 4.2.3 for surgery model. A summary of TN-C expression based on all of the IHC results is presented in Section 4.5.

### 3.6 Knockdown experiments using endoribonuclease-prepared small interfering RNAs

Small interfering RNAs (siRNAs) are a collection of short RNA molecules (20-25 bases) which bind to mRNA of a specific gene transcript and block the protein expression (Hamilton et al., 1999; Elbashir et al., 2001).

For our experiments, TN-C-specific siRNAs were introduced into primary newt chondrocytes. For this purpose, a custom-made TN-C siRNA pool was generated. The TN-C siRNA was derived from a RNase III digested 560-bp-TN-C-dsRNA fragment. This siRNA is called endoribonuclease-prepared siRNA (esiRNA). The preparation of the esiRNA was based on modification of the work which was reported elsewhere (Yang et al., 2002). TN-C esiRNA was designed from the newt's TN-C sequence data (TransID7000), which was kindly provided by Dr. rer. nat. Mario Looso and Dr. rer. nat Thilo Borchardt from the Max Planck Institute for Heart and Lung Research, Bad Nauheim, Germany. Synthesis of TN-C esiRNA was done with the help of BLOCK-iT RNAi TOPO Transcription Kit and ShortCut® RNase III as shown in Figure 11.

As control, *lacZ* esiRNA was generated. *lacZ* is a gene in enteric bacteria (e.g. *Escherichia coli*). It encodes  $\beta$ -galactosidase which hydrolyzes the disaccharide lactose into glucose and galactose. *lacZ* is not present in the newt's genome and, thus, is a suitable control.

The TN-C and *lacZ* esiRNA were introduced into newt chondrocytes using nucleofection, and the knockdown was determined with relative quantification using real-time PCR.

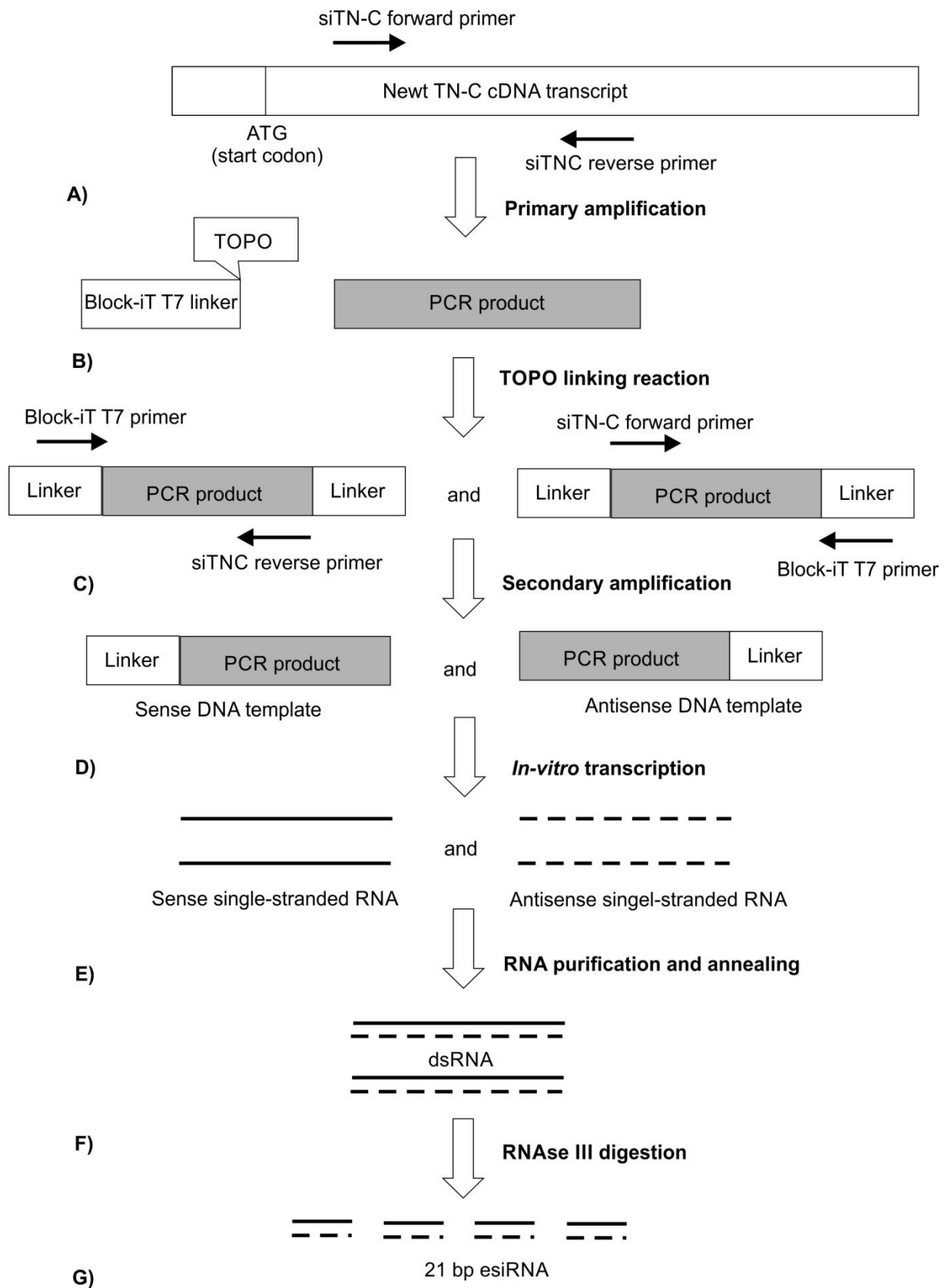


Figure 11: **esiRNA generation using BLOCK-iT RNAi TOPO Transcription Kit and RNase III.** (A) A primer pair (siTN-C forward and siTN-C reverse) was used to amplify a 560 bp newt TN-C cDNA product which was located 100 bp downstream of the start codon. (B) The 5'- and 3'- terminal of PCR product was then linked to the Block-iT T7 linker coupled with topoisomerase enzyme (TOPO).

(C) Afterwards, the secondary PCR was done with Block-iT T7 primer and siTN-C reverse to produce the sense DNA template. Antisense DNA template was produced by performing PCR of the linking reaction product with siTN-C forward and Block-iT T7 primer. (D) Sense RNA and antisense RNA products were synthesized by conducting *in-vitro* transcription of sense DNA template and antisense DNA template, respectively. (E) The sense RNA and the antisense RNA products were purified and annealed to produce dsRNA, then (F) the dsRNA was digested with RNase III to produce (G) 21 bp TN-C siRNA.

### 3.6.1 Generating TN-C and negative control *lacZ* esiRNA

In order to synthesize TN-C esiRNA, a 560 bp DNA fragment, which was located 100 bp downstream of the newt TN-C start codon, was amplified from a newt chondrocyte-derived cDNA template using siTN-C-F and siTN-C-R primers (the resulting DNA fragment is presented in Figure 12, lane B). For *lacZ* control esiRNA, a 1000 bp DNA fragment was amplified from plasmid containing *lacZ* (pcDNA™ 1.2/V5-GW/*lacZ*) with primers *lacZ*-forward and *lacZ*-reverse (Figure 12, lane C). The plasmid and *lacZ* primers were components of the kit. Both amplifications were prepared according to the following protocol:

Taq DNA Polymerase master mix	2.5 U/reaction
10 µM siTN-C-F or 10 µM <i>lacZ</i> forward	0.2 µM or 1.3 ng/µl
10 µM siTN-C-R or 10 µM <i>lacZ</i> reverse	0.2 µM or 1.3 ng/µl
cDNA template	1 µl
Final reaction volume	40 µl

The PCR reaction was done in a thermo cycler (GeneAmp PCR System 9700), with a reaction program as follows:

94°C	3 min	Initial denaturation	
94°C	30 sec	Denaturation	} 35 cycles
55°C	30 sec	Annealing	
72°C	1 min	Elongation	
72°C	10 min	Final elongation	

In order to evaluate the specificity of the amplification product, the PCR product was mixed with PCR loading buffer and run on a 1.5% (w/v) high-resolution agarose gel submerged in TAE buffer. A 100 bp DNA ladder was used. The gel was run by applying a constant voltage of 100 V for approximately 1 hr. The separated DNA was stained by incubating the agarose gel in ethidium bromide solution and visualized using a UV transilluminator.

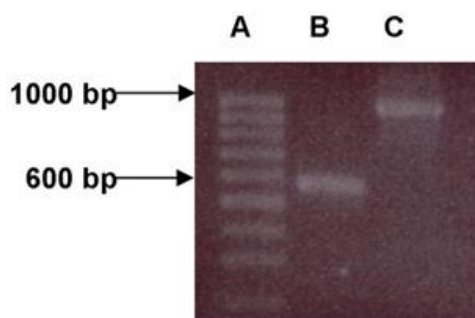


Figure 12: **Primary amplification products of newt TN-C (lane A) and *lacZ* (lane B)**

The amplification product was linked with a DNA linker containing T7 promoter through a bound-topoisomerase catalyzed linking reaction. The linking reaction mixture was composed of 3  $\mu$ l of supplied sterile water, 1  $\mu$ l of supplied salt solution, 1  $\mu$ l of Block-iT T7 TOPO® linker, and 1  $\mu$ l of PCR product. The reaction mixture was accomplished by incubating the mixture at 37°C for 15 min.

In order to provide antisense and sense DNA template for *in-vitro* transcription, two parallel amplifications with each DNA template TN-C and *lacZ* fragment-linked Block-iT T7 TOPO® linker were performed. The amplification reaction mixtures were prepared as follows:

***Reaction mixture to provide DNA template for generation of antisense TN-C ssRNA***

Taq DNA Polymerase master mix	2.5 U/reaction
75 ng/ $\mu$ l Block-iT™ T7 primer	1.5 ng/ $\mu$ l
10 $\mu$ M siTN-C-forward	0.5 $\mu$ M
TN-C TOPO linking reaction product	1 $\mu$ l
Final reaction volume	40 $\mu$ l

***Reaction mixture to provide DNA template for generation of sense TN-C ssRNA***

Taq DNA Polymerase master mix	2.5 U/reaction
75 ng/ $\mu$ l Block-iT™ T7 primer	1.5 ng/ $\mu$ l
10 $\mu$ M siTN-C-reverse	0.5 $\mu$ M
TN-C TOPO linking reaction product	1 $\mu$ l
Final reaction volume	40 $\mu$ l

***Reaction mixture to provide DNA template for generation of antisense *lacZ* ssRNA***

Taq DNA Polymerase master mix	2.5 U/reaction
75 ng/ $\mu$ l Block-iT™ T7 primer	1.5 ng/ $\mu$ l
65 ng/ $\mu$ l <i>lacZ</i> -forward	3.25 ng/ $\mu$ l
<i>lacZ</i> TOPO linking reaction product	1 $\mu$ l



Final reaction volume 40  $\mu$ l

**Reaction mixture to provide DNA template for generation of sense *lacZ* ssRNA**

Taq DNA Polymerase master mix	2.5 U/reaction
75 ng/ $\mu$ l Block-iT™ T7 primer	1.5 ng/ $\mu$ l
65 ng/ $\mu$ l <i>lacZ</i> -reverse	3.25 ng/ $\mu$ l
<i>lacZ</i> TOPO linking reaction product	1 $\mu$ l
Final reaction volume	40 $\mu$ l

The PCR reactions were done in a thermo cycler (GeneAmp PCR System 9700), with a reaction program as follows:

95°C	15 min	Initial denaturation	
94°C	30 sec	Denaturation	} 35 cycles
55°C	30 sec	Annealing	
72°C	1 min	Elongation	
72°C	10 min	Final elongation	

The amplification product resulted in generation of antisense and sense TN-C cDNA template (Figure 13, lane A, B), and antisense and sense *lacZ* cDNA template (Figure 13, lane C, D) respectively.

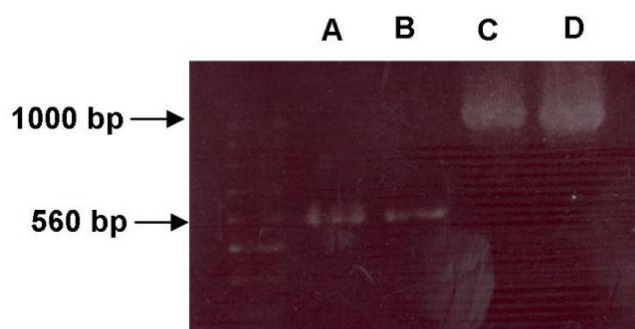


Figure 13: **Secondary amplification products of newt TN-C (lane A, B) and *lacZ* (lane C, D)**

The expected amplification reaction product was purified with Qiaquick Gel Extraction Kit according to the manufacturer's protocol.

Afterwards, RNA transcription reactions were performed with the four purified reaction products to synthesize ssRNA of sense and antisense of TN-C and *lacZ* RNA according to the BLOCK-iTRNAi TOPO Transcription Kit instruction.

Then, BLOCK-iT™ RNA Purification Kit was used to purify the RNA transcript products. The purification was performed by following the manufacturer's instructions. The concentration and quality of purified ssRNA were determined by a Nanodrop® spectrophotometer.

In order to generate dsRNA, 10 µg of each sense and antisense ssRNA of TN-C and *lacZ* were mixed and the mixtures were incubated in pre-boiled 250 µl of water in a 500 µl beaker glass and cooled slowly to RT for at least 2 hr.

esiRNA was generated using ShortCut®RNase III. The enzyme converts long dsRNA of TN-C and *lacZ* into 21-bp TN-C (lane A, Figure 14) and *lacZ* (lane B, Figure 14) esiRNAs respectively. The reaction was performed according to the manufacturer's instructions.

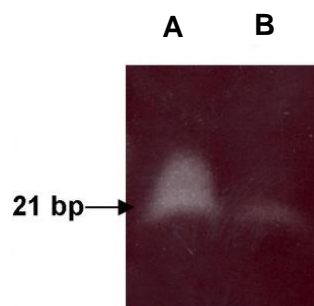


Figure 14: Polyacrylamide gel electrophoresis of (I) TN-C and (J) *lacZ* esiRNA showed RNA bands of 21 bp.

### 3.6.2 Purification of esiRNA product

The esiRNA products were mixed with 73 mM RNase-free sodium acetate pH 5.5, 0.8% (v/v) RNase-free glycogen and 70% RNase-free ethanol. To induce RNA precipitation, the mixture was incubated at -20°C for 2 hr. Then, the RNA was spun 20817xg for 15 min at RT to obtain a RNA pellet. The RNA pellet was washed with 120 µl of 80% (v/v) RNase-free ethanol by incubation at RT for 10 min. The ethanol was discarded by removing the ethanol after centrifugation at 20817xg for 5 min at RT. The RNA pellet was air-dried for 10 to 15 min. The RNA pellet was dissolved in 20 µl of RNase-free double-distilled water and stored at -80°C until further use.

### 3.6.3 Evaluation of esiRNA quality

Polyacrylamide gel electrophoresis (PAGE) can be applied for RNA detection and quality assessment. Polyacrylamide was chosen instead of agarose because polyacrylamide gel pore diameter is smaller compared to the one of agarose gels, which allows

differentiation of RNAs at the single nucleotide level (Alberts, 2002). The protocol of RNA PAGE was adapted from a previous study (Rio et al., 2010).

***Preparing RNA polyacrylamide gel :***

Urea	48% (w/v)
40% acrylamide/bis (19:1)	6% (v/v)
10x TBE buffer	1x
DEPC-treated ddH <sub>2</sub> O	up to 30 ml

The gel mixture was incubated in hot water to accelerate urea dissolution. After the urea was dissolved, the mixture was cooled down to RT, then the following reagents were added to the mixture sequentially:

10% ammonium persulfate	0.9% (w/v)
Tetramethylethylenediamine	0.08% (v/v)

After polymerization was completed, the gel was pre-run (without sample) at 118 V for 45 min in order to remove excess persulfate. Afterwards, the RNA sample was mixed with RNA loading buffer (see Section 2.3), the mixture was heated at 95°C for 5 min and then directly chilled on ice to denature RNA secondary structure. The gel was run by applying a constant voltage of 118 V.

In order to visualize the RNA, the gel was incubated in SYBR<sup>®</sup> Gold nucleic acid gel stain dissolved in TBE buffer pH 7.8. The incubation was performed under light agitation in the absence of light for 40 min. Finally, the RNA was visualized in an UV transilluminator.

### **3.6.4 Knockdown of TN-C expression in primary newt chondrocytes**

In order to knockdown the TN-C expression in primary newt chondrocytes, TN-C and *lacZ* esiRNA (negative control) were introduced into the cells by nucleofection using Human Chondrocyte Nucleofector™ Kit (Lonza).

#### **3.6.4.1 Introduction of esiRNA into primary newt chondrocytes**

In order to obtain reliable results, the nucleofection experiment was performed two times. Both experiments employed the same protocol. The differences between them were the number of the nucleofected primary newt chondrocytes. The first experiment used 400000 cells/nucleofected esiRNA and the second employed 725000 cells/nucleofected esiRNA.

In order to prepare the cells for the nucleofection experiment, the newt chondrocytes were incubated with culture medium supplemented with 5 U of hyaluronidase at 25°C overnight.

On the next day, the cells were washed with aPBS and detached with 0.5 mg/ml trypsin, 0.22 mg/ml EDTA in aPBS at RT. Two cell pellets, each containing 400000 cells (first experiment) or 725000 cells (second experiment), were prepared by centrifugation of the detached chondrocytes with 300xg for 10 min at RT.

Introduction of TN-C esiRNA into the primary newt chondrocytes was performed by mixing a cell pellet with 100  $\mu$ l of nucleofector final solution and 257.62 ng (20 pmole) of TN-C esiRNA. The mixtures were transferred to cuvettes and then the introduction of esiRNA in the cells was conducted in the nucleofector instrument with program T-023. Shortly after treatment, the chondrocytes were dissolved in 1 ml of culture medium. Afterwards, introduction of 257.62 ng (20 pmole) of *lacZ* esiRNA into the primary newt chondrocytes was performed according to the same protocol.

The nucleofected cells were then incubated at 25°C on 2% gelatin pre-coated 6 well-plates (first experiment) or 12 well-plates (second experiment) for RNA isolation to evaluate the knockdown of TN-C mRNA expression. In the second experiment, adhesion and scrape motility assays were performed after esiRNA nucleofection to evaluate the effect of TN-C knockdown on adherence and migration behavior of newt chondrocytes. Thus, 300000 nucleofected cells were seeded to 6 well-plates to perform these assays.

### 3.6.5 Scrape motility assay

The scrape motility assay required a confluent cell monolayer. Therefore, 24 hr after nucleofection, 30000 TN-C and *lacZ* esiRNA nucleofected cells from the 6 well-plates were detached and seeded onto two wells of a 24 well-plates pre-coated with 2% (w/v) gelatin. Thereafter, the newt chondrocytes were grown for 24 hr to form a confluent monolayer. Then, a defined area in the cell monolayer was uncovered by creating a straight line through the cell layer with a pipette tip. Afterwards, the cell debris was washed with aPBS and the remaining cells were incubated in 25°C for 12 hr. The migrated cells were investigated by taking images in defined areas of uncovered cell monolayer using phase-contrast microscope (Figure 15). For each nucleofected cells, the migrated cells in the two defined areas of two wells were calculated. 2 – 3 defined areas were selected for the image acquisition. The image acquisition was repeated every 2 hr until 22 hr of incubation time. The cells, which were migrated into two defined scraped area of each wells, were counted. Thereafter, the average and the standard deviation were calculated.

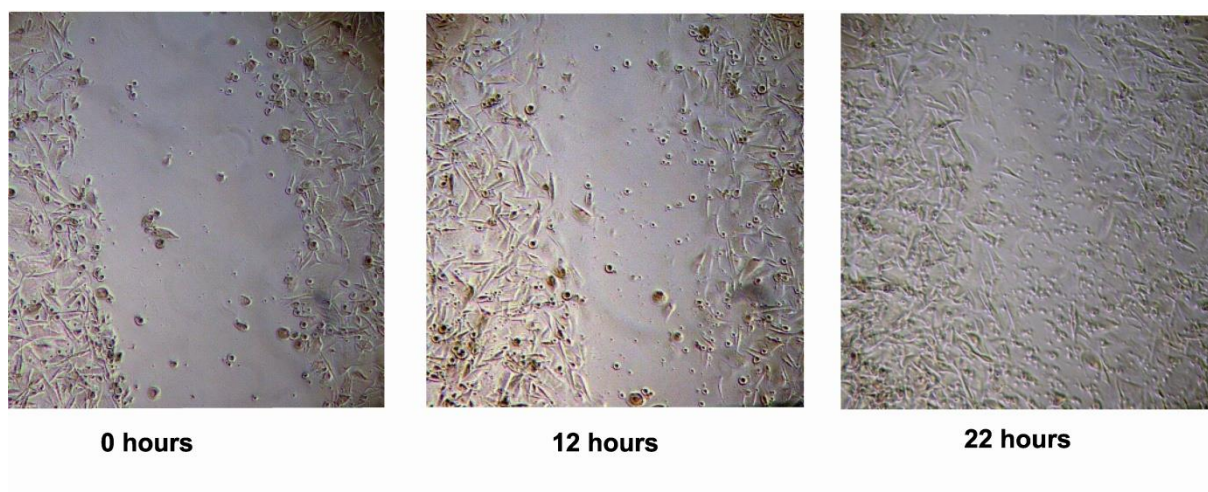


Figure 15: **The process of the newt chondrocytes migration in the scrape motility assay.** The cell monolayer was scratched with a pipett tip to form straight line of uncover cell layer (0 hr). After 12 hr, a movement of the cells were detected (12 hr). Finally, at 22 hr, the uncover area was closed by the migrated chondrocytes.

### 3.6.6 Adhesion assay

Confluent primary newt chondrocytes were detached with accutase. Afterwards, each of 15000 TN-C and *lacZ* esiRNA nucleofected cells were seeded on the three wells of 24 well-plates pre-coated with 2% (w/v) gelatin. Subsequently, the plate was incubated under light shaking in a water-bath with water temperature of 22°C for 1 hr. During this incubation, the plate was positioned just above the water surface. Thereafter, culture medium was aspirated and the plate was washed with aPBS to discard the non-adherent cells. Then, the attached chondrocytes were stained with crystal violet for 5 min. Then, the number of cells which had adhered to the bottom of the plate of each well was counted. Thereafter, the average cell number and the standard deviation were calculated.

## 4 Results

The cDNA microarray experiments were performed with regenerating newt knee joints after collagenase- and surgically-induced knee joint damage. The deregulated candidate genes, which were known to be involved in tissue repair and regeneration, were selected for further investigation. In addition, distinct candidate genes of the innate immune system and vitamin A biosynthesis, which were related to the cDNA microarray study, and supposed to be linked to the candidate genes collection. Afterwards, the deregulation of these genes was evaluated with relative quantification using real-time PCR.

### 4.1 Relative quantification of selected candidate genes

The quantification of gene expression of the candidate genes was calculated based on  $\Delta\Delta C_t$  (see Section 3.4.3). The complete results of the relative quantification of all 18 genes are presented in appendix (section 9.4). The key of the matricellular proteins (e.g. TN-C, SPARC, POSTN, and DCN), the innate-immune system (e.g. CFB and TLR2), and the vitamin A pathway (e.g. RARRES1) are presented in this section.

In the relative gene expression quantification, a gene was assigned to be upregulated when the deregulation value was higher than 2.0-fold, unregulated when the deregulation value was between 2.0 – 0.5-fold and downregulated when the deregulation value was between 0.5 – 0.0-fold.

There were some value differences in the candidate genes between the 2-pool (pool A) and the 3-pool animals (pool B). These discrepancies between the both pools might be explained by different degrees of knee joint damage.

#### 4.1.1 Relative quantification of selected candidate genes of matricellular proteins

##### 4.1.1.1 Relative quantification of TN-C

TN-C was selected because TN-C is known to be expressed during limb regeneration and limb development (Onda et al., 1990; Onda et al., 1991). An additional reason was the real-time PCR relative quantification of TN-C, which showed that TN-C was one of the strongly upregulated genes (upregulation value exceeded 5.0-fold, except on day 40 in the surgery model).

In the collagenase model (Figure 16), the TN-C upregulation pattern was obviously different between pool A and B. In the pool A, the upregulation decreased from 22.4-fold on day 10 after treatment to 3.8-fold on day 40 after treatment. In contrast, in the pool B, the

upregulation value of TN-C expression was increased from 3.5-fold on day 10 after treatment to 12.2-fold on day 40 after treatment.

In the surgery model, there were also obvious differences of the TN-C upregulation pattern between pool A and B. In the pool A, the TN-C upregulation decreased from 15.6-fold on day 10 after treatment to 10.1-fold on day 20 after treatment, then finally it returned to normal (1.2-fold) on day 40 after treatment. In contrast, the upregulation in the pool B increased from 12.3-fold on day 10 after treatment to 33.8-fold on day 20 after treatment, afterwards it decreased also to normal (0.7-fold) on day 40 after treatment.

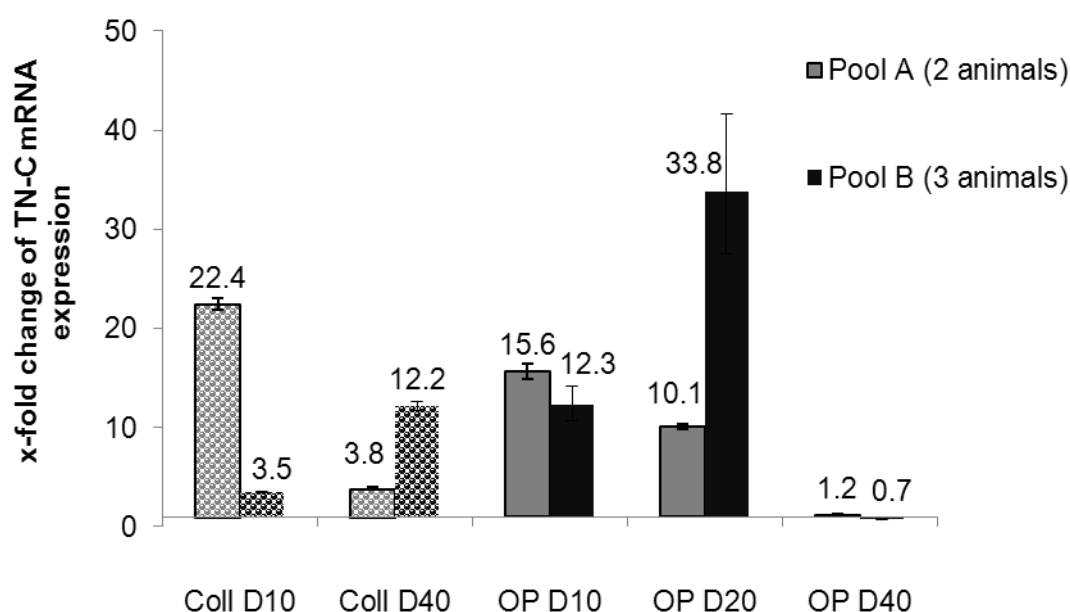


Figure 16: **Relative quantification of TN-C during newt knee joint regeneration after collagenase and surgically-induced OA.** The TN-C upregulation in pool A and B was analysed with real-time PCR relative to S21 ribosomal protein expression (normalisator gene) at day 10 (Coll D10) and at day 40 (Coll D40) after collagenase-induced OA and at day 10 (OP D10), at day 20 (OP D20), and at day 40 (OP D40) after surgically-induced OA. The presented values are the average of the x-fold change of TN-C mRNA expression and the standard deviation.

#### 4.1.1.2 Relative quantification of SPARC

SPARC was selected because SPARC is known to play important roles in bone development (Orlando et al., 2013) and is expressed in human knee joints in OA and rheumatoid arthritis (RA) (Nakamura et al., 1996).

In the collagenase model, there was a different expression of SPARC expression between the pool A and B (Figure 17). On day 10 after treatment, SPARC was only upregulated in the pool A (2.1-fold), and unregulated in the pool B (1.4-fold). On day 40 after treatment, SPARC was only upregulated in the pool B (2.6-fold), and normal in the pool A (1.7-fold).

In the surgery model, the different SPARC expression between the pool A and B occurred only on day 10 after treatment. In the pool B, SPARC was upregulated (2.5-fold), but in the pool A, SPARC was normal (1.4-fold). On day 20 after treatment, SPARC was upregulated in both pools (3.4-fold in the pool A; 2.4-fold in the pool B). On day 40 after treatment, SPARC was not dysregulated in both models.

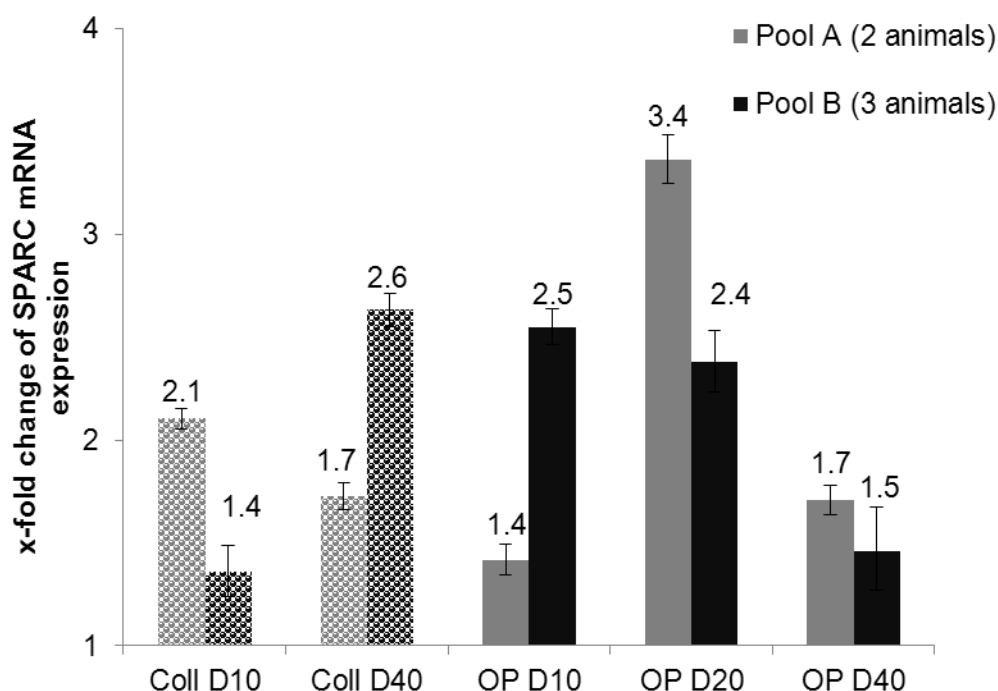


Figure 17: **Relative quantification of SPARC during newt knee joint regeneration after collagenase and surgically-induced OA.** The SPARC upregulation in pool A and B was analysed with real-time PCR relative to S21 ribosomal protein expression with real-time PCR relative to S21 ribosomal protein expression (normaliser gene) at day 10 (Coll D10) and at day 40 (Coll D40) after collagenase-induced OA and at day 10 (OP D10), at day 20 (OP D20), and at day 40 (OP D40) after surgically-induced OA. The presented values are the average of the x-fold change of SPARC mRNA expression and the standard deviation.

#### 4.1.1.3 Relative quantification of POSTN

POSTN was examined because it promotes wound healing in murine skin (Elliot et al., 2012) and bone (Horiuchi et al., 1999).

Relative quantification of POSTN expression is presented in Figure 18. In the collagenase model, there were some differences in expression between pool A and B. On day 10 after treatment, only the pool A showed that POSTN was upregulated (2.8-fold), whereas in the pool B, POSTN expression was normal (1.3-fold). Likewise, on day 40 after treatment, only in the pool B POSTN was upregulated (4.9-fold), whereas in the pool A, POSTN was not dysregulated (1.7-fold).



In the surgery model, POSTN was upregulated on day 10 after treatment (2.3-fold in the pool A; 3.3-fold in the pool B) and on day 20 after treatment (3.9-fold in the pool A and 8.9-fold in the pool B). However, on day 40 after treatment, POSTN expression returned to normal (1.3-fold in the pool A; 0.7-fold in the pool B).

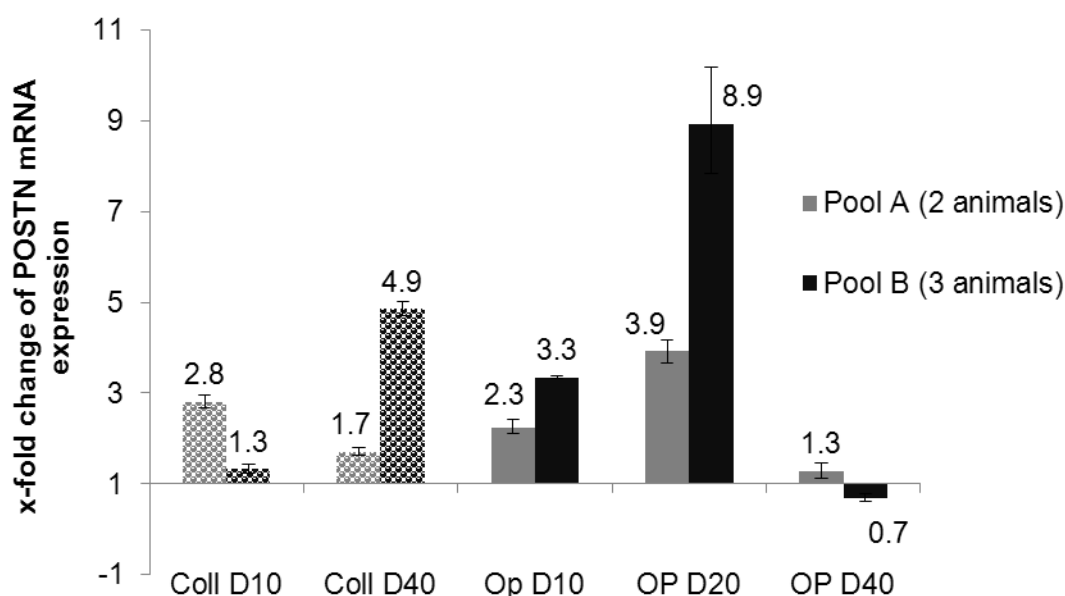


Figure 18: **Relative quantification of POSTN during newt knee joint regeneration after collagenase and surgically-induced OA.** The POSTN upregulation in pool A and B was analysed with real-time PCR relative to S21 ribosomal protein expression (normalisator gene) at day 10 (Coll D10) and at day 40 (Coll D40) after collagenase-induced OA and at day 10 (OP D10), at day 20 (OP D20), and after 40 days (OP D40) surgically-induced OA. The presented values are the average of the x-fold change of POSTN mRNA expression and the standard deviation.

#### 4.1.1.4 Relative quantification of DCN

DCN was examined because this protein is known to promote regeneration and repair in various tissues such as muscle (Li et al., 2007), skin (Shafritz et al., 1994), and tendon (Lu et al., 2013).

Relative quantification of DCN in the regenerating knee joints in the newts is presented in Figure 19. In the collagenase model, the deregulation values of DCN expression 10 days after treatment opposed each other between the pool A and B. They were upregulated in the pool A (8.6-fold) but downregulated in the pool B (0.4-fold). On day 40, DCN was slightly upregulated in the pool A (2.4-fold), whereas in the pool B, DCN was not dysregulated (1.7-fold).

In the surgery model, DCN was upregulated only on day 20 after treatment (2.1-fold in 2-pool animals), whereas at the other time points, DCN was normal (deregulation value was not higher than 2.0).

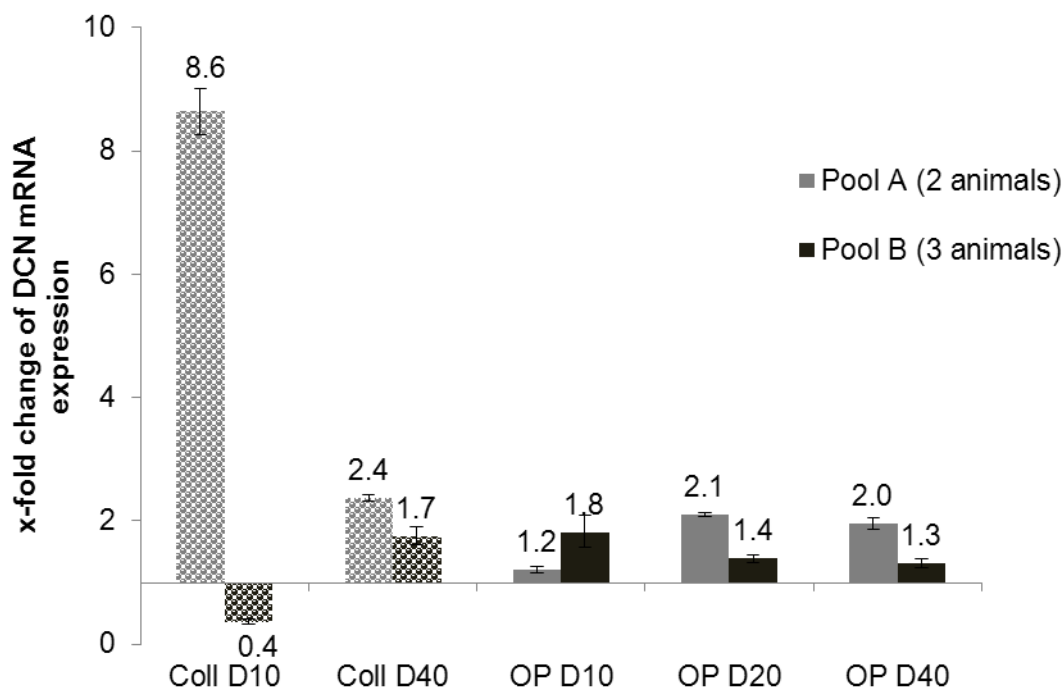


Figure 19: **Relative quantification of DCN during newt knee joint regeneration after collagenase- and surgically-induced OA.** The DCN upregulation in pool A and B was analyzed with real-time PCR relative to S21 ribosomal protein expression (normaliser gene) at day 10 (Coll D10) and at day 40 (Coll D40) after collagenase-induced OA, and at day 10 (OP D10), at day 20 (OP D20), and after 40 (OP D40) surgically-induced OA. The presented values are the average of the x-fold change of DCN mRNA expression and the standard deviation.

#### 4.1.2 Relative quantification of candidate genes from innate immune system

##### 4.1.2.1 Relative quantification of CFB

CFB was selected because complement components were expressed in the newt during regeneration of limbs after amputation and in regenerating lens vesicles after local eye injury (Kimura et al., 2003). In addition, based on real-time PCR relative quantification, CFB was strongly upregulated (deregulation value was higher than 5-fold) at day 10 and day 20 in the surgery model.

In both OA models, CFB was upregulated at all analyzed time points except in the pool A at day 40 of the collagenase model (Figure 20). In the collagenase model, at day 10 after treatment, CFB was upregulated in both pools (4.5-fold in the pool A and 3.2-fold in the pool B). However, at day 40 after treatment, CFB was upregulated only in the pool B (4.9-fold), whereas in the pool A, CFB was not dysregulated (0.8-fold).

In the surgery model, CFB was upregulated at all analyzed time points. However, the difference in values was large, for example at day 10 after treatment (11.8-fold in the pool A versus 4.5-fold in the pool B), and more prominent at day 20 after treatment (4.4-fold in the

pool A versus 23.6-fold in the pool B). At day 40 after treatment, the differences were less (5.2-fold in the pool A versus 6.9-fold in the pool B) in comparison to the previous time points.

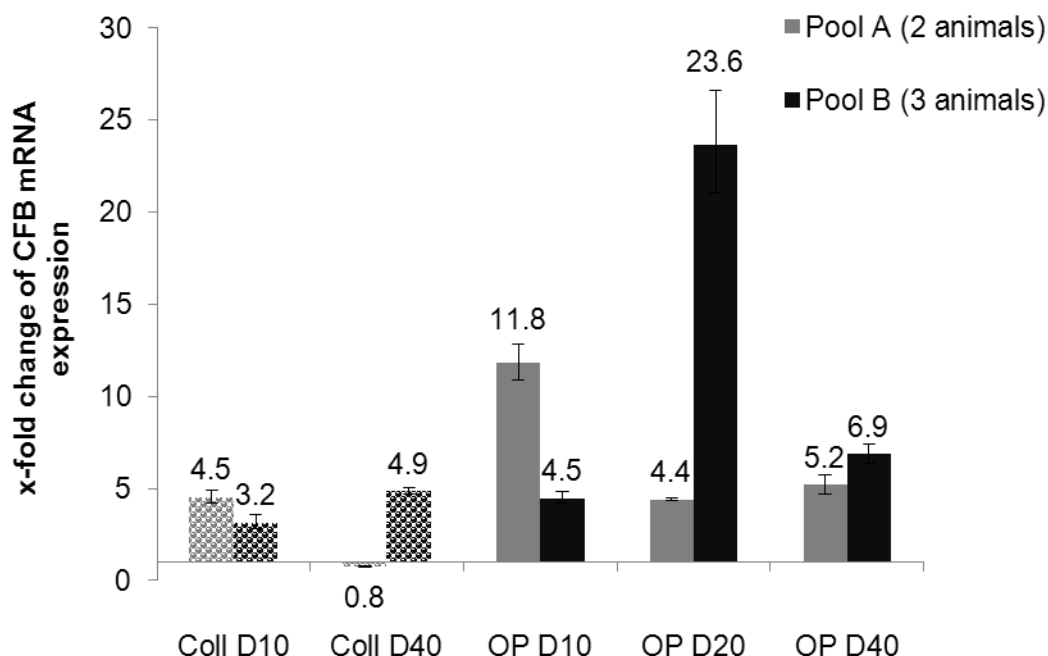


Figure 20: **Relative quantification of CFB during newt knee joint regeneration after collagenase and surgically-induced OA.** The CFB upregulation in pool A and B was analysed with real-time PCR relative to S21 ribosomal protein expression (normalisator gene) at day 10 (Coll D10) and at day 40 (Coll D40) after collagenase-induced OA and at day 10 (OP D10), at day 20 (OP D20), and at day 40 (OP D40) after surgically-induced OA. The presented values are the average of the x-fold change of CFB mRNA expression and the standard deviation.

#### 4.1.2.2 Relative quantification of TLR2

TLR2 was included because of the involvement of TLR2 in regeneration and repair in various tissues (Brown et al., 2007). The result of relative quantification of TLR2 in the surgery model (Figure 21) showed that TLR2 was upregulated only at day 10 after treatment (8.9-fold in the pool A and 6.6-fold in the pool B). At day 20 after treatment, however, the TLR2 upregulation decreased (2.1-fold in the pool B) or became normal in the pool A (0.6-fold). Finally, at day 40 after treatment, TLR2 was normal (0.7-fold in the pool A and 0.5-fold in the pool B). In the collagenase model, TLR2 seemed not to be activated during the regeneration process, because TLR2 was not found to be present at all time points.

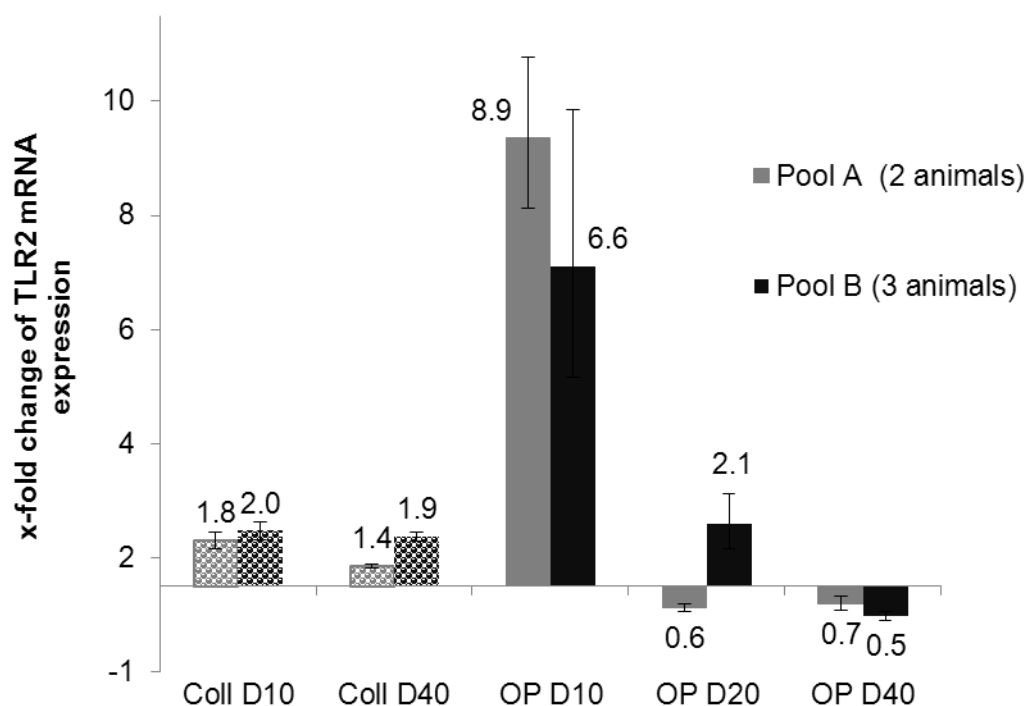


Figure 21: **Relative quantification of TLR2 during newt knee joint regeneration after collagenase and surgically-induced OA.** The TLR2 upregulation in pool A and B was analysed with real-time PCR relative to S21 ribosomal protein expression (normalisator gene) at day 10 (Coll D10) and at day 40 (Coll D40) after collagenase-induced OA and at day 10 (OP D10), at day 20 (OP D20), and at day 40 (OP D40) after surgically-induced OA. The presented values are the average of the x-fold change of TLR2 mRNA expression and the standard deviation.

### 4.1.3 Relative quantification of genes of the vitamin A pathway

#### 4.1.3.1 Relative quantification of RARRES1

RARRES was included as it is involved in tissue proliferation and differentiation (Ohnishi et al., 2009). In addition, it was the only gene from the vitamin A pathway found to be upregulated in the cDNA microarray.

The disagreement of deregulation values between the pool A and B was found to be pronounced in RARRES1 (Figure 22). In the collagenase model, at day 10 after treatment, RARRES1 was only upregulated in the pool A (4.6-fold), but not dysregulated in the pool B (1.7-fold). In the surgery model, at day 10 after treatment, RARRES1 was upregulated only in the pool A (2.7-fold) but normal in the pool B (1.0-fold). Likewise, at day 20 after treatment, the RARRES1 upregulation only occurred in the pool B (3.7-fold) but not in the pool A (1.0-fold). At day 40 after treatment in both models, RARRES1 was normal again.

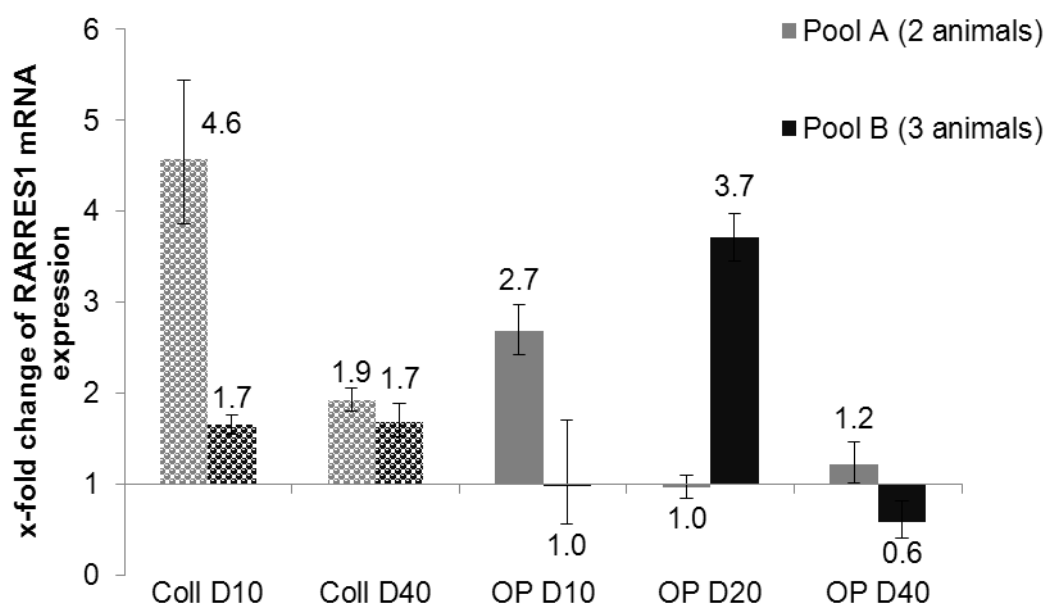


Figure 22: **Relative quantification of RARRES1 during newt knee joint regeneration after collagenase and surgically-induced OA.** The RARRES1 upregulation in pool A and B was analysed with real-time PCR relative to S21 ribosomal protein expression (normalisator gene) at day 10 (Coll D10) and at day 40 (Coll D40) after collagenase-induced OA and at day 10 (OP D10), at day 20 (OP D20), and at day 40 (OP D40) after surgically-induced OA. The presented values are the average of x-fold change of RARRES1 mRNA expression and the standard deviation.

## 4.2 Spatial expression of dysregulated proteins

### 4.2.1 Expression of TN-C and physiological appearance of a healthy newt knee joint

In a healthy newt knee joint, TN-C was localized in the periosteum (black arrow, Figure 23B), and absent in the femoral and tibial articular cartilage (green arrow, Figure 23B). In addition, there was no immunoreactivity of the rabbit polyclonal IgG (isotype control) in the newt knee joint (Figure 23C).

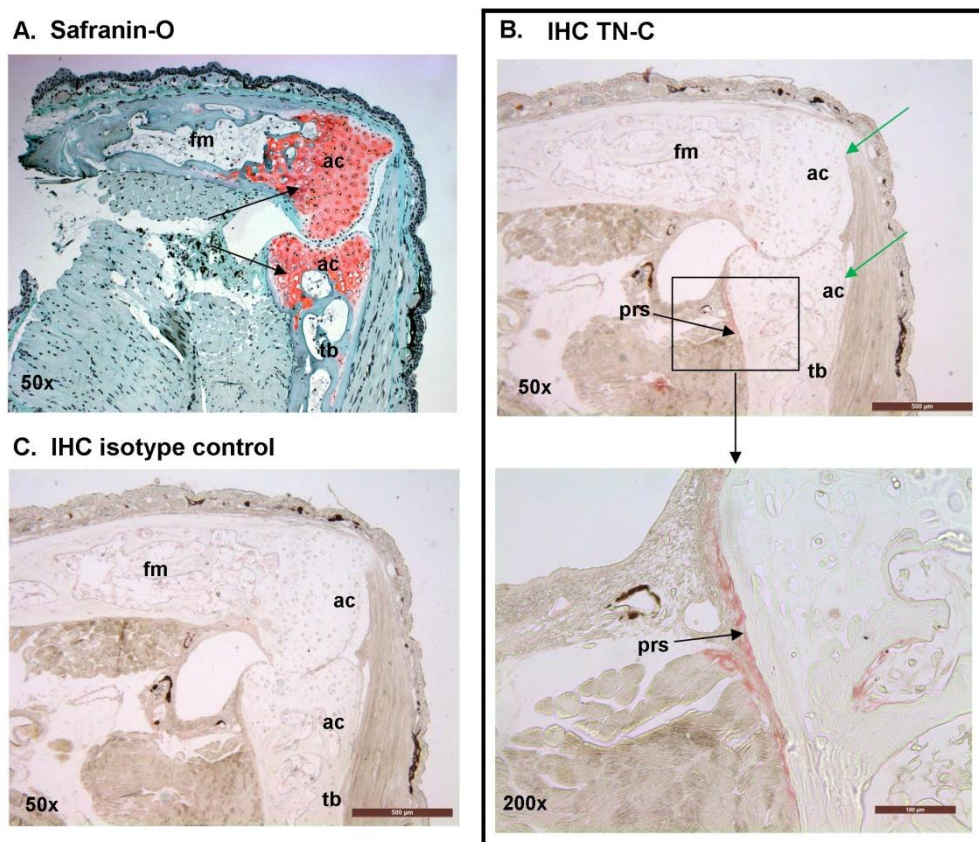


Figure 23: **TN-C expression and physiological appearance of a healthy newt knee joint.** (A) **Safranin-O staining.** Due to its high proteoglycan content, articular cartilage was stained red. **IHC staining (B) against TN-C and (C) against rabbit polyclonal IgG (isotype control).** A 5-µm healthy newt knee joint section was incubated with 10 µg/ml anti-human TN-C or rabbit polyclonal IgG (isotype control). TN-C was detected along the periosteum after staining with AEC substrate (black arrow). There was no antibody reactivity in the newt knee joint incubated with the isotype control. Original magnification x 50. The inset shows the situation in more detail (original magnification x 200). ac, articular cartilage; fm, femur; tb, tibia; prs, periosteum.

In order to validate the result and to check the cross-reactivity of the antibody, TN-C expression in a healthy newt knee joint was further investigated using the newt-specific

antibody, MT-1 (Onda et al., 1990). Similar results were obtained. Strong reactivity of the MT1 antibody in the periosteum was detected (see Figure 24).

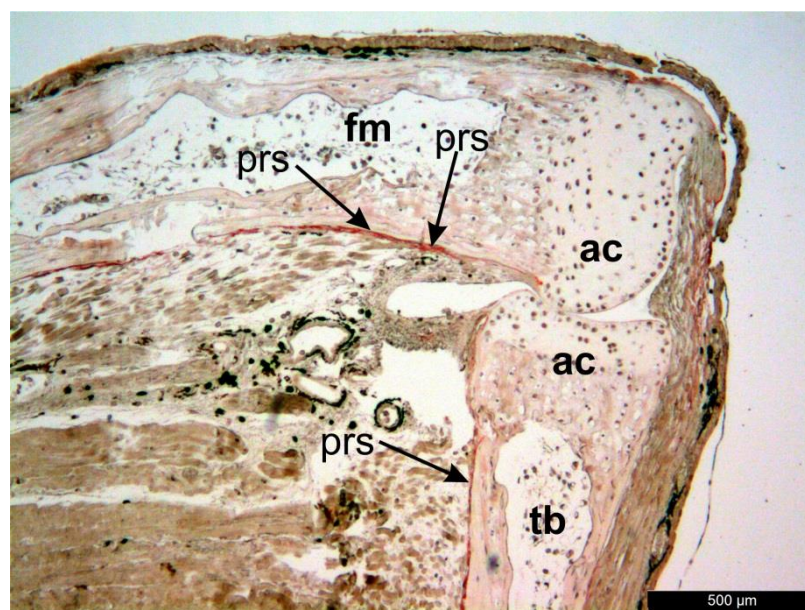


Figure 24: **Validation of TN-C expression in healthy newt knee joint using the newt-specific antibody MT-1.** A 5- $\mu$ m healthy newt knee joint section was incubated with MT-1 antibody. TN-C was detected along the periosteum after staining with AEC substrate (arrows). Original magnification x 50. ac, articular cartilage; fm, femur; tb, tibia; prs, periosteum.

#### 4.2.2 Spatiotemporal TN-C expression during newt knee joint regeneration in the collagenase model

Previous examinations showed that joint-luxation and detachment of muscles from bone and the periarticular zone were observed as early as at day 6 after collagenase injection (Geyer et al., 2010). In this study, at 10 days after collagenase injection, there was no disruption of the anatomical axis of femur and tibia (joint-luxation) as a consequence of collagen degradation due to intra-articular collagenase injection into newt knee joint (see Figure 25A). Safranin-O staining showed that the effect of collagenase injection was already evident by a reduction of the proteoglycan density within the femoral and tibial articular cartilage (arrows, Safranin-O, Figure 25A). This alteration was not seen in the corresponding buffer-injected knee joint section (arrows, Safranin-O, Figure 25B).

At day 10 after treatment, TN-C was found along the periosteum surrounding the femur and tibia (arrow, IHC, Figure 25A). The TN-C localization along the periosteum on the 10-day collagenase-injected newt knee joint was similar to that in the healthy newt knee joint (Figure 23B).



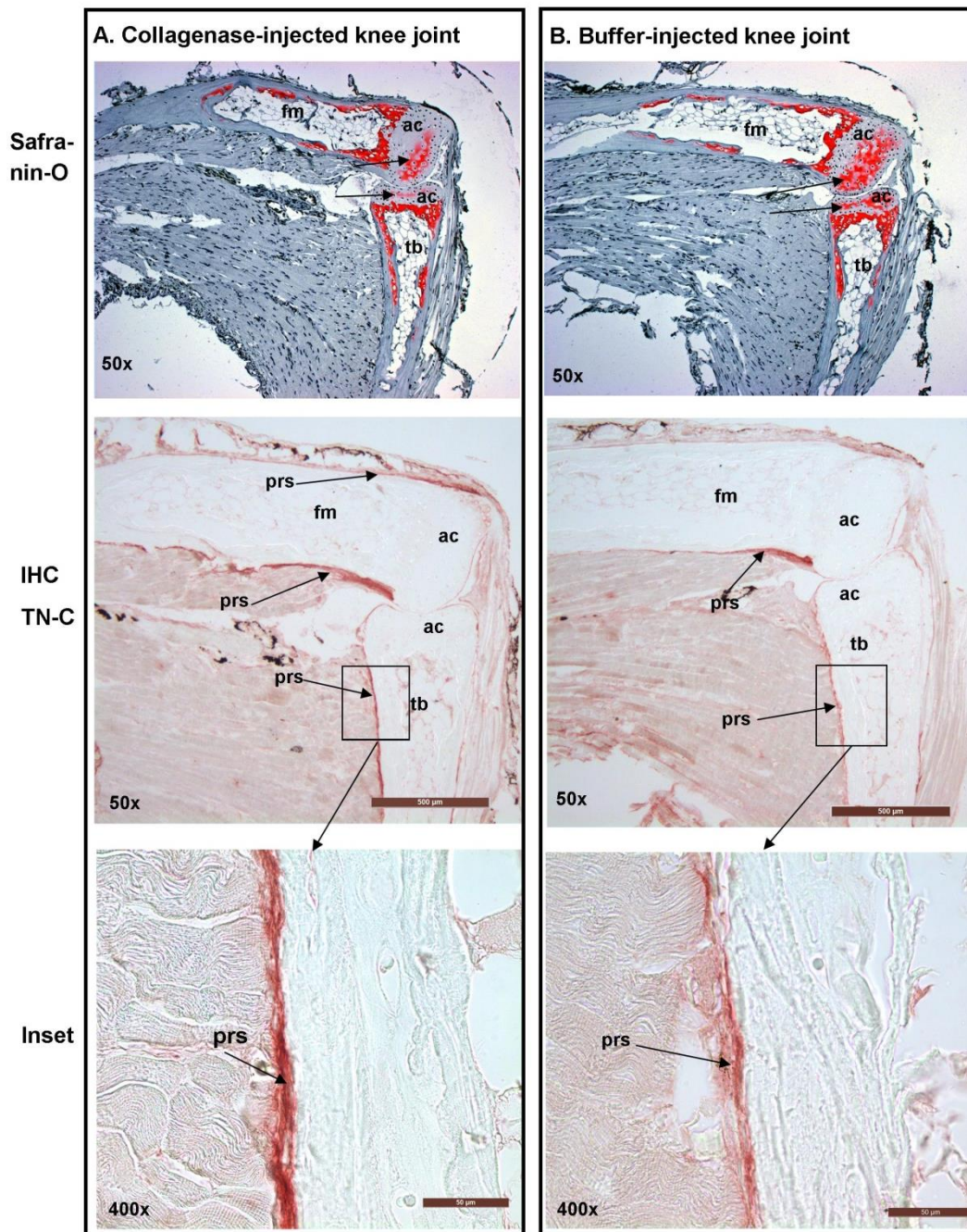


Figure 25: **TN-C expression and physiological appearance of a newt knee joint 10 days after (A), collagenase injection and (B) buffer injection. (A), (B) Safranin-O staining.** Due to its high proteoglycan content, articular cartilage was stained red. **(A), (B) IHC staining of TN-C.** A 5-µm 10 days post intra-articular collagenase- or buffer-injected newt knee joint section was incubated with 10 µg/ml anti-human TN-C. The reactivity of the antibody (red signal) was detected along the periosteum after staining with AEC substrate (arrow). Original magnification x 50. The inset shows the situation in more detail (original magnification x 400). **Depicted here are images from a representative IHC staining / representative IHC stainings.** ac, articular cartilage; fm, femur; prs, periosteum; tb, tibia.



At day 20 after collagenase injection, the disruption of the anatomical axis (joint-luxation) was evident (Safranin-O and H&E, Figure 26A). The disruption of the articular cartilage was also noticeable. The Safranin-O staining (proteoglycan staining) was absent in the deep zone of the femoral articular cartilage (green arrow, Safranin-O, Figure 26A). Nevertheless, in the buffer-injected knee joint, proteoglycan staining covered the complete femoral and tibial articular cartilage (Safranin-O, Figure 26B).

In the treated knee joint, there was amorphous-looking undifferentiated tissue, surrounding the femur and tibia at the site of the defect. The H&E staining revealed that the appearance of the cells in the amorphous-looking tissue was fusiform and they had relatively big and distinct nuclei (H&E, Figure 26A). In contrast to the collagenase-injected joint, no undifferentiated tissue in the corresponding buffer-injected knee joint section was detected (H&E, Figure 26B).

The IHC 20 days post collagenase treatment showed a TN-C localization along the periosteum (black arrow, IHC, Figure 26A) and in the undifferentiated tissue (blue arrow, IHC, Figure 26A). In the buffer-injected knee joint, TN-C appeared only along the periosteum (arrow, IHC Figure 26B).

At day 40 after collagenase injection in the newt knee joint, additional alterations emerged in the regenerating newt knee joint. First, the normal anatomical axis was restored (Figure 27A). However, the joint gap between the femoral and tibial articular cartilages was still clearly visible (black arrow, Safranin-O, Figure 27A). Second, the undifferentiated tissue, which was located adjacent to the femur and tibia at the site of damage, was no longer detectable. A newly-formed tissue appeared next to the damaged area. The tissue was stained red with Safranin-O staining, this meant that it was composed of proteoglycan, indicating that new articular cartilage was formed (nac, Safranin-O, Figure 27A).

Safranin-O staining of the femoral and the tibial old-defected articular cartilages at day 40 of the treated knee joint of the collagenase model indicated slightly lower proteoglycan density (blue arrows, Safranin-O, Figure 27A) in comparison with the femoral and tibial articular cartilage of the corresponding buffer-injected knee joint (arrows, Safranin-O, Figure 27B).

IHC at day 40 after collagenase treatment showed localization of TN-C that was distributed in the newly-formed articular cartilage (arrow, IHC, Figure 27A). Interestingly, the TN-C localization was absent in the femoral and tibial old-defected articular cartilages (oac, IHC, Figure 27A). In contrast, the IHC of the corresponding buffer-injected knee joint section against TN-C showed only specific TN-C localization along the periosteum (arrows, IHC, Figure 27B).

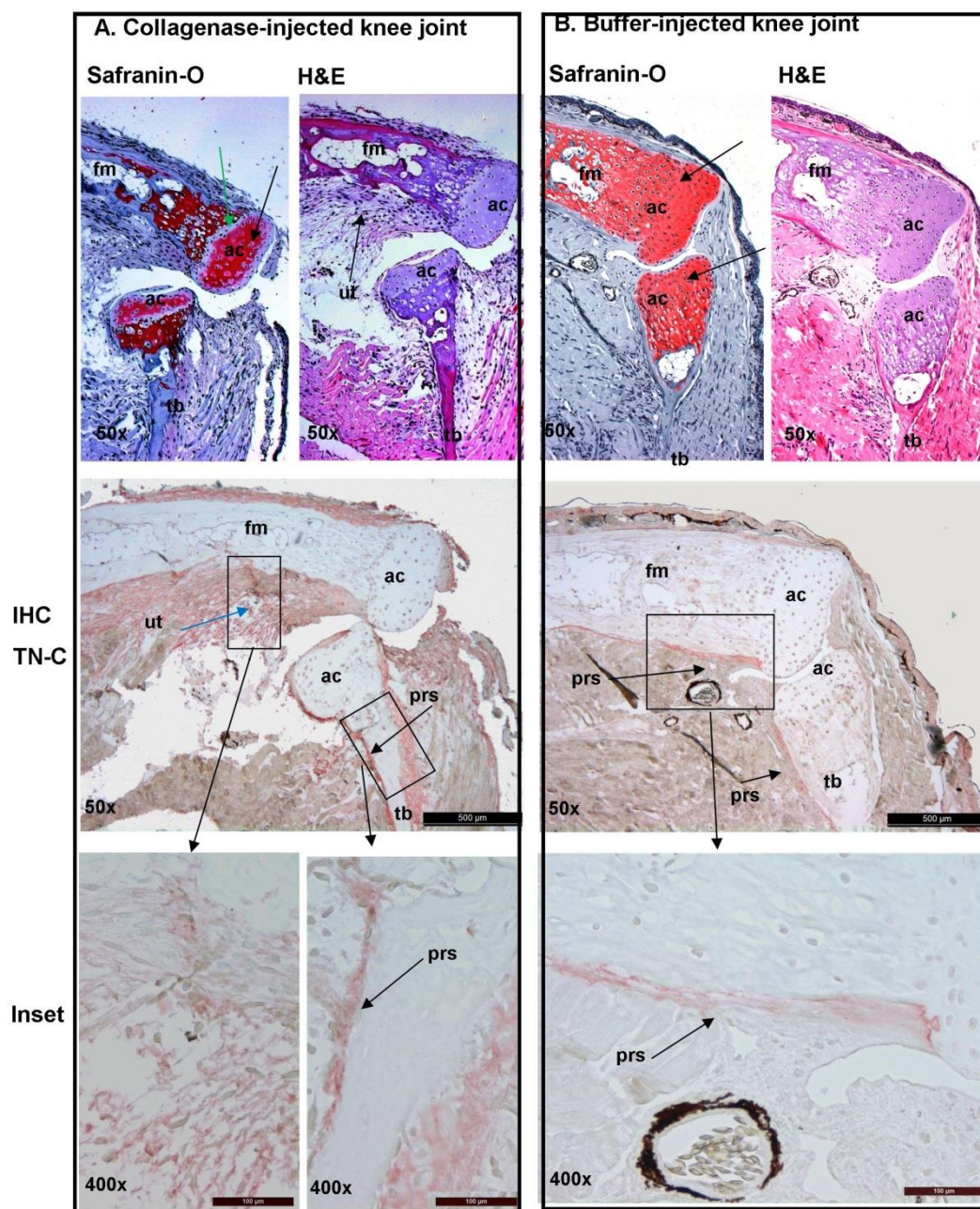


Figure 26: **TN-C expression and physiological appearance of a newt knee joint 20 days after (A) collagenase- and (B) buffer injection. (A), (B) Safranin-O staining.** Due to its high proteoglycan content, articular cartilage was stained red (black arrow). **(A)** Absence of proteoglycan in the articular cartilage of collagenase-treated joint was shown (green arrow). Original magnification x 50. **(A), (B) H&E staining for tissue overview.** Original magnification x 50. **(A), (B) IHC staining of TN-C.** A 5-µm 10 days post intra-articular collagenase- or buffer-injected newt knee joint was incubated with 10 µg/ml anti-human TN-C. The reactivity of the antibody (red signal) was detected in the undifferentiated tissue and in the periosteum after staining with AEC substrate (arrow). Original magnification x 50. The inset shows the situation in more detail (original magnification x 400). **Depicted here are images from a representative IHC staining / representative IHC stainings.** The IHC images are a



representative result from two IHC stainings ac, articular cartilage; fm, femur; tb, tibia; prs, periosteum; ut, undifferentiated tissue.

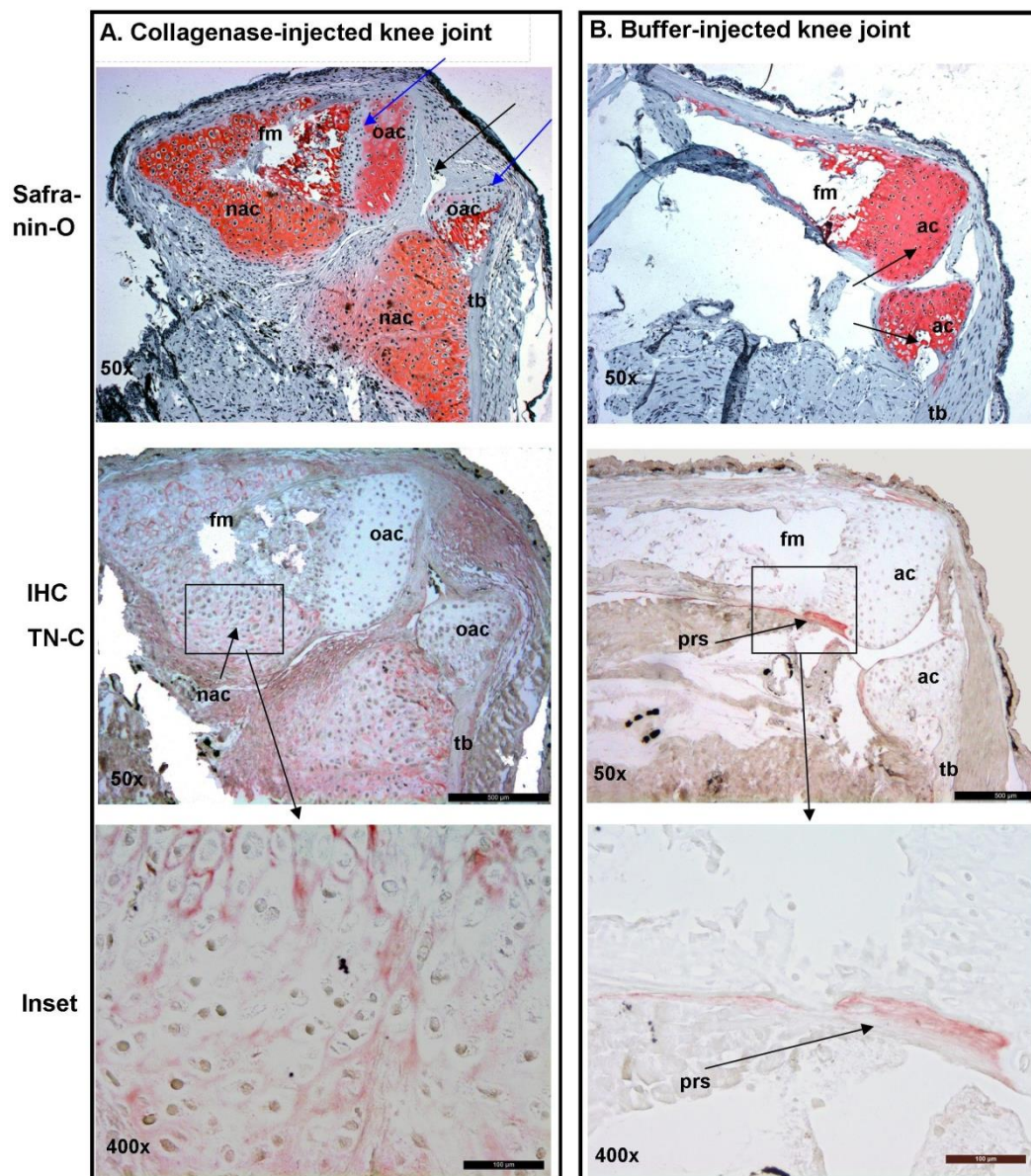


Figure 27: **TN-C expression and physiological appearance of a newt knee joint 40 days after (A) collagenase- and (B) buffer-injection. (A), (B) Safranin-O staining.** Due to its high proteoglycan content, articular cartilage was stained red. Original magnification x 50. **(A), (B) IHC staining for TN-C.** A 5- $\mu$ m 40-day post intra-articular collagenase- or buffer-injected newt knee joint section was incubated with 10  $\mu$ g/ml anti-human TN-C. The reactivity of the antibody (red signal) was detected within **(A)** the newly-formed articular cartilage and **(B)** along the periosteum after staining with AEC substrate (arrow). Original magnification x 50. The inset shows the situation in more detail (original magnification x 400). **Depicted here are images from a representative IHC staining / representative IHC stainings.** ac, articular cartilage; fm, femur; tb, tibia; nac, newly-formed articular cartilage; prs, periosteum; oac, old-defected articular cartilage.

### 4.2.3 Spatiotemporal TN-C expression during newt knee joint regeneration in the surgery model

At day 10 after the surgically-induced knee joint defect, due to the surgical procedure, a small area of the superficial zone of femoral articular cartilage was defected (blue arrow, Figure 28A). Pappenheim staining of the knee joint showed that proteoglycan loss was found in and around the defect area (blue arrow, Pappenheim, Figure 28A). On the other hand, the proteoglycan density of the corresponding knee joint negative control undergoing sham surgery was intact (ac, Pappenheim, Figure 28B).

To study TN-C localization 10 days after surgically-induced knee joint defect, IHC was performed with treated and sham operated newt knee joint sections using TN-C antibody. TN-C was localized in the defect area (blue arrow, IHC, Figure 28A) and along the periosteum (black arrow, IHC, Figure 28A). On the sham operated knee joint, TN-C was restricted to the periosteum (arrow, IHC, Figure 28B).

Investigation of TN-C expression 20 days after treatment showed newts with their femoral and tibial articular cartilage of the treated knee joint almost completely removed. The surgery treatment had left debris of the old-defected articular cartilage, which could be visualized with Safranin-O staining of the knee joint (black arrow, Safranin-O, Figure 29A). Another result of the surgery treatment was a disruption of the anatomical axis or joint-luxation of the treated joint.

In addition, at this time point, undifferentiated tissue was formed adjacent to the femur and tibia at the defect site (ut, Safranin-O, Figure 29A).

Meanwhile, the corresponding control sham operated knee joint was morphologically intact. There was no alteration of the proteoglycan density of the femoral and the tibial articular cartilages (arrows, Safranin-O, Figure 29B).

The IHC of the 20-day surgically-treated knee joint showed a TN-C localization in the undifferentiated tissue (blue arrow, IHC, Figure 29A) and in the old-defected articular cartilage (black arrow, IHC, Figure 29A). In the sham operated knee joint, TN-C was detected only along the periosteum (arrow, IHC, Figure 29B).

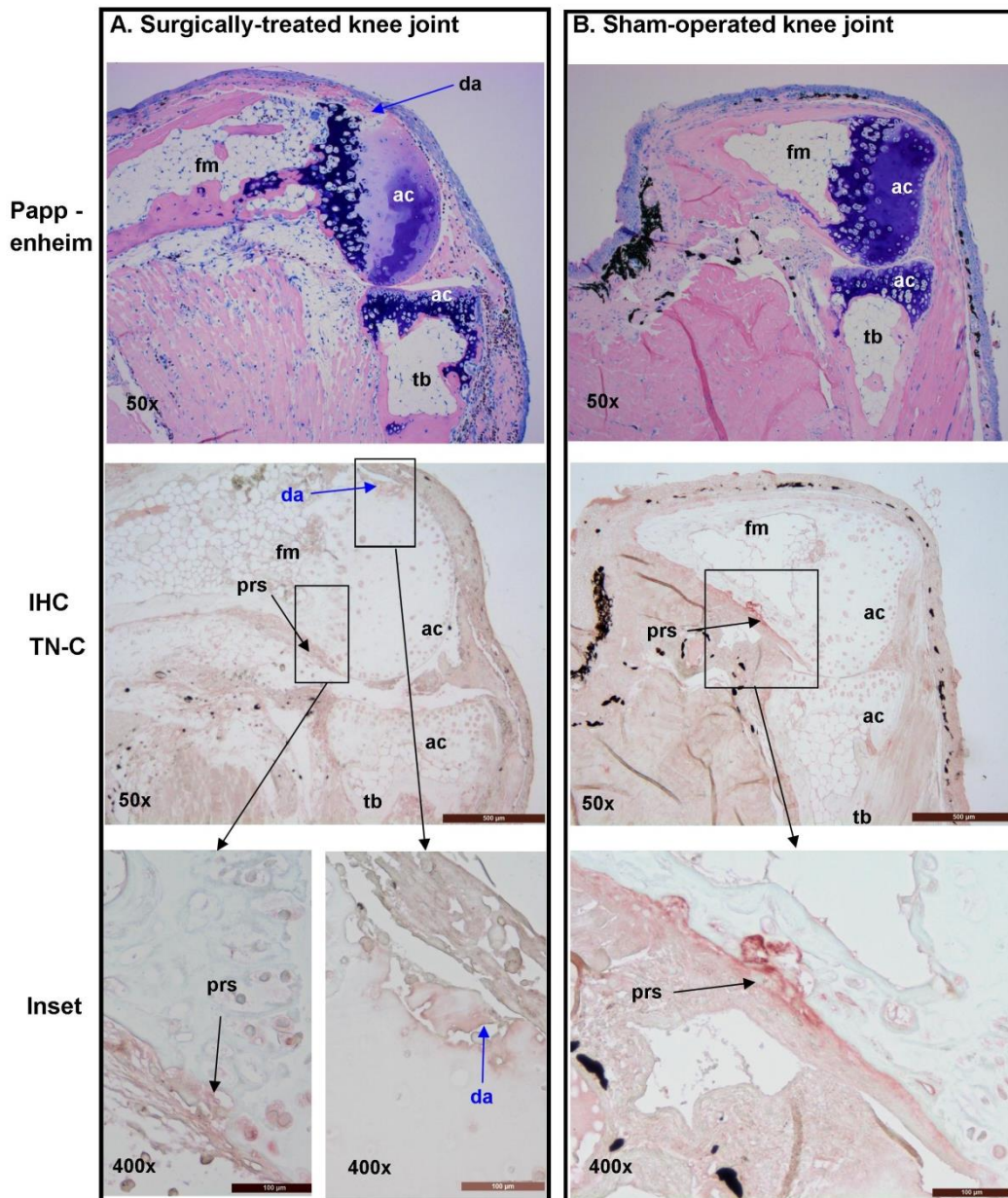


Figure 28: **TN-C expression and physiological appearance of a newt knee joint 10 days after (A) surgery and (B) sham surgery treatment. (A), (B) Pappenheim staining.** Due to its proteoglycan content, articular cartilage was stained blue. Original magnification x 50. **(A), (B) IHC against TN-C.** A 5-µm 10 day post surgery or sham operated newt knee joint section was incubated with 10 µg/ml anti-human TN-C. The reactivity of the antibody (red signal) was detected at the defect area (blue arrow) and along the periosteum (black arrows). Original magnification x 50. The inset shows the situation in more detail (original magnification x 400). **Depicted here are images from a representative IHC staining / representative IHC stainings.** ac, articular cartilage; fm, femur; tb, tibia; da, defect area; prs, periosteum;



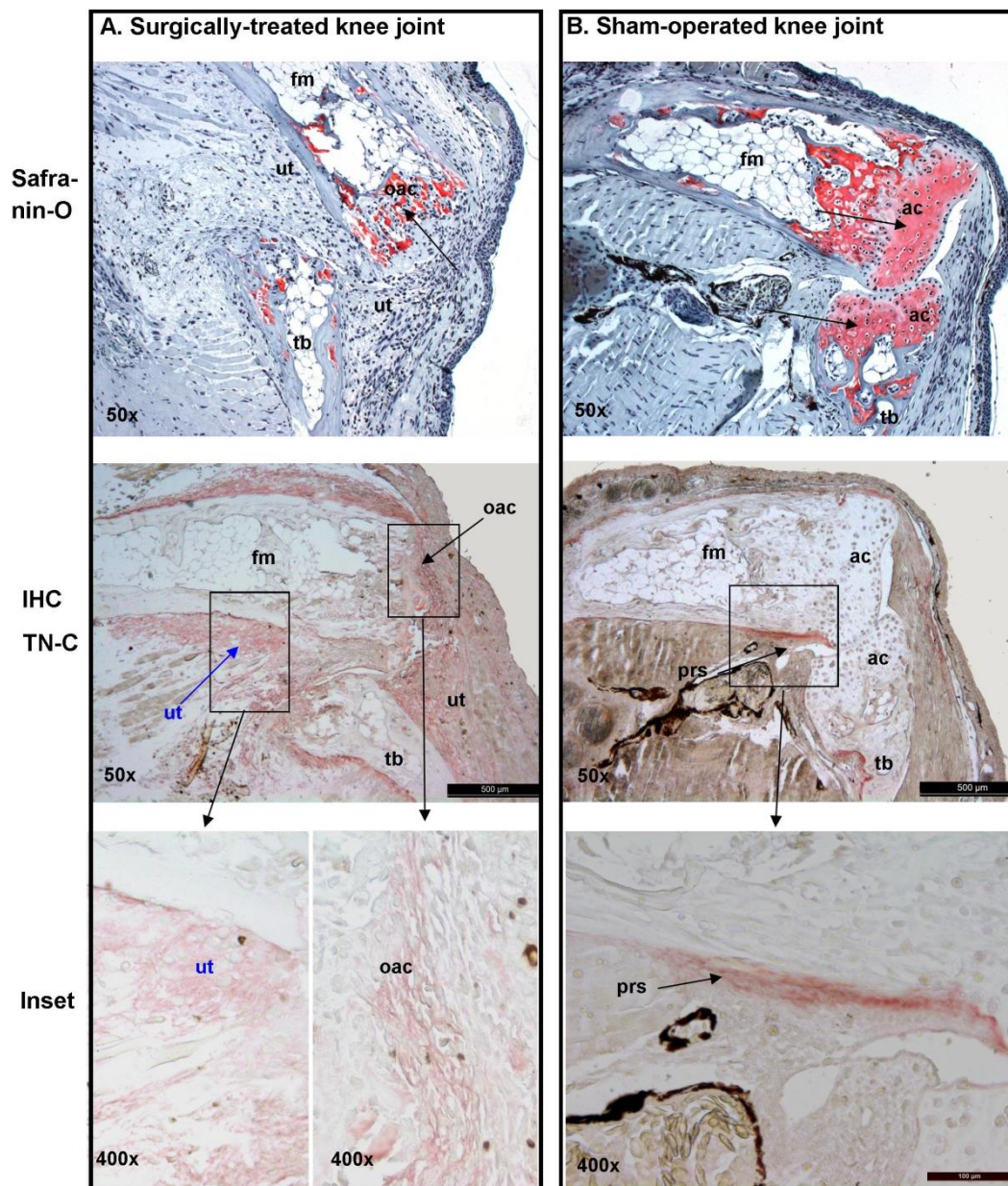


Figure 29: **TN-C expression and physiological appearance of a newt knee joint 20 days after (A) surgery or (B) sham surgery treatment.** (A), (B) **Safranin-O staining.** Due to its proteoglycan content, articular cartilage was stained red. Original magnification x 50. (A), (B) **IHC against TN-C** A 5- $\mu$ m 20-day post-surgery or sham operated newt knee joint section was incubated with 10  $\mu$ g/ml anti-human TN-C. The reactivity of the antibody (red signal) was detected in the undifferentiated tissue (blue arrow) and in the old-defected articular cartilage (black arrow). Original magnification x 50. The inset shows the situation in more detail (original magnification x 400). **Depicted here are images from a representative IHC staining / representative IHC stainings.** ac, articular cartilage; oac, old-defected articular cartilage, fm, femur; tb, tibia; ut, undifferentiated tissue; prs, periosteum.

At day 40 after surgery treatment, the anatomical axis of the treated knee joint was restored (Figure 30A). The Safranin-O staining of this tissue showed that the old-defected articular cartilage had been repaired. The proteoglycan density of the femoral cartilage increased substantially (black arrow, Figure 30A) and covered all of the femoral cartilage area, whereas in the tibia articular cartilage proteoglycan was detected only at the deep zone of the tibial articular cartilage (blue arrow, Figure 30A). The medial and superficial zones had not yet been covered by proteoglycan. In addition, the corresponding sham operated knee joint was morphologically intact (Figure 30B).

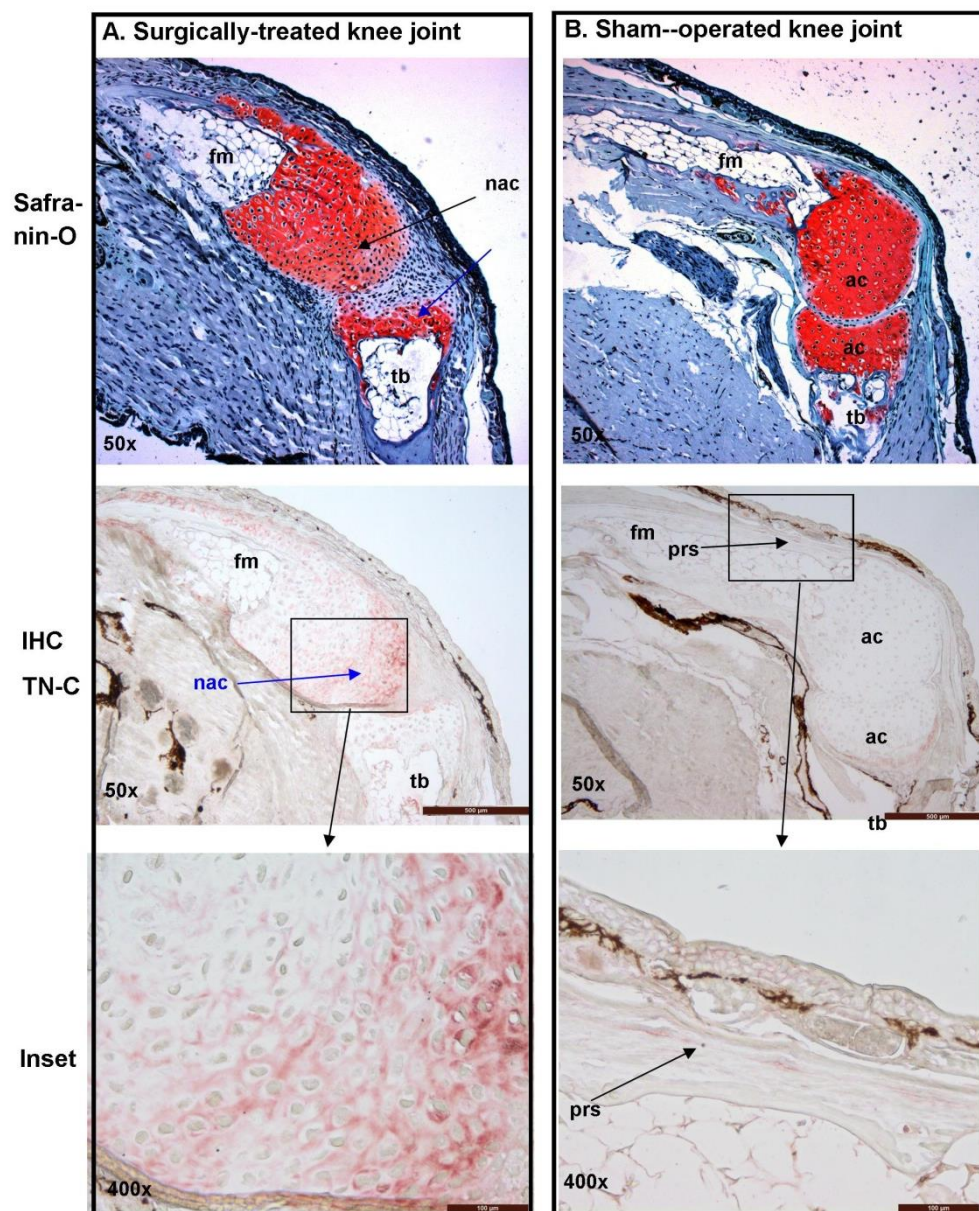


Figure 30: TN-C expression and physiological appearance of a newt knee joint 40 days after (A) surgery or (B) sham surgery treatment. (A), (B) Safranin-O staining. Due to its proteoglycan content, articular cartilage was stained red. Original magnification x 50. (A), (B) IHC against TN-C. A 5- $\mu$ m 40-day post-surgery or sham operated newt knee joint section was incubated with 10  $\mu$ g/ml anti-

human TN-C. The reactivity of the antibody (red signal) was detected in the undifferentiated tissue (blue arrow). Original magnification x 50. The inset shows the situation in more detail (original magnification x 400). **Depicted here are images from a representative IHC staining / representative IHC stainings.** ac, articular cartilage; oac, old-defected articular cartilage, fm, femur; tb, tibia; ut, undifferentiated tissue; prs, periosteum.

The IHC of the 40-day surgery or sham operated knee joint section revealed that the TN-C localized extracellularly in the newly-formed articular cartilage (arrow, IHC, Figure 30A). Moreover, the IHC of the corresponding control sham operated newt knee joint against TN-C showed localization of TN-C only along the periosteum (arrow, IHC, Figure 30B).

### 4.3 Summary of spatiotemporal TN-C expression of the collagenase and surgery model

Expression of TN-C at the protein level could be demonstrated in all IHC stainings of treated and control knee joint sections of the surgery and collagenase model. The IHC experiments were performed with newt knee joint sections from 2 animals (n=2) of collagenase and 3 animals (n=3) of surgery models. Representative images were already presented previously (Section 4.2). The summary of the spatial expression of TN-C in the regenerating newt knee joint in the surgery model and collagenase model is presented in Table 14:



Table 14: **Summary of TN-C spatial expression from collagenase and surgery model.** For each OA model, locations of TN-C expressions are listed. In the collagenase model, IHC staining was performed with two animals (n=2) and in surgery model, IHC experiments were conducted with three animals (n=3). T, treated knee joint; C, control knee joint; coll, collagenase; 1/2, TN-C was detected in the respected tissue in one from two animals; 2/2, TN-C was detected in the respected tissue in all two animals; 1/3, TN-C was detected in the respected tissue in one from three animals; 2/3, TN-C was detected in the respected tissue in two from three animals; 3/3, TN-C was detected in the respected tissue in all three animals.

	Perioste- um	Trabecular bone	Undifferenti- ated tissue	Newly-formed articular cartilage	Old-defected articular cartilage
T coll day 10	2/2				
C coll day 10	2/2				
T coll day 20	2/2		2/2		
C coll day 20	2/2				
T coll day 40	2/2		1/2	1/2	
C coll day 40	2/2				
T surgery day 10	3/3	1/3			2/3
C surgery day 10	3/3	1/3			
T surgery day 20	3/3	1/3	3/3		3/3
C surgery day 20	3/3	1/3			
T surgery day 40	3/3			3/3	
C surgery day 40	3/3				

## 4.4 Evaluation of TN-C contribution to the regenerative process

TN-C was shown to be involved during knee joint regeneration. In order to investigate whether the participation of TN-C was essential in this process, gene expression knockdown experiments were performed. In order to conduct this experiment, a newt cell population, which expressed constitutively abundant TN-C, was selected.

### 4.4.1 TN-C expression levels in different newt cell populations

To analyze the mRNA expression level of TN-C, total RNA from different newt chondrocyte populations (2, 4, and 5 months), newt myotubes (A1), and newt blastemal cells (B1H1) was isolated. Afterwards, cDNA was synthesized by reverse transcription reaction from equal RNA concentrations. Thereafter, real-time PCR was performed with the cDNA to obtain the TN-C expression relative to ribosomal protein S21 ( $\Delta Ct$ ) (Figure 31). TN-C expression levels varied among the cell populations tested. The highest expression was in the 5-month-old newt chondrocytes, followed by the 4-month-old newt chondrocytes, and the A1 cells, afterwards the 2-month-old newt chondrocytes, and finally the B1H1. Based on the abundant constitutive TN-C expression in 5 months old primary newt chondrocytes, these cells were selected for TN-C knockdown *in vitro* using esiRNA.

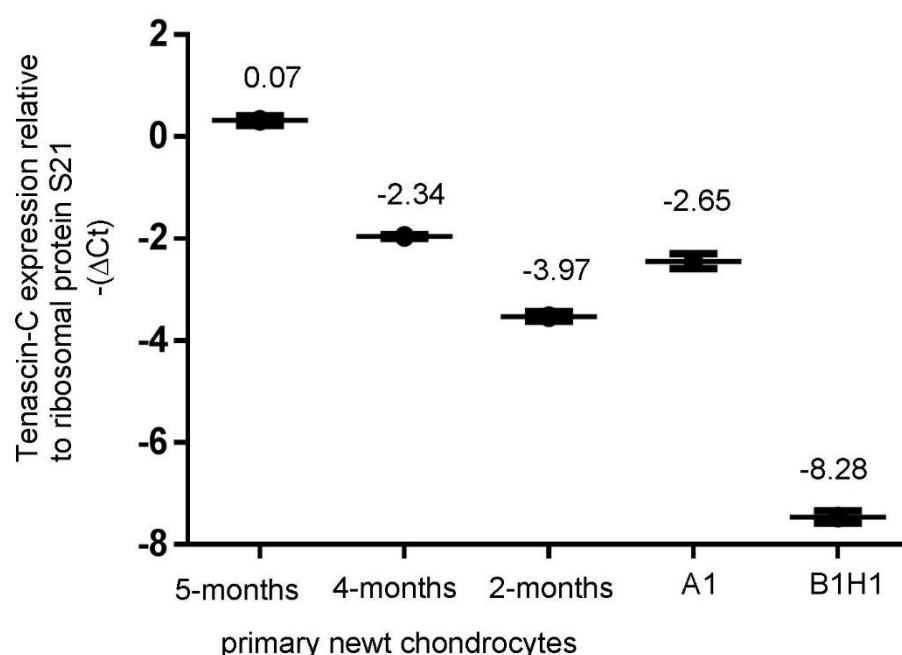


Figure 31: **Relative quantification of TN-C in different newt chondrocyte populations, newt A1 cells, and newt B1H1 cells.** Relative quantification of TN-C expression in different primary newt chondrocyte populations (5-, 4- and 2-months), newt myotube cells (A1) and newt blastema cells (B1H1) was performed using real-time PCR. The presented values are the average of  $-\Delta Ct$  and the standard deviation.

#### 4.4.2 TN-C knockdown in primary newt chondrocytes

After producing TN-C esiRNA and *lacZ* esiRNA, they were introduced into primary newt chondrocytes using the human chondrocyte nucleofector kit (Amaxa, Lonza). In order to confirm the reliability of the knockdown experiment, the nucleofection was performed two times. All of the two experiments showed that the self-made esiRNA was able to silence the expression of TN-C in newt chondrocytes. 48 hr after the first nucleofection experiment, TN-C expression was reduced to 0.55-fold or 45% ( $p < 0.01$ ) in the TN-C esiRNA nucleofected cells in comparison to the control (Figure 32). The second experiment even exhibited a stronger gene silencing than the first. The gene expression from the TN-C esiRNA nucleofected cells was reduced to 0.29-fold or 71% ( $p < 0.01$ ) in comparison to the control (Figure 33).

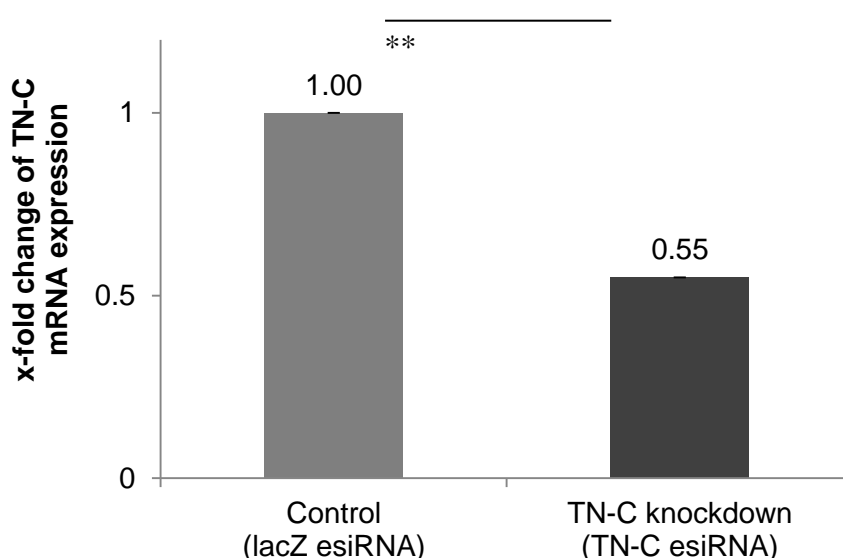


Figure 32: **First experiment of TN-C knockdown in primary newt chondrocytes.** TN-C expression was reduced to 0.55-fold or 45% reduction ( $p < 0.01$ ) in TN-C esiRNA nucleofected newt primary chondrocytes in comparison to *lacZ* esiRNA nucleofected cells. The presented values are the average of x-fold changes and the standard deviation.

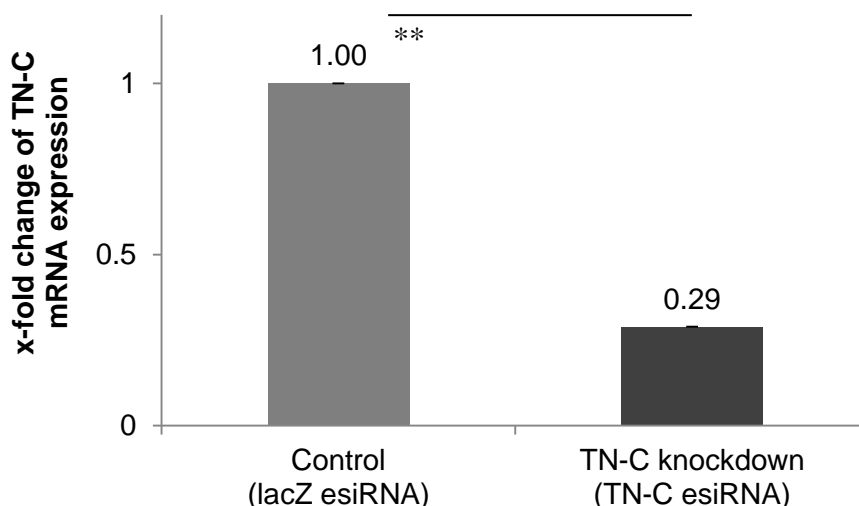


Figure 33: **Second experiment of TN-C knockdown in primary newt chondrocytes.** TN-C expression was reduced to 0.29-fold or 71% reduction ( $p < 0.01$ ) in TN-C esiRNA nucleofected newt primary chondrocyte in comparison to *lacZ* esiRNA nucleofected cells. The presented values are the average of x-fold changes and the standard deviation.

#### 4.4.3 Effect of TN-C knockdown on adhesion and motility of the primary newt chondrocytes

In order to evaluate the effect of the TN-C knockdown in the primary newt chondrocytes to their adhesion capacity, 48 hr after esiRNA introduction into the primary newt chondrocytes, adhesion assay was performed. The result of the quantification experiment showed that TN-C knockdown newt chondrocytes appeared to have reduced capacity to attach to the bottom surface of the cell culture plate (545 adherent cells) as compared to the control (634 adherent cells) (see Figure 34). But the reduction was not statistically significant ( $p = 0.133$ ).

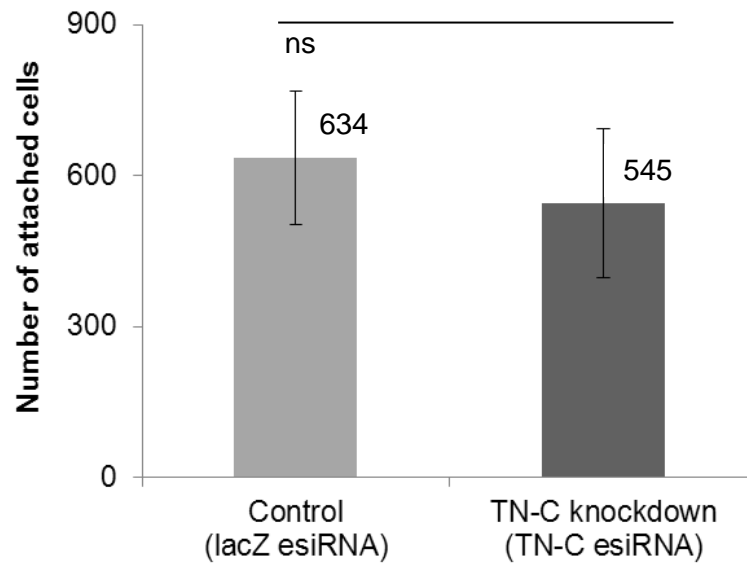


Figure 34: **The effect of TN-C knockdown to the adhesive capacity of the primary newt chondrocytes 48 hr after esiRNA nucleofection.** The capacity of TN-C knockdown chondrocytes to adhere on the bottom of the cell culture appeared to be lower than the control cells, but the reduction was not statistically significant ( $p=0.133$ ). The presented values are the average number of adherent TN-C knockdown and control newt chondrocytes with the standard deviation.

The effect of TN-C knockdown on the migratory capacity of the primary newt chondrocytes were analyzed using scrape motility assay. The result of this experiment showed that the migratory capacity of the TN-C knockdown cells was lower than the control at 12 hr incubation time. However, at the later time points, the number of migrated TN-C knockdown cells was higher than the control (Figure 35). Taken together, the difference of the migrated cell numbers was not statistically significant ( $p>0.1$ ).

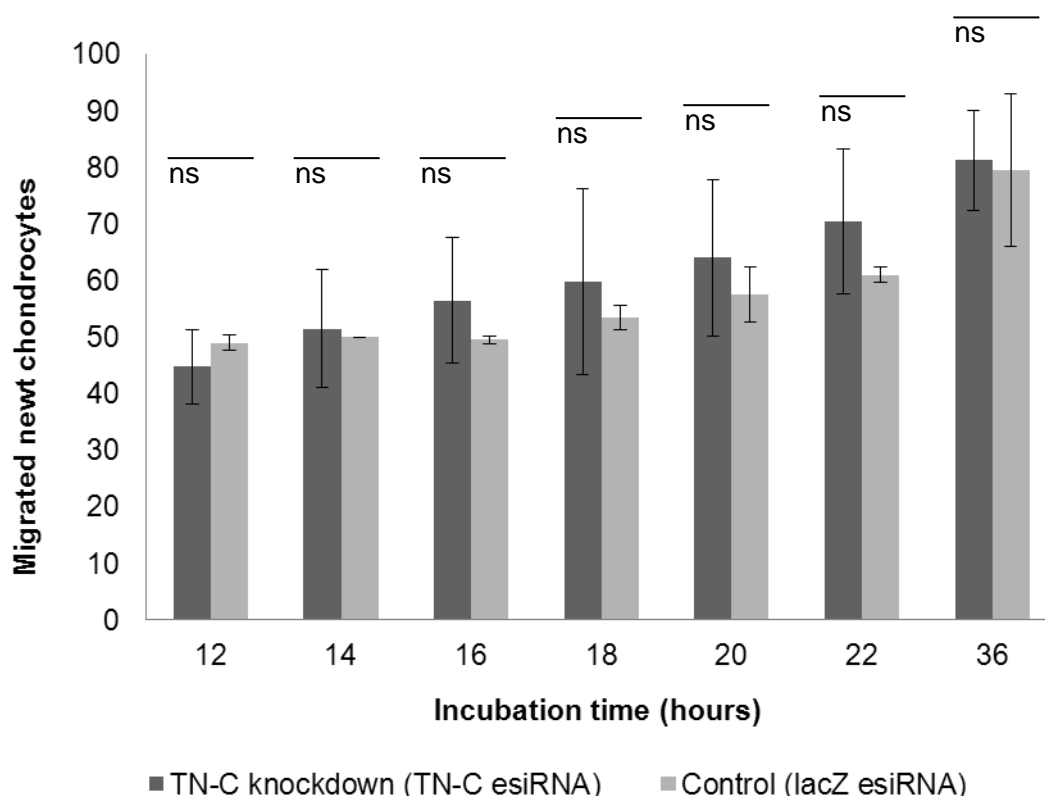


Figure 35: **The effect of TN-C knockdown in the motility capacity of the primary newt chondrocytes.** The number of the migrated TN-C knockdown newt chondrocytes appeared to be lower than the control at 12 hr incubation time. However, at the later time points, the number of the migrated TN-C knockdown cells was higher than the respective control. Taken together, the difference of the number was not statistically significant ( $p > 0.1$ ). The presented values are the number of migrated cell and their standard deviations.

#### 4.4.4 Effect of TN-C knockdown on expression level of SPARC and DCN

SPARC and DCN are matricellular proteins which are known to be involved in the knee joint regeneration process. In order to evaluate the effect of TN-C knockdown at the mRNA expression level of SPARC and DCN, a relative quantification ( $\Delta\Delta C_t$ ) of these genes was calculated with the TN-C and *lacZ* esiRNA nucleofected cells at 48 hr after treatment using real-time PCR. The result of the quantification showed that TN-C knockdown did not affect SPARC (Figure 36) and DCN (Figure 37) expression.

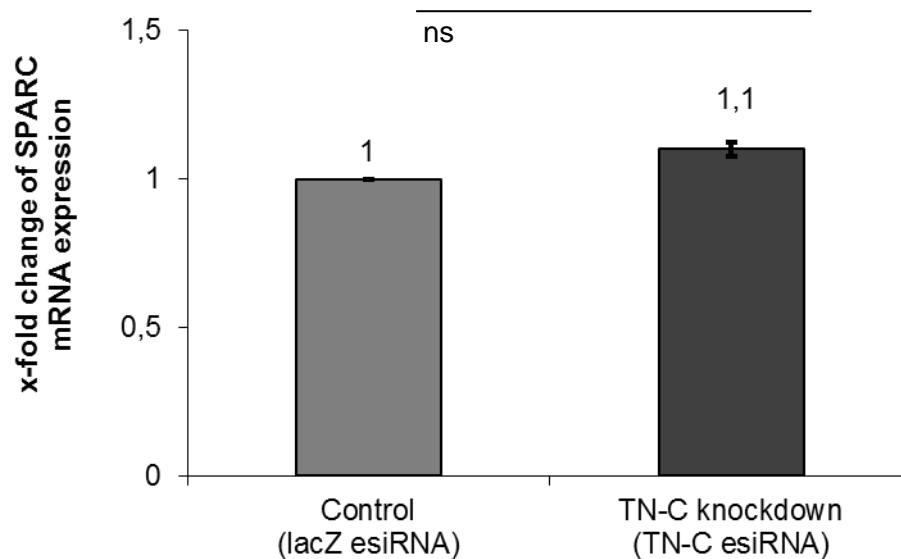


Figure 36: **SPARC expression in TN-C-knockdown primary newt chondrocytes.** Primary newt chondrocytes were nucleofected with 20 pmole of TN-C esiRNA and *lacZ* esiRNA (control). Using real-time PCR, x-fold change of SPARC mRNA expression was calculated using relative quantification ( $\Delta\Delta C_t$ ). SPARC expression was not altered in TN-C esiRNA nucleofected cells in comparison to *lacZ* esiRNA nucleofected cells. The presented values are the average of x-fold and the standard deviation.

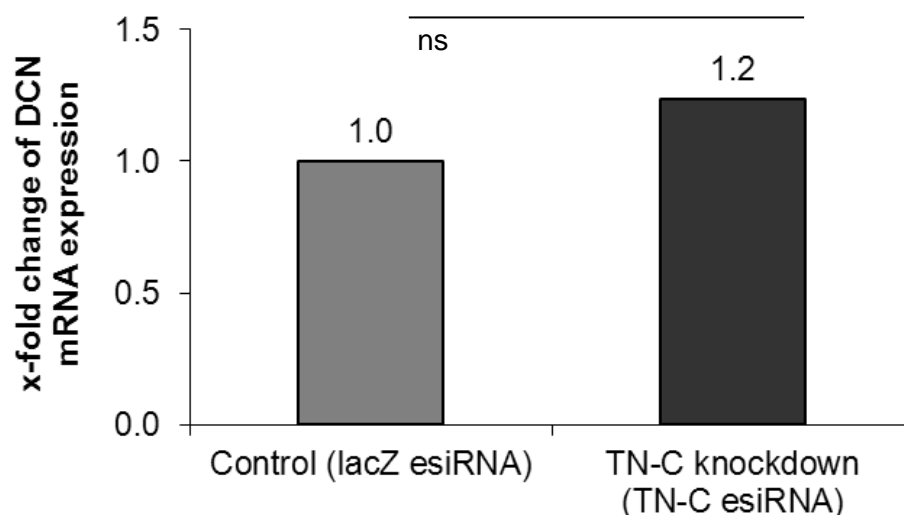


Figure 37: **DCN expression in TN-C knockdown primary newt chondrocytes.** Primary newt chondrocytes were nucleofected with 20 pmole of TN-C esiRNA and *lacZ* esiRNA (control). Using real-time PCR, x-fold change of DCN mRNA expression was calculated using relative quantification ( $\Delta\Delta C_t$ ). DCN expression was not altered in the TN-C esiRNA nucleofected cells in comparison to *lacZ* esiRNA nucleofected cells. The presented values are the average of x-fold changes and the standard deviation.

## **4.5 Expression of SPARC during newt knee joint regeneration**

SPARC is expressed during remodelling and repair in different tissues (e.g. muscle and bones) and some investigators suggested its function in regeneration (Jorgensen et al., 2009). Based on the results from microarray and real-time PCR analysis, SPARC was found to be upregulated in regenerating newt knee joint. Therefore, the expression pattern of this protein was investigated with IHC. Before applying this experiment in the newt tissue, establishment of a reliable IHC protocol was performed.

### **4.5.1 Optimization of newt non-specific SPARC antibody in human RA bone tissue**

There was no newt-specific SPARC antibody commercially available. Therefore, a polyclonal SPARC antibody, which was specific for mouse and human tissue, was selected for the IHC study. Subsequently, a preliminary protocol optimization was performed with human RA bone tissue, before applying this antibody in IHC of newt knee joint sections.

In the human tissue, there was a remodeling zone, where new bone was formed in the cartilage. It was characterized by pink color after staining with H&E (Figure 38A). Osteoblasts were found in the remodeling zone (green arrow, Figure 38B), and in the later process of bone remodeling, some of the cells were embedded into bone matrix and turned into osteocytes (blue arrow, Figure 38B). Osteoblasts are known to express SPARC, therefore the optimization was performed in this tissue.

Establishment of the IHC protocol using the chosen antibody was successful. SPARC expression was detected in the remodeling zone (Figure 38C, D), and specifically along the osteoid layer wherein osteoblasts were located (black arrow, Figure 38D).

In addition, a background signal, which is usually derived from non-specific binding of Fc receptor of the antibody, was absent, and there was no immunoreactivity of isotype control antibody in the remodeling zone (Figure 38E).



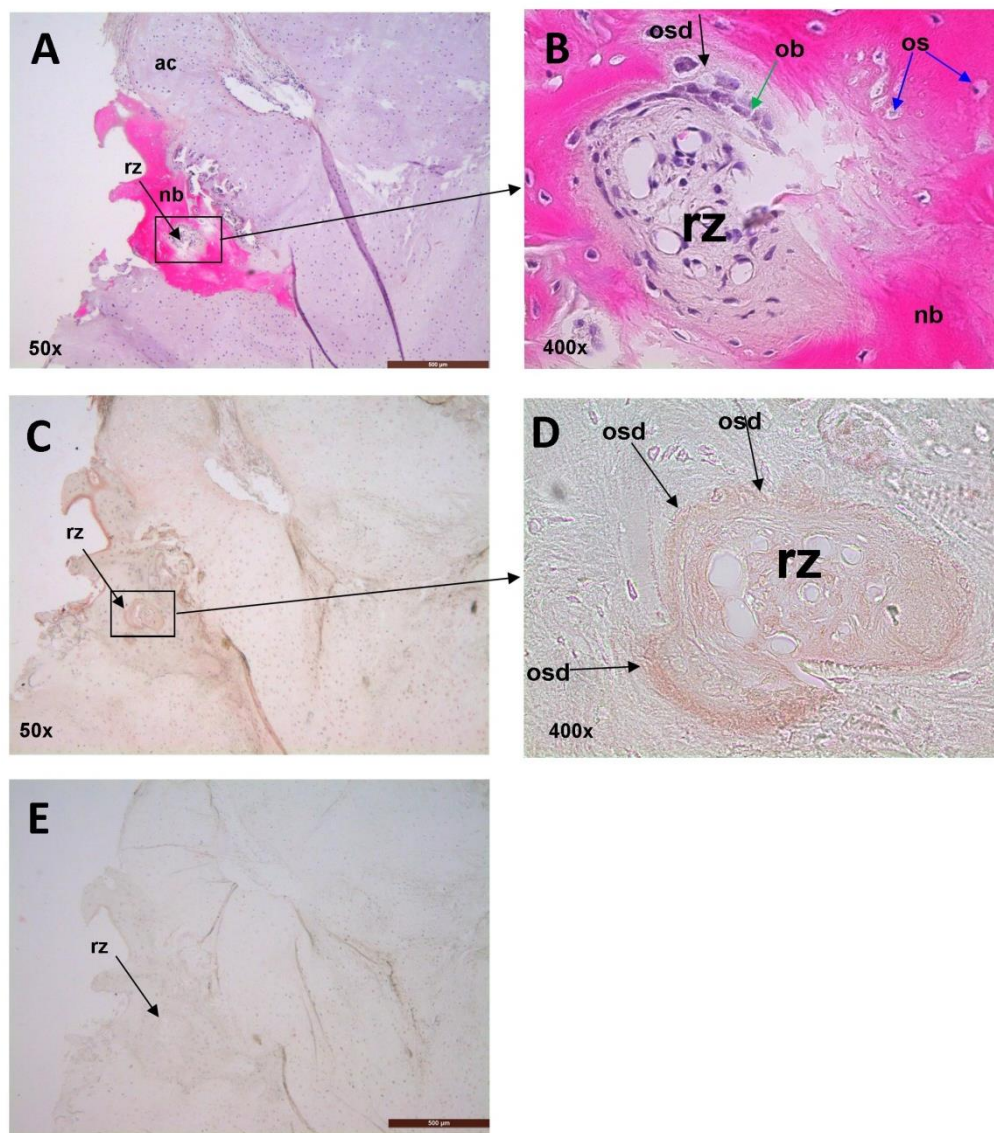


Figure 38: **SPARC expression in human bone from an RA patient. (A) H&E staining of a RA bone tissue section for tissue overview.** Original magnification x 50. **(B) The inset shows a remodeling zone surrounded by newly-formed bone.** Original magnification x 400. **IHC staining against (C), (D), SPARC and against (E) goat polyclonal IgG (isotype control).** A decalcified RA bone tissue section (5-µm) was incubated with 4 µg/ml anti-SPARC or goat polyclonal IgG. A specific cellular SPARC expression was detected in the remodeling zone after staining with AEC substrate (arrow, C). Strong SPARC expression was detected along the osteoid layer in the remodeling zone (arrow, D). **(D) The inset shows the situation in more detail (original magnification x 400).** **(E) Isotype control showed no signal.** Original magnification x 50. rz, remodeling zone; ac, articular cartilage; nb, newly-formed bone; os, osteocytes; osd, osteoid; ob, osteoblasts.

#### 4.5.2 SPARC expression in healthy newt knee joint

The IHC for SPARC in healthy newt knee joints revealed its localizations in different areas (arrows, Figure 39A, B, C). This matricellular protein could be observed on the subchondral bone (green arrow, Figure 39B), the calcified zone of the articular cartilage

(black arrow, Figure 39B), the deep zone of articular cartilage (blue arrow, Figure 39B), the osteocytes in the bone (black arrow, Figure 39C), the blood vessel (yellow arrow, Figure 39C), and on the skin (red arrow, Figure 39C).

Background signal, which is usually derived from non-specific binding of Fc receptor of the antibody, was absent. The isotype control of the SPARC antibody (goat polyclonal IgG) did not show immunoreactivity in the remodeling zone (Figure 39D).

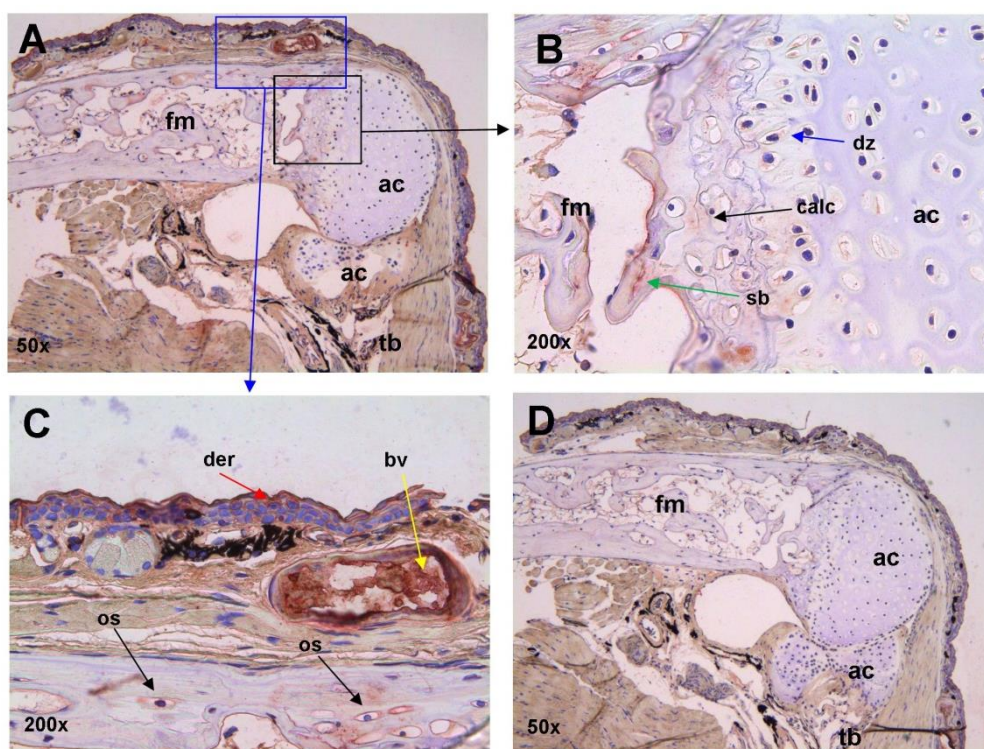


Figure 39: **SPARC expression in a healthy newt knee joint. IHC staining against (A), (B), (C) SPARC and against (D) goat polyclonal IgG (isotype control).** A 5- $\mu$ m newt knee joint section was incubated with 4  $\mu$ g/ml anti-SPARC or goat polyclonal IgG. Then, the section was counterstained with hematoxylin. The SPARC expression was detected on the subchondral bone (green arrow, B), on the calcified zone of the articular cartilage (black arrow, B), on the deep zone of articular cartilage (blue arrow, B), on the osteocytes in the bone (black arrow, C), on the blood vessel (yellow arrow, B), and on the skin (red arrow, B). **(A)** IHC staining against SPARC with original magnification x 50. **(B), (C)** The inset shows the situation in more detail. Original magnification x 200. **(D)** There was no signal in the isotype control. Original magnification x 50. ac, articular cartilage; bv, blood vessel; der, dermis; dz, deep zone of articular cartilage; calc, calcified zone of articular cartilage; fm, femur; sb, subchondral bone; tb, tibia.

### **4.5.3 SPARC expression in regenerating newt knee joints after 20 and 40 days of surgery treatment**

After optimization of IHC protocol for usage in newt tissue, the antibody was then used to evaluate the spatiotemporal expression of SPARC during knee joint regeneration after surgically-induced OA. Twenty-days after surgical removal of articular cartilage in the newt knee joint, SPARC was differentially upregulated in the cDNA microarray and was confirmed with real-time PCR (see Section 4.1.1.2). However, 40 days after surgery treatment, SPARC expression was not dysregulated on microarray and real-time PCR. In order to observe the spatiotemporal expression of SPARC during knee joint regeneration, IHC experiments using samples 20 and 40 days after surgery treatment were performed.

In the 20-day post-surgical knee joint tissue, SPARC expression was restricted to the osteocytes (arrow, Figure 40A, B; blue arrow, Figure 40C, D), on the skeletal muscle (black arrow, Figure 40C, D), along the periosteum (red arrow, Figure 40C, D).

Interestingly, in the control newt knee joint undergoing sham surgery, SPARC could not be detected in the osteocytes (Figure 40E, F, G) and the skeletal muscle (Figure 40G). Instead, it was found to be expressed along the endosteum (black arrow, Figure 40F) and the periosteum (red arrow, Figure 40F).

In contrast to the strong expression of SPARC in the femur and the tibia, no SPARC signal was observed at the defected articular cartilage, and the undifferentiated tissue (data not shown).

At day 40 after treatment, SPARC expression in the surgically-treated (Figure 41A, B) and in the sham operated knee joint (Figure 41C, D) was restricted only to the skin.



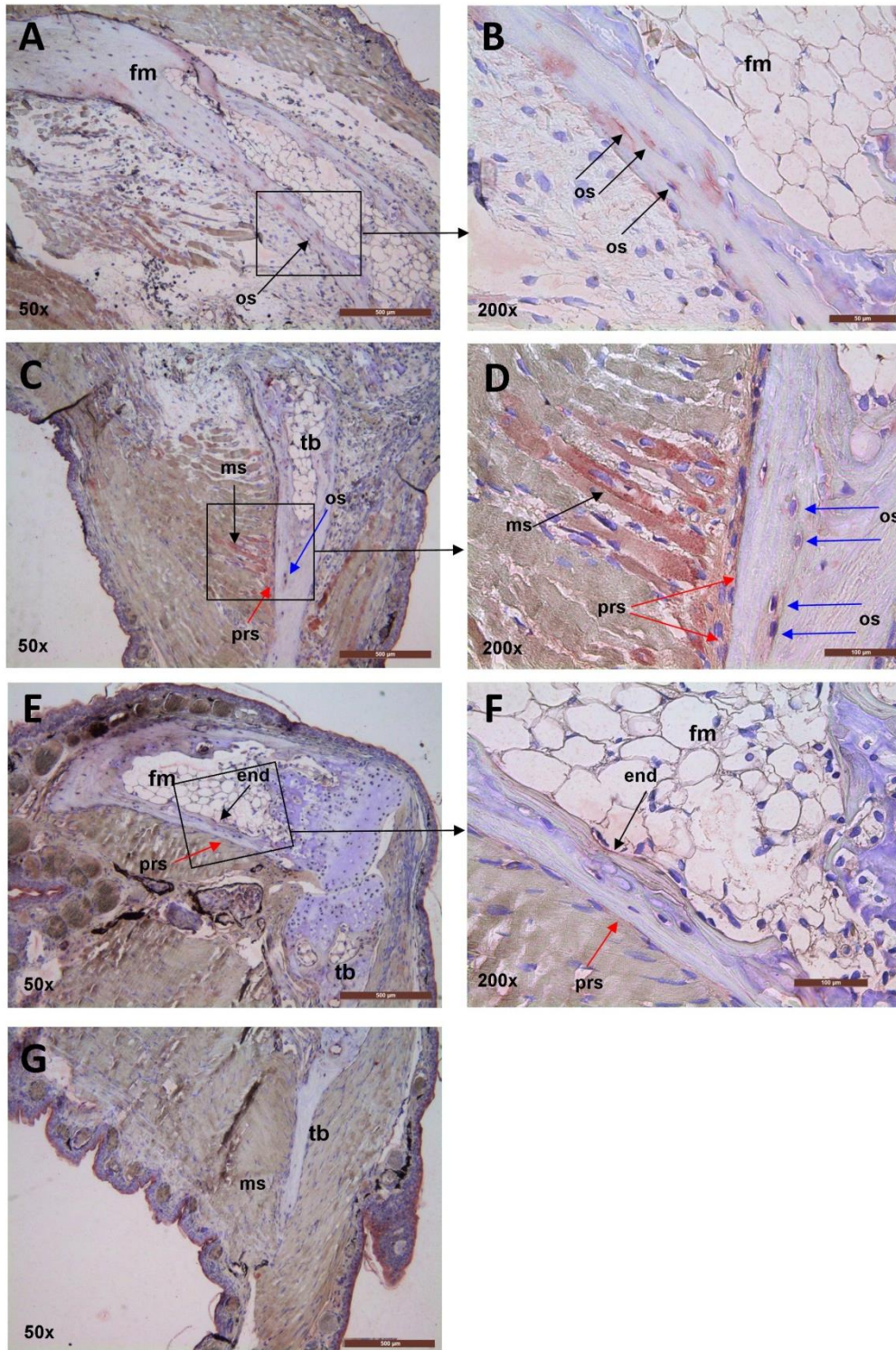


Figure 40: **SPARC** expression in the 20-day post-surgically-induced knee joint defect. IHC staining of (A), (B), (C), (D) surgically-treated and (E), (F), (G) sham operated knee joint against **SPARC**. A 5-µm 20-day post-surgically-induced knee joint defect or sham operated newt knee joint section was incubated with 4 µg/ml anti-SPARC or goat polyclonal IgG. Then, the section was counterstained with hematoxylin. SPARC expression was detected in the osteocytes (black arrow, A, B; blue arrow, C, D), on the muscle (black arrow, C, D), along the periosteum (red arrow, C, D, E, F), and along the endosteum (black arrow, E, F). (A), (C), (E), (G) IHC staining against SPARC with

original magnification x 50. **(B), (D), (F)** The inset shows the situation in more detail. Original magnification x 200. fm, femur; os; osteocytes; tb, tibia; ms, muscle; prs, periosteum; end, endosteum.

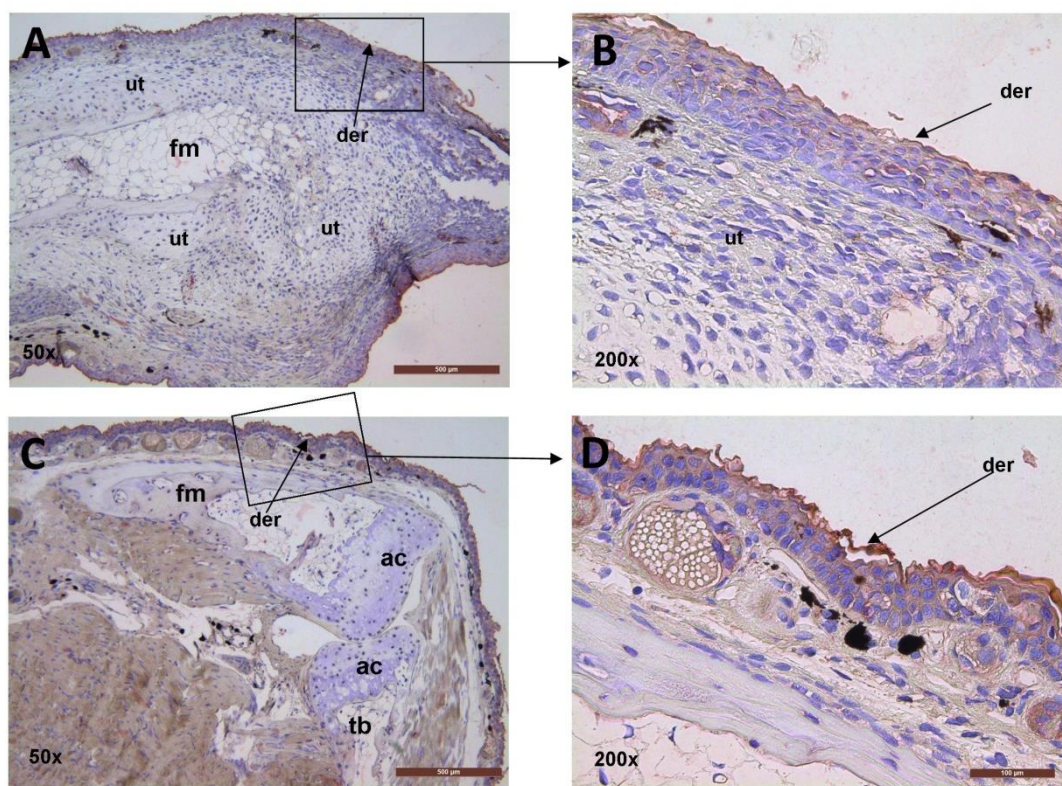


Figure 41: **SPARC expression in a 40-day post-surgical inflicted newt knee joint defect. IHC staining for SPARC in (A), (B) surgically-treated and (C), (D) sham operated newt knee joints.** A 5- $\mu$ m 40-day post-surgical inflicted knee joint defect or post-sham operated newt knee joint section was incubated with 4  $\mu$ g/ml anti-SPARC or goat polyclonal IgG. Thereafter, the section was counterstained with hematoxylin. The SPARC reactivity was observed only on the skin (arrow, A, B, C, D). **(B), (D)** The inset shows the situation in more detail (original magnification x 200). ac, articular cartilage; der, dermis; fm, femur; tb, tibia; ut, undifferentiated tissue.



## 5 Discussion

The remarkable ability of newt to regenerate many kinds of tissues is well known. An example of this is the knee joint restoration after collagenase- (Geyer et al., 2010) and surgically-induced knee joint damage (unpublished work from Dr. Matthias Geyer and Prof. Dr. med. Robert Dinser<sup>‡</sup>). The animals restore the defect until the formation of a functional knee joint is achieved. In contrast, mammals such as human and mice cannot repair this defect, and finally the affected knee joint will lose its function. In order to elucidate why and how the newt can perform this kind of regeneration, expression analysis using cDNA microarray was performed that showed several genes which were upregulated during this repair process (unpublished work from Dr. med. Matthias Geyer, Prof. Dr. med. Robert M. Dinser<sup>‡</sup>, and Dr. rer. nat. Thilo Borchardt). The involvement of these genes in the newt knee joint regeneration suggested potential molecular mechanisms, which have been addressed in this doctoral thesis.

### 5.1 Molecular mechanisms during knee joint regeneration in newt

The suggested mechanisms, which might play an important role in the newt knee joint regeneration process, were the innate immune system, the vitamin A pathway, and matricellular proteins.

#### 5.1.1 Role of the innate immune system during knee joint regeneration in the newt

Evidence for the involvement of the innate immune system during regeneration in newt was shown by participation of the complement system during newt limb and eye repair (Kimura et al., 2003). They showed that complement component 3 was expressed in the blastema during newt limb regeneration and in the cornea and iris during newt eye repair. In addition, they showed that other members of the complement family such as complement component 5 were also expressed in the wound epithelium, regenerating newt limb, as well as lens vesicles and cornea during newt eye repair (Kimura et al., 2003).

In this doctoral work, CFB (another member of complement system of the alternative pathway) appeared to be involved in knee joint regeneration, because its expression was strongly upregulated at every time point during knee joint regeneration. Real-time PCR quantification of CFB confirmed the results of the cDNA microarray.

TLRs and their adaptor molecule MyD88 are known to be involved in lung repair processes after acute injury (Jiang et al., 2005). Activation of these molecules is essential to prevent apoptosis of airway epithelial and endothelial cells in the injured lung (Jiang et al., 2005).

In our experiments, participation of TLRs in knee joint regeneration was demonstrated by upregulation of TLR2 and TLR5 at day 10 of the surgery model. At later time points, their expression decreased. In contrast, in the collagenase model, TLRs appeared not to be involved. However, the strong upregulation of these receptors at this time point was not supported by the activation of MyD88 (see Section 9.4). This finding contrasts the fact that MyD88 is usually mediating TLR2 and TLR5 activation in the innate immune system (Akira et al., 2001). In order to confirm the expression of these receptors at day 10 in the surgery model, spatial expression analysis was tried to be established with IHC. Nevertheless, the effort was hampered by unspecificity of the antibody when it was applied on newt tissues. An alternative method like ISH was not conducted because of some technical problems which are discussed in Section 5.2.3.

### **5.1.2 Role of the retinoic acid pathway during knee joint regeneration in the newt**

Upregulation of RARRES1 in the cDNA microarray indicated an involvement of the retinoic acid pathway during knee joint regeneration. This molecule was selected as candidate gene in this doctoral study because it has the capability to inhibit growth of human colon tumor cells (Wu et al., 2011). Tumor growth and tissue repair are related events, since tumor development is known to be an uncontrolled repair process (Haddow, 1972; Schäfer and Werner, 2008). In addition, the relation between tumor growth and tissue repair can be observed from similarity of the gene expression profile between the renal regeneration / repair process and the development of renal cell carcinoma (Riss et al., 2006). Of note, almost 77% of genes expressed during both events are regulated concordantly.

In this doctoral study, relative quantification of RARRES1 did not confirm the upregulation of this protein in the cDNA microarray. The real-time PCR analysis demonstrated that the upregulation of RARRES1 was only present in one pool of the animals (see Figure 22). Therefore, it was difficult to deduct, whether this gene is really deregulated during the repair process.

Nonetheless, the idea to investigate the role of the vitamin A and its derivatives in knee joint regeneration was continued by selecting vitamin A receptors including RAR $\alpha$ ,  $\beta$ , and  $\delta$ . They were selected because they play an important role in newt limb regeneration (Brockes, 1997). They mediate proximodistal respecification of blastema cells. Another ability of the cells is to locate their position during blastema formation (Brockes, 1997). However, our real-time PCR experiments showed that RARs and RXR were not dysregulated (see Table 15). Therefore, it can be concluded that the role of RARs and RXR during knee joint healing in newt was not prominent.

### 5.1.3 Role of matricellular proteins during knee joint regeneration in newt

Matricellular proteins are matrix proteins with an important function as regulator of cell behavior such as cell adhesion, proliferation, and apoptosis (Bornstein and Sage, 2002). They are also known to be associated with regeneration (Midwood et al., 2004). Dynamic expressions of these proteins (e.g. TN-C, hyaluronic acid, and fibronectin) direct cellular behaviors and provide instructive cues in newt muscle cell repair (Calve et al., 2010).

In this doctoral work, matricellular proteins such as DCN, POSTN, TN-C, and SPARC were differentially upregulated in newt knee joint regeneration in the collagenase- and surgically-treated animal groups. Their activation suggested a possible involvement in this process.

The role of DCN in newt's tissue regeneration is still unknown. From other animal models, including humans, this matricellular protein has been supposed to promote cartilage healing (Grogan et al., 2014). In this process, DCN induces COL2A1 expression, a gene which is responsible for the production of the alpha 1(II) chain of type II collagen that is found primarily in articular cartilage (Grogan et al., 2014).

Likewise, the role of POSTN in tissue regeneration of the newt is also still unknown. In other animal models such as rats, involvement of this protein is reported during the regeneration of bone tissue. In rat, POSTN promotes healing of bone fractures by recruiting preosteoblastic cells into provisional callus (a temporary tissue which is formed after bone fracture). The tissue is then removed after bone repair is completed (Kojima et al., 2007; Nakazawa et al., 2004).

The role of SPARC in newt tissue regeneration is also unknown. In mammals, this matricellular protein is involved in bone repair after injury (Alford and Hankenson, 2006). cDNA microarray and subsequent real-time PCR quantification indicated that SPARC is involved in knee joint regeneration, and in order to analyze the expression of this matricellular protein during the repair process, IHC against SPARC was performed.

#### 5.1.3.1 SPARC expression: Analysis, predicted function, and role in knee joint regeneration

Due to its properties as the most abundant non-collagenous protein in the bone (Termine et al., 1981), SPARC localization was predominantly located in this tissue and also in cartilage of a healthy newt knee joint.

##### 5.1.3.1.1 SPARC expression in healthy knee joint

In the bone of the healthy newt knee joints, SPARC was expressed in osteocytes. There is no scientific report which had already showed SPARC in osteocytes of newt's bone. In other animals including humans, Metsäranta and coworkers showed that expression of



SPARC is involved in development processes. They found that this matricellular protein is expressed in the osteocytes of calvarial bone matrix of the developing fetus (Metsäranta et al., 1989). This was also supported by other findings that showed only young (mineralizing) osteocytes expressing SPARC while aged, quiescent osteocytes did not synthesize this protein (Jundt et al., 1987). Therefore, SPARC expression in the osteocytes of healthy adult newt bone might be a false positive IHC result, because this tissue was not in the development phase. For future studies, in order to confirm this assumption, detection of quiescent osteocyte markers such as sclerostin should be conducted (Robling et al., 2008). If the SPARC expressing osteocytes express sclerostin, then the SPARC signal in the healthy adult newt bone is a false positive result. In order to investigate, whether the SPARC expressing osteocytes are part of mineralizing tissue, detection of dentin matrix protein-1 (DMP-1) can be performed, as dentin matrix protein-1 (DMP1) is a protein which is synthesized only by actively mineralizing osteocytes (Bonewald, 2011).

In articular cartilage of healthy newt knee joints, SPARC expression was found in the calcified, and the deep zone of articular cartilage. Until this time, there is no scientific report about appearance of this protein in this tissue in the newt model system. In other animals including humans, the expression of SPARC in these locations was already described. Nakamura and coworkers observed that in the deep zone of healthy articular cartilage, SPARC expression could be detected weakly in some chondrocytes (Nakamura et al., 1996). However, the appearance of this protein in healthy cartilage seems to be controversial. Some recent publications showed that detectable SPARC expression can only be observed in hypertrophic chondrocytes in cartilage undergoing calcification (Ikeda-Isogai et al., 2012) or degenerative disease such as OA (Goyal et al., 2010). Therefore, in order to evaluate the validity of IHC staining, which showed SPARC expression in the healthy articular cartilage, confirmatory experiments should be performed in the future, e.g. detection of collagen type X to elucidate whether SPARC expressing cells are hypertrophic chondrocytes (Kielty et al., 1985).

In addition to bone and cartilage, SPARC was also expressed in the skin, and in blood vessels. Scientific reports that describe the expression of SPARC in these tissues in newt have not yet been published. Investigation of SPARC expression in human skin was performed by Hunzelmann and coworkers. By using northern blotting, ISH, and IHC, they noticed that in healthy skin, this matricellular protein was present in the vascular cells and basement membranes of the dermis. They suggested that this protein might play a role in differentiation and maintenance of healthy human skin (Hunzelmann et al., 1998).

#### **5.1.3.1.2 SPARC expression in the regenerating newt knee joint**

Spatial SPARC expression in regenerating and control newt knee joint beginning at day 20 in surgery model was different when compared with the healthy tissue. In the treated

knee joint, SPARC could be detected in the osteocytes, the skeletal muscle and the periosteum. SPARC expression in the skeletal muscle was most prominent during knee joint regeneration at day 20 of the surgery model. Based on investigations in other animal models, it could be shown that the expression of SPARC in the skeletal muscle was important for regeneration. Studies in the human fetuses showed that SPARC is detected only in differentiating tissues such as developing myofibers; afterwards, the expression level decreases when the tissue becomes differentiated (Jorgensen et al., 2009). SPARC was therefore suggested to induce regeneration and muscle reformation (Jorgensen et al., 2009). However, in the knee joint regeneration, abundant SPARC expression in the skeletal muscle did not relate to any regeneration/repair process. The location of SPARC was quite distant from the damaged area (see Section 4.5.3). In order to confirm this result, it would have been very helpful, if there had been other IHC experiments with regenerating knee joint from other animals at the same time point (day 20 of the surgery model). Unfortunately, the experiment could not be performed, due to tissue limitation.

Abundant SPARC appearance was also found in the periosteum, which was located adjacent to the SPARC expressing skeletal muscle (see Section 4.5.3). This matricellular protein is synthesized by osteoblasts, which are located in the inner surface of the periosteum (Gilbert, 2000; Baldini et al., 2008). SPARC supports the mineralization process during new bone formation. It provides healthy bone for tissue maintenance. Increased expression of this protein is observed only during fracture repair (Delany et al., 2003). It could not be completely clarified, why the expression of this protein was elevated in the treated tissue in comparison to the control knee joint. Thus, in order to confirm this result, some additional IHC stainings should be performed with different animals in the same time point in the future. In this doctoral work, the experiment could only be performed once due to tissue limitation.

These additional experiments should also evaluate the difference in spatial expression pattern between the healthy and the control knee joint. For example, the presence of SPARC in the articular cartilage and the blood vessel, which emerged only in the healthy tissue but were absent in the control knee joint. Here, both tissues should have similar SPARC expression pattern.

As conclusion, SPARC could be observed in different areas in a healthy newt knee joint. Although, its expression is required for the normal maintenance of the tissue, in the regenerating knee joint, based on the SPARC IHC staining, the appearance of this matricellular protein seemed not to correlate with the repair process. Therefore, additional experiments are required to confirm this assumption in the future, which is also important to elucidate the different of spatial expression pattern between healthy and control knee joint.

In contrast to SPARC with its expression in the regenerating tissue not correlating with regeneration processes, the presence of TN-C during the healing process seemed to be important and one of the most interesting findings of this doctoral work.

### **5.1.3.2 TN-C and its role in knee joint regeneration in newt**

As early as in 1990, a research group led by Roy A. Tassava pioneered the work that detected TN-C in the blastema tissue during newt limb regeneration. They noticed that appearance of this matricellular protein was related to the repair, because it appeared only in the tissue related to this process such as wound epithelium, blastema, and condensing mesenchyme. After these tissues were completely differentiated and finally became a functional limb, the TN-C expression disappeared (Onda et al., 1990). One year later, another group showed that this matricellular protein was present during scar free skin wound healing. By using IHC staining, they found that TN-C expression in this process was involved in the regeneration process (Donaldson et al., 1991). Until today, there are some more reports that show the involvement of this protein during regeneration processes in different newt's tissues such as in the caudal spinal cord (Caubit et al., 1994), neural retina (Mitashov et al., 1995), skeletal muscle (Calve et al., 2010), and recently in the heart (Mercer et al., 2012)

Although numerous investigations in different tissues have already been performed, none of them showed that this protein is actually required for regeneration, for example by conducting knockdown experiments. Therefore in this doctoral work, the investigation was not only performed on the mRNA (real-time PCR) and protein expression level (IHC), an additional functional analysis (knockdown) was also conducted. The results of this experiment are discussed in more detail in Section 5.1.3.2.3.

In the knee joint regeneration, the expression pattern of TN-C was also associated with the repair process. It emerged in the defect area, undifferentiated tissue, and newly-formed articular cartilage. Interestingly, the expression pattern seemed to be unique in each OA model.

#### **5.1.3.2.1 TN-C expression in both OA models**

On day 10 after treatment, there was already a spatial expression difference between both OA models. In the surgery model, from three analyzed animals, TN-C was present in the periosteum, while expression in the defected articular cartilage was present only in two of them. Meanwhile, in the collagenase model, from two analyzed animals, TN-C localization was found only in the periosteum but not in the articular cartilage (see Section 4.3).

It can therefore be speculated that the TN-C expression in the defected articular cartilage in the surgery model was a part of the inflammatory response because this

matricellular protein is highly upregulated in the damaged articular cartilage and synovial joint (Chevalier et al., 1994). The appearance of TN-C in these tissues can induce inflammatory factors such as IL-1 and IL-6 (Patel et al., 2011). In inflammatory arthritis including RA, TN-C is also abundantly expressed in the cartilage and synovium (a thin layer of membrane that lines joint capsule and secretes synovial fluid) (Salter, 1993). The elevated amounts of this protein in the RA joints are thought to induce joint inflammation through interaction of the fibrinogen-like globe domain of TN-C with TLR4 (Midwood et al., 2009). The appearance of TN-C during inflammation can also be found in humans during injury such as skin wounds (Betz et al., 1993), and asbestos-induced lung damage (Kaarteenaho-Wiik et al., 2000). TN-C does not only induce inflammatory responses but is also activated by infections such as in the lung of tuberculosis patients (Kaarteenaho-Wiik et al., 2000).

It is interesting to analyze why TN-C expression was not present in the damaged articular cartilage in the newt knee joint of collagenase model. It can be speculated that the absence of this matricellular protein probably correlates with the inflammatory response. In the previous report, it was shown that the severity of the disease peaked on day 6 after intra-articular injection of collagenase (Geyer et al., 2010). At this time point, the treated knee joint was already inflamed, the joint was swelling (Geyer et al., 2010). Thus, the inflammatory process had already been initiated. Consequently, TN-C should also be upregulated. However, it could not be clarified, whether the inflammatory response still exists on day 10 after treatment. In fact, each treated animal developed an unique disease kinetic. Therefore, in order to investigate whether inflammatory response exists in the treated newt knee joint of collagenase model, expression of TLR4 and IL-1 can be analyzed in the future using IHC or ISH.

In addition, the absence of TN-C expression in the articular cartilage of newt knees joint in the collagenase model can also be related to the absence of structural damage of the treated articular cartilage. Veje and coworkers investigated TN-C expression in femoral head cartilages of human knee OA. They demonstrated that TN-C accumulated only in the areas displaying structural damage such as fibrillated cartilage (Veje et al., 2003).

At day 20 after treatment, the difference of the TN-C expression pattern still emerged between both models. In all of the three surgically-treated animals, traces of TN-C were present in the defected cartilage remnant and additionally in the undifferentiated tissue. In contrast, in the collagenase model, TN-C signals were absent in the damaged articular cartilage of two analyzed animals. This protein emerged only in the undifferentiated tissue.

The TN-C appearance in the defected articular cartilage in the knee joint of all animals in the surgery model was still hypothesized as part of the inflammatory response. These ideas are derived from our previous study, which demonstrated that the clinical score that assesses the severity of the disease, was still high at day 20 after intra-articular

collagenase injection (Geyer et al., 2010). Logically, this inflammatory response also occurred in the damaged articular cartilage of animals in the collagenase model. TN-C should therefore be expressed in the damaged articular cartilage in the knee joint at 20 days post collagenase-treated animals. This assumption should also be confirmed by investigating the expression of relevant inflammatory factors such as IL-1 and IL-6 as previously mentioned.

Expression of TN-C in the defected articular cartilage in the knee joints of surgically-treated animals can also be elicited by tissue remodeling and repair process. The appearance and the involvement of TN-C during epimorphic regeneration including limb regeneration after amputation (Onda et al., 1990; Onda et al., 1991) and muscle regeneration (Goetsch et al., 2003; Calve et al., 2010) is already known. The proposed function of this matricellular protein is providing an extracellular environment, which promotes regeneration process (Calve et al., 2010).

Interestingly, TN-C did not appear in the articular cartilage in the knee joint 20 days after collagenase treatment, although there is a visible repair process in this tissue. The Safranin-O staining demonstrated an increase of proteoglycan content in the damaged articular cartilage 20 days after treatment in comparison with 10 days after treatment. This assumption that there was a repair process in the articular cartilage should be confirmed, because the differences of the proteoglycan content in the articular cartilage in knee joints between the 20 and the 10 day collagenase treated animals can also be caused by the variability of disease severity. For future studies, in order to investigate, whether repair processes occur in the articular cartilage of collagenase treated animals, the chondrocyte proliferation activity can be investigated using IHC staining against proliferating cell nuclear antigen (PCNA) (Nakoshi et al., 2010).

20 days after artificially induced knee joint damage, all of the animals in the surgically- and collagenase-treated groups demonstrated an undifferentiated tissue formation in their treated newt knee joint. The formation of this tissue structure was also found in the previous knee joint regeneration after intra-articular collagenase injection study (Geyer et al., 2010). In this doctoral study, it could be shown that TN-C was expressed abundantly in this tissue. During limb regeneration after amputation, this matricellular protein appears abundantly in blastema (Onda et al., 1990; Onda et al., 1991), and in dedifferentiated mononucleate progenitor cells in muscle regeneration (Calve et al., 2010). TN-C expression in the damaged skeletal muscle can promote fragmentation and cell cycle reentry which result in formation of mononucleate progenitor cells (Calve et al., 2010). Thus, the function of TN-C in the undifferentiated tissue is promoting synthesis of the undifferentiated tissue.

On the last analysis time point (on day 40 after treatment), the newly formed articular cartilage was detected in the regenerating knee joint of all three analyzed animals in the

surgery model. The newly formed tissue was assembled in the area where the defected articular cartilage was located at day 20 after treatment. Interestingly, TN-C could be detected abundantly in this newly formed articular cartilage. The function of this matricellular protein in chondrogenesis is already known (Mackie et al., 1987). TN-C promotes differentiation of mesenchymal progenitor cells into mature cartilage (Mackie et al., 1987). The capability of TN-C to promote chondrogenesis is mediated by its FN-III domain (Murphy et al., 2000). This domain modulates adhesion behavior of the mesenchymal cells and induces proliferation of these cells (Murphy et al., 2000).

In the corresponding collagenase model, the newly formed cartilage emerged only in one of the two analyzed animals. This tissue was formed adjacent to the damaged cartilage. TN-C was expressed in this newly formed tissue. However, this matricellular protein was absent in the old-damaged articular cartilage. The selective appearance of TN-C indicated that the repair activity of cartilage occurred only in the newly formed cartilage but is absent in the old-defected tissue. This idea is derived from the fact that TN-C promotes chondrocyte differentiation and proliferation in the developing and OA articular cartilage (Mackie et al., 1987; Nakoshi et al., 2010). For future studies, this assumption should be confirmed by performing experiments such as IHC against proliferating cell nuclear antigen (PCNA) to prove whether the TN-C expressing chondrocytes really exhibit proliferation activity. In order to confirm chondrocyte differentiation, IHC against SOX9 can also be performed. SOX9 is a transcription factor of the sex-determining region Y-chromosome family, which is required for differentiation of different cell lineages including chondrocytes (de Crombrughe et al., 2000; Hattori et al., 2008). Because SOX9 can also induce differentiation of several cell lineages, identification of its target gene including Col2a1 should be performed to show chondrocyte differentiation in the newly formed and old-defected articular cartilage (Hattori et al., 2008).

Another animal at day 40 of the collagenase model showed undifferentiated tissue formation and the TN-C expression co-localized in this tissue (data not shown). It can be speculated that this treated animal had a different disease kinetic than the other animals. i.e. the regeneration process of this animal seemed to proceed longer than others

In addition, in the spatial expression study, there was also TN-C expression in tissue not related to the regeneration process. For example, the appearance of TN-C in the bone marrow in the treated and control knee joint of day 10 and 20 after surgery treatment. There are two possible explanations for this observation: First, it can be speculated that TN-C localization in the bone marrow is derived from adipocytes, which have recently been reported to express this matricellular protein (Catalan et al., 2012). Adipocytes can originate from bone marrow mesenchymal stem cells, which in mammals such as human and mice, exist abundantly in the bone marrow (Beresford et al., 1992; Nuttall et al., 2014). Unfortunately, there is no report in newt which shows that adipocytes can originate from

bone marrow. Second, the other speculation proposes that the TN-C expression in bone marrow is required for hematopoiesis (formation of blood cellular component) (Nakamura-Ishizu et al., 2012). Probably, due to surgery treatment, in the surgically-treated and sham-operated knee joint, the animals lost some blood that had to be replaced by hematopoiesis. This activity could also have triggered TN-C expression in the bone marrow of both tissues.

As conclusion, based on the assumption that the appearance of TN-C is important in regeneration, its selective expression in certain tissues implicates different regeneration mechanisms in both OA models. In order to confirm this assumption, additional experiments need to be performed (e.g. investigating the animals at later time points).

#### **5.1.3.2.2 Relative quantification versus spatiotemporal analysis of TN-C expression during newt knee joint regeneration**

Real-time PCR quantification of TN-C in both OA models showed that this matricellular protein was highly expressed at 10 days after treatment and then the expression level was reduced dramatically at 40 days after treatment (except pool animals B in collagenase model) (see Figure 16). This fact seemed to contradict the result of spatiotemporal analysis by IHC which showed that there was no abundant TN-C expression in both models at 10 days after treatment. The expression of this matricellular protein was only restricted to the small defect area and periosteum in the surgically-treated animals and only along the periosteum in the collagenase-treated newts. The contradiction was also evident at 40 days after treatment. At this time point, IHC results showed that TN-C expression was increased dramatically especially in the articular cartilage.

There were some possibilities why the result of IHC analysis of TN-C expression did not correlate with the real-time PCR quantification of this matricellular protein. One possibility could be the difference of the transcription and the translation kinetic of this gene during knee joint regeneration. Another possibility is the variability of the TN-C expression in each treated animals due to variability of disease severity (see Section 5.2.2)

The assumption that TN-C played important roles in the knee healing process needed also to be validated. Thus, functional analyses were carried out by performing a TN-C knockdown in newt-derived cells / cell lines.

#### **5.1.3.2.3 Establishing expression knockdown in newt and its implication in functional analysis of TN-C**

Establishing gene expression knockdown in the newt is a challenging effort due to the limited number of sequence informations and commercial reagents for performing knockdown experiments such as siRNA. So far, only three sets of experiments are reported. Recently, Witman and coworkers were able to knockdown the expression of micro RNA 128 (miR-128) using antagomirs (Witman et al., 2013). An antagomir is a chemically engineered

oligonucleotide which binds specifically to microRNA and elicits its degradation (Krützfeld et al., 2005). Two other groups employed morpholino oligonucleotides (MOs) to knockdown genes including pax-6 (Madhavan et al., 2006) and the oocyte-type linker histone B gene (Maki et al., 2010) in the newt. MO-mediated expression knockdown is a widely used tool to conduct functional analysis of a gene of interest *in vivo* (Summerton et al., 1997). MOs employ oligomers which are composed of approximately 25 morpholine bases that are specifically targeted via complementary base pairing to the transcription product of interest. The binding of the MOs with the mRNA creates a steric hindrance for proper transcript processing and translation, therefore, protein synthesis is not possible (Summerton et al., 1997; Summerton et al., 1999).

In this doctoral work, the MO technique was not selected for the TN-C expression knockdown, due to the limited financial budget and the unavailability of animals. As alternative, *in vitro* knockdown was performed using esiRNA-mediated gene silencing. A TN-C-specific esiRNA was produced based on nucleotide information from newt-omics, a database which was recently established at the Max Planck Institute in Bad Nauheim (Bruckskotten et al., 2012). Two separate knockdown experiments were performed in primary newt chondrocytes and the expression of the gene reduced to 0.45-fold in the first experiment and to 0.29-fold in the second.

In this doctoral work, a direct examination (*in vivo*) of the influence of TN-C knockdown in the restoration of the tissue could not be performed. Some representative experiments, which were able to be performed *in vitro*, were selected to investigate the effect of the TN-C gene silencing on cellular properties of newt chondrocytes. The adhesion assay was one of the selected methods to address this objective, since an earlier studies showed that this experimental setting can be used for investigating and measuring the repair capacity of a tissue (Park et al., 2009). Park and coworkers investigated the role of TLR4 blockade in the induction of tooth regeneration. They evaluated the adhesive capacity of odontoblasts (a cell type which covers the outer space of dental pulp that produces the dentin of a tooth) to collagen-coated plate. They found an increase of the adhesive capacity of the cells that correlated with tooth regenerative capacity (Park et al., 2009). In newt regeneration, Brookes showed that cellular properties such as adhesion, was required during tissue patterning (a process which controls the position and organization of cells in a certain tissue) of differentiated blastema cells during newt appendage regeneration (Brookes, 1997).

In this study, it was hypothesized that the silencing of TN-C in newt chondrocytes resulted in a reduction of the regenerative capacity, reflected by the reduction of the adherence ability of the TN-C knockdown newt chondrocytes (Ishida et al., 1997). In order to evaluate the hypothesis, an adhesion assay was performed, and the result of the experiments showed that the TN-C expression knockdown decreased the adhesion of the



cells to the surface of cell culture plates. However, the difference between TN-C knockdown cells and control cells was not statistically significant.

The second study, which was performed to evaluate the effect of TN-C knockdown in newt chondrocytes, was the scrape motility assay. Some experiments demonstrated the relation between cell motility and tissue repair (Lallier et al., 2007; Zhang et al., 2013). Lallier and coworkers investigated periodontal regeneration, and they found that the process relied on migratory capacity of distinct cell types including gingival fibroblasts (a cell type found in periodontal connective tissue). They conducted a motility assay to prove their hypothesis (Lallier et al., 2007). Studies in a human gastric wound healing *in vitro* model showed that also the migrative capacity of gastric epithelial cells increased during the wound healing process (Zhang et al., 2013). In the newt model system, there is also evidence of a correlation between migratory capacity in tissue repair process during skeletal muscle regeneration (Calve et al., 2012). Calve and coworkers observed that TN-C-coated substrates enhanced the migration of primary newt muscle cells (myoblasts) in comparison to control substrates (laminin- and matrigel- coated substrates). This event correlated with myoblast fragmentation, which is a process of muscle dedifferentiation for subsequent epimorphic regeneration to restore the damage tissue (Calve et al., 2012).

Based on the same principle, in this doctoral work, it was hypothesized that the silencing of TN-C expression of newt chondrocytes may cause a reduction of the regenerative capacity of the cells, which was shown in the reduction of their migratory capacity. In order to answer this hypothesis, the motility of newt chondrocytes was investigated using the scrape assay. The result of the study exhibited that in the majority of analyzed incubation times, TN-C knockdown cells exhibited a tendency of higher migratory capacity than the control, but altogether, it was not statistically significant.

In addition, we hypothesized that in supporting regeneration, TN-C probably collaborated with or influenced other ECM components, that were also upregulated in this process e.g. SPARC and DCN. This idea derived from the newt muscle regeneration model. Here, TN-C collaborates with other ECM components such as fibronectin and hyaluronic acid. They form a dynamic expression pattern during skeletal muscle regeneration (Calve et al., 2010). The result of relative quantification of SPARC and DCN mRNA from the TN-C knockdown in primary newt chondrocytes showed that the silencing of TN-C transcript did not affect the expression of these matricellular proteins.

## 5.2 Analysis of obstacles during investigation of knee joint regeneration in newt

Although newts are an attractive animal model to study molecular mechanisms, which underlie knee joint regeneration, some obstacles, which significantly influenced the results in this thesis, emerged during this doctoral study.

### 5.2.1 The newt as animal model for research

The red-spotted newts are not endemic in Europe. Their natural habitat is located at the east coast of North America. Therefore, this research project relied substantially on the delivery from the country of origin. In one case, there was a delay in the shipping of the animals due to regulations that limit amphibian shipping to Europe from the USA in order to prevent spreading of infectious disease (unpublished report from Prof. Dr. med. Robert Dinser<sup>‡</sup> and Dr. rer. nat. Thilo Borchardt). The consequence of this regulation was a limited number of animals available for the investigations. As solution to resolve this problem, recently the Max Planck Institute in Bad Nauheim has been trying to breed and culture the animal in an artificial environment. Until now, the effort has not yet been fully successful, due to the long breeding (6 months) and culturing time (3 years) until the animals become adult and ready to be used for research purposes. As a comparison, other animal model for studying regeneration, the axolotl (*Ambystoma mexicanum*), can be easily bred in animal housing facilities. They have also a relatively short period to reach sexual maturity (approximately 5 months; Clare, 2012).

The low number of animals as planned which could be used in this study increased the variability of the results. This is reflected by the expression analysis of the newt knee joint tissue after artificially induced damage as discussed below.

### 5.2.2 Problem during transcriptome analysis

The initial transcriptome analysis using cDNA microarray was performed in order to reveal molecular mechanisms underlying knee joint regeneration. Several experimental approaches were conducted in order to achieve the best possible result. Nevertheless, some problems arose due to limitations of the utilized technique. One of the weaknesses was the moderate sensitivity of the cDNA microarray (Hicks et al., 2008). It was reflected in the susceptibility of the assay against background interferences. The hybridization signal from fluorescently labeled cDNA samples of day 20 of the collagenase model was disturbed by a high background signal. Therefore, only hybridization signals from two investigated time points (days 10 and 40) could be used (unpublished report from Prof. Dr. med. Robert M. Dinser<sup>‡</sup>, Dr. med. Matthias Geyer, and Dr. rer. nat. Thilo Borchardt). In contrast to the

collagenase technique, the surgery method produced a reliable hybridization signal (data not shown). The background level was low and did not disturb the specific signal from the deregulated genes.

Validation of deregulation values of the selected genes from the cDNA microarray with real-time PCR was also accompanied by variability. There was a disagreement of deregulation values of some selected genes between pool A and B animals. An obvious example is the deregulation values of DCN at day 10 after collagenase treatment (see Section 4.1.1.4). In this selected example, there was an extreme value difference (pool A, 8.6-fold; pool B, 0.4-fold). In this doctoral work, the exact reason of the discrepancy of the deregulation status and value differences of selected gene expressions between pool A and B could not be fully investigated. A possible explanation could be that each treated animal developed a varying degree of disease severity. Thus, it presumably reflects to the dissimilarity of expression values between both pool animals. These differences between the two animal pools in some genes generated the problematic situation to deduce the importance of these genes during the knee joint restoration process. In order to solve this problem, spatial expression analysis using IHC was performed for some selected genes such as TN-C and SPARC to provide additional information for the role of the selected genes in the repair mechanism.

### **5.2.3 Problem during establishment of spatial expression analysis**

The spatial expression analysis using IHC was also challenged by the lack of cross-reactivity of commercially available primary antibodies to newt-specific proteins. Therefore, tedious investigations of antibodies cross-reactivities were performed before applying them for spatial expression analysis in newt tissues. In this doctoral study, only two antibodies including anti-human TN-C and anti-mouse and –human SPARC were used for spatial expression analysis.

ISH can be used as alternative approach for investigating spatial expression of gene of interest. This technique allows the detection of specific nucleic acid molecules by using a DNA/RNA probe that specifically detects newt-specific gene transcription products in morphologically preserved tissue sections. The probe was synthesized based on nucleotide sequence information from newly-established newt-omics database (Bruckskotten et al., 2012).

During this doctoral work, the protocol to investigate the spatial expression of TN-C using ISH was developed. Unfortunately, the established ISH protocol was only able to detect gene transcripts in newt blastema cryosections (data not shown). ISH of healthy newt knee joint paraffin sections to detect TN-C expression in periosteum was unsuccessful. The reason could be that due to the long preparation time of paraffin-embedded tissue, the

quality and abundance of the mRNA of interest was strongly reduced (Salmon et al., 2012; Shao et al., 2006).

However, it is feasible that ISH can be performed in paraffin preserved tissues in the future. A recent study showed that the integrity of mRNA step can be preserved by using RNAlater/EDTA mixture in decalcification step during establishment of paraffin sections of bone-containing tissue and shorter decalcification time (overnight) (Belluoccio et al., 2013). In this technique, RNAlater (Life Technologies), a proprietary tissue storage reagent, which stabilizes and protects cellular RNA is mixed with EDTA, and this solution is used to decalcify the bone tissue (Belluoccio et al., 2013).

## 6 Summary

Lesions of articular cartilage are still leading to irreversible degenerative joint diseases including osteoarthritis (OA). Aside pain, the disease results in loss of function of the affected joint and severe disability and a substantial reduction of quality of life of the affected patient. The human does not have the endogenous capacity to restore the structure and the function of the osteoarthritic knee joint damage. In contrast, animals such as the red-spotted newt (*Notophthalmus viridescens viridescens*) are able to repair complete organs and tissues including joints after artificial damage by collagenase treatment and surgery. The underlying mechanisms of this regenerative process can be further investigated by cDNA microarray showing distinct genes, which were differentially upregulated in both models for OA.

Based on these results, in this doctoral project, the genes, that were found to be upregulated in the cDNA microarray study and additional genes from the vitamin A pathway, and the innate immune system, both known to be involved in repair processes were selected for real-time PCR analysis to primarily quantify their deregulation status. Here, real-time PCR study confirmed the deregulation of distinct molecules including secreted protein acidic and rich in cysteine (SPARC), periostin (POSTN), decorin (DCN), complement factor B (CFB), tenascin-C (TN-C), toll-like receptor 2 (TLR2), and retinoic acid receptor responder 1 (RARRES1).

Among these selected factors, TN-C was the most interesting one, because the deregulation of this matricellular protein was the most prominent among the other selected candidates.

IHC analysis revealed that the spatial expression of TN-C during the knee joint regeneration process was unique in each OA model. At day 10 and 20 after surgery treatment, TN-C appeared in the defected articular cartilage of the treated knee joints in two of three analyzed animals. In contrast, in the animals of the collagenase model, the TN-C expression was absent in the defected articular cartilage. It supported the idea of a differential initiation of the repair process depending on the type of the damage inflicted. The appearance of this matricellular protein in the defected articular cartilage in the animals of the surgery model can be seen as a part of an inflammatory response during the injury process. At day 20 after treatment, undifferentiated tissue emerged in the regenerating newt knee joint of all analyzed animals. TN-C was expressed abundantly in this tissue, which is a further indication of its involvement in the knee joint regeneration. At day 40 after treatment, all of the three analyzed animals in the surgery model and one animal of the two analyzed animals in the collagenase model demonstrated expression of TN-C in the newly formed articular cartilage. Here, TN-C could promote the formation of this tissue. In the regenerating knee

joint of one analyzed animal in the surgically-treated animals, TN-C appeared only in the newly formed articular cartilage, but it was absent in the old-defected cartilage.

In order to investigate whether the involvement of TN-C was functionally important for the knee joint regeneration process, gene silencing experiments were conducted in newt primary chondrocytes using TN-C esiRNAs *in vitro*, introduced into the primary newt chondrocytes by nucleofection. In two independent experiments, TN-C expression could be reduced to 0.55-fold (45% reduction) and 0.29-fold (71% reduction), the effect of one-time TN-C gene silencing on regenerative capacity of newt chondrocytes with respect to migration and adhesive capacity of these cells did not result in a statistically significant effect. In addition, in order to elucidate the effect of TN-C knockdown on other dysregulated candidate genes including SPARC and DCN, relative quantification of the transcription product of both genes was performed. The result of the measurement demonstrated that TN-C knockdown in newt chondrocytes did not alter the expression levels of these molecules.

SPARC, another prominent candidate gene, which was selected from the cDNA microarray, was present in several tissues in untreated newt legs including osteocytes, articular cartilage, blood vessels and skin. As SPARC is known to be important for the normal function of these tissues, in the regenerating newt knee joint already at day 20 after surgery treatment, this matricellular protein was localized abundantly in distinct areas in the skeletal muscle and periosteum. Of note, this expression was not directly related to the regeneration process since these tissues were not primarily damaged by the surgical treatment.

Similar to the results obtained from the TN-C and SPARC experiments, several other matrix repair associated molecules were found to be upregulated and expressed at different time points during the newt knee joint regeneration process, providing interesting new insights into this fascinating phenomenon. However, the experiments of this doctoral thesis also showed the still existing limitations of an experimental approach in an organism, for which the technical systems still need to be fully established.

## 7 Zusammenfassung

Läsionen des Gelenkknorpels führen zu einer irreversiblen degenerativen Gelenkerkrankung, einschließlich der Osteoarthritis. Die Krankheit verursacht neben Schmerzen einen Funktionsverlust des betroffenen Gelenks, eine schwere Behinderung sowie eine erhebliche Einschränkung der Lebensqualität der betroffenen Patienten. Der menschliche Organismus besitzt keine Möglichkeit, die Struktur und Funktion eines arthrotisch erkrankten Gelenkes selbst wiederherzustellen. Im Gegensatz hierzu besitzen verschiedene Tierarten wie z.B. der rotgetüpfelte Teichmolch (*Notophthalmus viridescens viridescens*), die Fähigkeit verletzte Organe und Gewebe z.T. vollständig zu regenerieren. Nach Verletzung des Gelenkknorpels durch Kollagenase-Injektion und OP sind diese Molche z.B. in der Lage, den Knorpel zu reparieren und die Funktionsfähigkeit des Gelenkes wiederherzustellen.

Die zu Grunde liegenden Mechanismen dieses Regenerationsprozesses wurden primär durch einen cDNA-Microarray untersucht. Es wurden aus diesem verschiedene Gene in beiden OA Modellen als hochreguliert nachgewiesen und im Rahmen dieser Arbeit im Detail untersucht. Basierend auf diesen Ergebnissen wurden die Gene, die in der zuvor durchgeführten cDNA-Microarray-Untersuchung als dysreguliert nachgewiesen wurden, Gene aus dem gelenkaktiven Vitamin A Signalweg sowie dem angeborenen Immunsystem näher untersucht. Die Expression der ausgewählten Kandidatengene wurde mittels Real-time-PCR-Analyse bestätigt und eine Deregulierung von unterschiedlichen Molekülen, einschließlich des secreted protein acidic and rich in cysteine (SPARC), periostin (POSTN), decorin (DCN), complement factor B (CFB), tenascin-C (TN-C), toll-like receptor 2 (TLR2) und retinoic acid receptor responder 1 (RARRES1) auf mRNA Ebene verifiziert werden.

Die immunohistochemische Analyse zeigte, dass die Lokalisation der Expression von TN-C im Kniegelenkregenerationsprozess spezifisch für jedes OA-Modell zeichnete. TN-C war im defekten Knorpel des behandelten Kniegelenks in zwei von drei Tieren am Tag 10 und 20 nach der OP-Behandlung nachweisbar. Im Gegensatz dazu konnte bei den Kollagenase-behandelten Tieren keine TN-C-Expression im defekten Knorpel nachgewiesen werden. Diese Ergebnisse unterstützen die Hypothese, dass unterschiedliche Reparaturvorgänge in Abhängigkeit von der Art der Schädigung ablaufen. Das Erscheinen dieses matrizellulären Proteins im defekten Knorpel der OP behandelten Tiere kann auch im Rahmen einer lokalen Entzündungsreaktion gesehen werden. Am Tag 20 nach der Behandlung war noch undifferenziertes mesenchymales Gewebe in den regenerierenden Molch-Kniegelenken aller untersuchten Tiere histologisch erkennbar. TN-C wurde in diesen noch nicht differenziertem Geweben ausgeprägt exprimiert. Diese Beobachtung deutet ebenfalls daraufhin, dass dieses matrizelluläre Protein wesentlich an der Kniegelenk-

regeneration beteiligt ist. An Tag 40 nach der Behandlung konnte bei allen drei Kollagenase-behandelten Tieren und in einem von zwei OP-Tieren eine TN-C-Expression im bis dahin neu gebildeten Gelenkknorpel nachgewiesen werden. Hier könnte TN-C in die Neubildung dieses Gewebes involviert sein. Im regenerierenden Kniegelenk eines analysierten Tieres in den OP behandelten Tieren war TN-C nur im neuen gebildeten Gelenkknorpel sichtbar, es fehlte aber im alten, defekten Gelenkknorpel.

Um die Beteiligung von TN-C im Reparaturvorgang des Kniegelenks näher zu untersuchen, wurden *Gene Silencing*-Experimente in primären Molchchondrozyten mithilfe von TN-C esiRNA, die mittels Nukleofektion in die Zellen eingebracht wurde, *in vitro* durchgeführt. In zwei voneinander unabhängigen Experimenten konnte die TN-C-Expression hiermit bis zu 45% bzw. 71% reduziert werden. Das Migrations- und Adhäsionsverhalten der primären Molchchondrozyten nach TN-C *Knockdown* im Vergleich zu Kontrollzellen war hierbei nicht signifikant verändert. Um den Effekt des TN-C-*Knockdowns* auf andere deregulierte Kandidaten Gene einschließlich SPARC und DCN näher zu untersuchen, wurde deren Expression mittels Real-time PCR untersucht. Das Ergebnis der Messung zeigte, dass der TN-C-Knockdown in Molchchondrozyten die Expression dieser beiden matrizellulären Proteine nicht beeinflusst.

Basierend auf dem cDNA-Microarray wurde SPARC ebenfalls als vielversprechender Kandidat aus den cDNA-Microarray ausgewählt. Die Expression dieses Proteins konnte in verschiedenen Geweben z.B. Osteozyten, Gelenkknorpel, Blutgefäßen und in der Haut in unbehandelten Molchbeinen nachgewiesen werden. Während der Regeneration nach OP Schädigung konnte dieses matrizelluläre Protein verstärkt in verschiedenen Bereichen des Skelettmuskels und des Periosts ab Tag 20 nachgewiesen werden. Die SPARC-Expression in diesen Geweben war wahrscheinlich nicht direkt mit dem Regenerationsprozess verbunden, da diese Gewebe nicht direkt durch den Eingriff alteriert wurden.

Neben den Ergebnissen für die matrizellulären Proteine TN-C- und SPARC konnte mehrere andere Matrixreparatur-assoziierte Moleküle zu verschiedenen Zeitpunkten während des Regenerationsprozess des Molch-Kniegelenks ebenfalls als hochreguliert nachgewiesen werden, was interessante neue Einblicke in diese faszinierende Phänomen der Regeneration bietet. Allerdings zeigten die Experimente in dieser Doktorarbeit auch die noch vorhandenen Grenzen eines experimentellen Ansatzes in einem Organismus auf, für den die technischen Systeme noch nicht vollständig etabliert sind.



## 8 References

1. Afanador E, Yokozeki M, Oba Y, Kitase Y, Takahashi T, Kudo A, Moriyama K. Messenger RNA expression of periostin and Twist transiently decrease by occlusal hypofunction in mouse periodontal ligament. *Arch Oral Biol* 2005; 50: 1023-1031
2. Akira S, Takeda K, Kaisho T. Toll-like receptors: critical proteins linking innate and acquired immunity. *Nat Immunol* 2001; 2: 675-680
3. Alberts B, Johnson A, Lewis J, et al. Isolating, Cloning, and Sequencing DNA: Molecular Biology of the Cell. 4th edition [Internet]. New York: Garland Science; 2002. Available from: <http://www.ncbi.nlm.nih.gov/books/NBK26837/>
4. Alford AI, Hankenson KD. Matricellular proteins: extracellular modulator of bone development, remodeling, and regeneration. *Bone* 2006; 38: 749-757
5. Athanasiou KA, Darling EM, DuRaine GD, Hu JC, Reddi AH. Articular cartilage. Boca Raton Florida: CRC Press Taylor & Francis Group; 2013
6. Aukhil I, Joshi P, Yan Y, Erickson HP. Cell- and heparin- binding domains of the hexabrachion arm identified by tenascin expression proteins. *J Biol Chem* 1993; 268: 2542-2533
7. Bailey AJ, Sims TJ, Knott L. Phenotypic expression of osteoblast collagen in osteoarthritic bone: production of type I homotrimer. *Int J Biochem Cell Biol* 2002; 34: 176-182
8. Baldini G, Pointi C, Bortul R, Narducci P, Grill V, Martelli AM. Sparc localizes to the blebs of hobit cells and human primary osteoblasts. *J Cell Biochem* 2008
9. Bau B, Gebhard PM, Haag J, Knorr T, Bartnik E, Aigner T. Relative messenger RNA expression profiling of collagenases and aggrecanases in human articular chondrocytes in vivo and in vitro. *Arthritis Rheum* 2002; 46: 2648-2657
10. Behler JL, King FW. National audubon society field guide to north american reptiles and amphibians. New York: Knopf; 1996.
11. Belluoccio D, Rowley L, Little CR, Bateman JF. Maintaining mRNA integrity during decalcification of mineralized tissues. *PLOS one* 2013; 8: e58154
12. Bennet GA, Waine H, Bauer W. Changes in the knee joint at various ages, with particular reference to the nature and development of degenerative joint disease. New york: Commonwealth Fund; 1942
13. Beresford JN, Bennett JH, Devlin C et al., Evidence for an inverse relationship between the differentiation of adipocytic and osteogenic cells in rat marrow stromal cell cultures. *J Cell Sci* 1992; 102: 341-351
14. Berg DA, Kirkham M, Beljajeva A, Knapp D, Habermann B, Ryqe J, Tanaka EM, Simon A. Efficient regeneration by activation of neurogenesis in homeostatically quiescent regions of the adult vertebrate brain. *Development* 2010; 137: 4127-4137
15. Betz P, Nerlich A, Tubel J, Penning R, Eisenmenger W. Localization of tenascin in human skin wounds an immunohistochemical study. *Int J Legal Med* 1993; 105: 325-328

16. Billingham RC, Dahlberg L, Ionescu M, Reiner A, Bourne R, Rorabeck C, Mitchell P, Hambor J, Diekmann O, Tschesche H, Chen J, Van Wart H, Poole AR. Enhanced cleavage of type II collagen by collagenase in osteoarthritic articular cartilage. *J Clin Invest* 1997; 99: 1534-1545
17. Bock HC, Michaeli P, Bode C, Schultz W, Kresse H, Herken R, Miosqe N. The small proteoglycans decorin and biglycan in human articular cartilage of late-stage osteoarthritis. *Osteoarthritis Cartilage* 2001; 9: 654-663
18. Bollet AJ, Handy JR, Sturgil BC. Chondroitin sulfate concentration and protein-polysaccharide composition of articular cartilage in osteoarthritis. *J Clin Invest* 1963; 6: 853-859
19. Bonewald LF. The amazing osteocyte. *J Bone Miner Res* 2011; 26: 229-238
20. Borchardt T, Braun T. Cardiovascular regeneration in non-mammalian model systems: What are the differences between newts and man. *Thromb Haemost* 2007; 98: 311-318
21. Bornstein P, Sage EH. Matricellular proteins: extracellular modulators of cell function. *Curr Opin Cell Biol* 2002; 14: 608 - 616
22. Bourne GH. The relative importance of periosteum and endosteum in bone healing and the relationship of vitamin C to their activities. *Proc R Soc Med* 1944; 37: 275-279
23. Bradshaw AD, Graves DC, Motamed K, Sage EH. SPARC-null mice exhibit increased adiposity without significant differences in overall body weight. *Proc Natl Acad Sci USA* 2003; 100: 6045-6050
24. Bradshaw AD, Reed MJ, Sage EH. SPARC-null mice exhibit accelerated cutaneous wound closure. *J Histochem Cytochem* 2002; 50: 1-10
25. Bradshaw AD, Sage EH. SPARC, a matricellular protein that functions in cellular differentiation and tissue response to injury. *J Clin Invest* 2001; 107: 1049-1054
26. Bradshaw AD. The role of SPARC in extracellular matrix assembly. *J. Cell Commun. Signal.* 2009; 3: 329-246
27. Brittberg M, Lindahl A, Nilsson A, Ohlsson C, Isaksson O, Peterson L. Treatment of deep cartilage defects in the knee with autologous chondrocyte transplantation. *N Engl J Med* 1994; 331: 889-895
28. Brockes JP. Amphibian limb regeneration: rebuilding a complex structure. *Science* 1997; 276: 81
29. Brockes JP, Kumar A, Velloso CP. Regeneration as an evolutionary variable. *J Anat* 2001; 199: 3-11
30. Brown SL, Riehl TE, Walker MR, Geske MJ, Doherty JM, Stenson WF, Stappenbeck TS. Myd88-dependent positioning of Ptgs2-expressing stromal cells maintains colonic epithelial proliferation during injury. *J Clin Invest* 2007; 117: 258-269
31. Bruckskotten M, Looso M, Reinhardt R, Braun T, Borchardt T. Newt-omics: a comprehensive repository for omics data from the newt *Notophthalmus viridescens*. *Nucleic Acids Res* 2012; 40: D895-900

32. Buckwalter JA, Mankin HJ, Grodzinsky AJ. Articular cartilage and osteoarthritis. *Instr Course Lect* 2005; 54: 465-480
33. Bushue N, Wan YV. Retinoid pathway and cancer therapeutics. *Adv drug deliv rev* 2010; 62: 1285-1298
34. Calve S, Odelberg SJ, Simon HG. A transitional extracellular matrix instructs cell behavior during muscle regeneration. *Dev Biol* 2010; 259-271
35. Calve S, Simon HG. Biochemical and mechanical environment cooperatively regulate skeletal muscle regeneration. *FASEB J* 2012; 26: 2538-2545
36. Carlson BM. Principles of regenerative biology. London: Elsevier; 2007. p 379
37. Carlson BM. Factors controlling the initiation and cessation of early events in the regenerative process. In: Neoplasia and cell differentiation. Basel:Karger 1974; p60-105
38. Carragher NO, Levkau B, Ross R, Raines EW. Degraded collagen fragments promote rapid disassembly of smooth muscle focal adhesions that correlates with cleavage of p125 (FAK), paxillin, and talin. *J Cell Biol* 1999; 147: 619 -629
39. Catalan V, Gomez-Ambrosi J, Rodriguez A, Ramirez B, Rotellar F, Valenti V, Silva C, Gil MJ, Salvador J, Frühbeck G. Increased tenascin C and Toll-like receptor 4 levels in visceral adipose tissue as a link between inflammation and extracellular matrix remodeling in obesity. *J Clin Endocrinol Metab* 2012; 97: E1880-E1889
40. Caubit X, Riou JF, Coulon J, Arsanto JP, Benraiss A, Boucaut JC, Thouveny Y. Tenascin expression in developing adult and regenerating caudal spinal cord in the urodele amphibians. *Int J Dev Biol* 1994; 38: 661-672
41. Chaar ZY, Tsilfidis C. New opportunities for understanding the dedifferentiation process. *Scientific World Journal* 2006; 6: 55-64
42. Chernoff EAG, Stocum D. Developmental aspects of spinal cord and limb regeneration. *Dev. Growth Diff* 1995; 37: 133–147
43. Chevalier X, Groult N, Larget-Piet B, Zardi L, Hornebeck W. Tenascin distribution in articular cartilage from normal subjects and from patients with osteoarthritis and rheumatoid arthritis. *Arthritis Rheum* 1994; 37: 1013-1022
44. Chiba K, Eutani M, Kido Y, Ito M, Okazaki N, Taguchi K, Shindo H. Osteoporotic changes of subchondral trabecular bone in osteoarthritis of the knee: a 3-TMRI study. *Osteoporos Int* 2011; 23: 589-597
45. Clare JP. Breeding Axolotls; 2012. available from: [www.axolotl.org/breeding.htm](http://www.axolotl.org/breeding.htm)
46. Clark RK. Anatomy and physiology: Understanding the human body. Sudbury: Jones and Bartlett Publisher 2005
47. Clarke B. Normal bone anatomy and physiology. *Clin J Am Soc Nephrol* 2008; 3: S131-S139
48. Cole BJ, Gomoll AH. Biologic joint reconstruction alternatives to arthroplasty. SLACK Incorporated, 2009
49. Colnot C, Zhang X, Knothe Tate ML. Current insights on the regenerative potential of the periosteum: molecular, cellular, and endogenous engineering approaches. *J Orthop Res* 2012; 30: 1869-1878

50. Conaghan P, Birrell F, Burke M, Cumming J, Dickson J, Dieppe P, Doherty M, Dziedzic K, Francis R, Grant R, Kell C, Latimer N, MacGregor A, Naisby C, O'Mahony R, Oliver S, Underwood M. OSTEOARTHRITIS national clinical guideline for care and management in adults. London: Royal College of Physicians; 2008
51. Coons AA, Creech HJ, Jones RN et al., The demonstration of pneumococcal antigen in tissues by use of fluorescent antibodies. *J. Immunol* 1942; 45: 159-170
52. Danielson KG, Baribault H, Homes DF, Graham H, Kadler KE, Iozzo RV. Targeted disruption of decorin leads to abnormal collagen fibril morphology and skin fragility. *JCB* 1997; 136: 729-743
53. De Crombrughe B, Lefebvre V, Behringer RR, Bi W, Murakami S, Huang W. Transcriptional mechanisms of chondrocyte differentiation. *Matrix Biol* 2000; 19: 389-394
54. Delany AM, Kalajzic I, Bradshaw AD, Sage EH, Canalis E. Osteonectin-null mutation compromises osteoblast formation, maturation, and survival. *Endocrinology* 2003; 144: 2588-2596
55. Donaldson DJ, Mahan JT, Yang H, Crossin KL. Tenascin localization in skin wounds of the adult newt *Notophthalmus viridescens*. *Anat Rec* 1991; 230: 451-459
56. Elbashir S, Harborth J, Lendeckel W, Yalcin A, Weber K, Tuschl T. Duplexes of 21-nucleotide RNAs mediate RNA interference in cultured mammalian cells. *Nature* 2001; 411: 494-988
57. Elliot CG, Wang J, Guo X, Xu SW, Eastwood M, Guan J, Leask A, Conway SJ, Hamilton DW. Periostin modulates myofibroblast differentiation during full-thickness cutaneous wound repair. *J Cell Sci* 2012; 125: 121-132
58. Epker BN, Kellin M, Frost HM. Magnitude and location of cortical bone loss in human rib with aging. *Clin Orthop* 1965; 41: 198-203
59. Erickson HP. Tenascin-C, tenascin-R and tenascin-X: a family of talented proteins in search of functions. *Curr Opin Cell Biol* 1993; 869-876
60. Eriksen EF. Cellular mechanisms of bone remodeling. *Rev Endocr Metab Disord* 2010; 11: 219-227
61. Felson DT, Zhan Y, Hannan MT et al., The incidence and natural history of knee osteoarthritis in the elderly. *Arthritis and Rheumatism* 1995; 38: 1500-1505
62. Fischer D, Brown-Ludi M, Schulthess T, Chiquet-Ehrismann R. Concerted action of tenascin-C domains in cell adhesion, anti-adhesion and promotion of neurite outgrowth. *J Cell Sci* 1997; 110: 1513-1522
63. Forester DC, Lykens DV. Age structure in a population of Red-spotted newts from the Allegheny plateau of Maryland. *J Herpetol* 1991; 25: 373 - 376
64. Fosang AJ, Neame PJ, Hardingham TE, Murphy G, Hamilton JA. Cleavage of cartilage proteoglycan between G1 and G2 domains by stromelysins. *J Biol Chem* 1991; 266: 15579-15582
65. Gage SH. Life-history of the vermilion-spotted newt (*Diemyctylus viridescens* Raf.). *Amer Nat* 1891; 25: 1084 - 1110

66. Geyer M, Borchardt T, Schreyäck C, Wieteleman A, Müller-Schrobsdorff F, Müller C, Müller-Ladner U. Endogenous regeneration after collagenase-induced knee joint damage in the adult newt *Notophthalmus viridescens*, *Ann Rheum Dis* 2010; 70: 214-220
67. Gilbert SF. Developmental biology. 6th edition. Sunderland (MA): Sinauer Associates. 2000
68. Gill DE. The metapopulation ecology of the red-spotted newt, *Notophthalmus viridescens viridescens* (Rafinesque). *Ecol Monogr* 1978; 48: 145-166
69. Gilmour DT, Lyon GJ, Carlton MB, Sanes JR, Cunningham MJ, Anderson JR, Hogan BL, Evans MJ, Colledge WH. Mice deficient for the secreted glycoprotein SPARC/osteonectin/BM40 develop normally but show severe age-onset cataract formation and disruption of the lens. *EMBO J* 1998; 17: 1860-1870
70. Globus M, Vethamany-Globus S, Lee YC. Effect of apical epidermal cap on mitotic cycle and cartilage differentiation in regeneration blastemata in the newt, *Notophthalmus viridescens*. *Anat Rec* 1960; 136: 27-40
71. Godwin JW, Pinto AR, Rosenthal NA. Macrophages are required for adult salamander limb regeneration. *PNAS* 2013; 110: 9415-9420
72. Goetsch SC, Hawke TJ, Gallardo TD, Richardson JA, Garry DJ. Transcriptional profiling and regulation of the extracellular matrix during muscle regeneration. *Physiol Genomics* 2003; 14: 261-271
73. Götz M, Bolz J, Joester A, Faissner A. Tenascin-C synthesis and influence of axonal growth during rat cortical development. *Eur J Neurosci* 1997; 9: 496-506.
74. Goyal N, Gupta M, Joshi K, Naqi ON. Immunohistochemical analysis of ageing and osteoarthritic articular cartilage. *J Mol Histol* 2010; 41: 193-197
75. Grogan SP, Chen X, Sovani S, Taniguchi N, Colwell CW Jr, Lotz MK, D'Lima DD. Influence of cartilage extracellular matrix molecules on cell phenotype and neocartilage formation. *Tissue Eng Part A*. 2014; 20: 264-274
76. Haddow A. Molecular repair, wound healing, and carcinogenesis: tumor production a possible overhealing? *Adv. Cancer Res.* 1972; 16: 181-234
77. Hadjidakis DJ, Androulakis II, Bone remodeling. *Ann. N.Y. Acad. Sci.* 2006; 1092: 385-396
78. Häkkinen L, Strassburger S, Kähäri VM, Scott PG, Eichstetter I, Iozzo RV, Larjava H. A role for decorin in the structural organization of periodontal ligament. *Lab Invest* 2000; 80: 1869-1880
79. Haller O, Kiessling, Örn A, Wigzell H. Generation of natural killer cells: An autonomous function of the bone marrow. *J Exp Med* 1977; 145: 1411-1416
80. Hamilton A, Baulcombe D. A species of small antisense RNA in posttranscriptional gene silencing in plants. *Science* 1999; 286: 950-952
81. Hardy MA. The biology of scar formation. *Phys Ther* 1989; 69: 1014-1024
82. Harty M, Neff AW, King MW, Mescher AL. Regeneration or scarring: An immunologic perspective. *Dev Dyn* 2003; 226: 268-279

83. Hattori T, Coustry F, Stephens S, Eberspaecher H, Takigawa M, Yasuda H, de Crombrughe B. Transcriptional regulation of chondrogenesis by coactivator Tip60 via chromatin association with Sox9 and Sox5. *Nucleic Acids Res* 2008; 36: 3011-3024
84. Hazard L. Regeneration of the extremities of the adult Axolotl, at the expense of embryonal grafts. *C R Hebd Seances Acad Sci* 1959; 21: 2857-2859
85. Healy WR. Population consequences of alternative life histories in *Notophthalmus viridescens*. *Copeia* 1974; 221-229
86. Hecht JT, Sage EH. Retention of the matricellular protein SPARC in the endoplasmic reticulum of chondrocytes from patients with pseudoachondroplasia. *J Histochem Cytochem* 2006; 54: 269-274
87. Hegde P, Qi R, Abernathy K, Gay C, Dharap S, Gaspard R, Hughes JE, Snesrud E, Lee N, Quackenbush J. A concise guide to cDNA microarray analysis. *Biotechniques* 2000; 29: 548-550
88. Henry JJ, Tsonis PA. Molecular and cellular aspects of amphibian lens regeneration. *Prog Retin Eyes Res* 2010; 29: 543-555
89. Hicks C, Khorasanee J, Gamelli RL. Genomics of burn injury and its promise in clinical practice. *J Burn Care Res* 2008; 29: 877-886
90. Hirakawa K, Hirota s, Ikeda T, Yamaguchi A, Takemura T, Nagoshi J, Yoshiki S, Suda T, Kitamura Y, Nomura S. Localization of the mRNA for bone matrix proteins during fracture healing as determined by in situ hybridization. *J Bone Miner Res* 1994; 9: 1551-1557
91. Hocking AM, Shinomura T, McQuillan DJ. Leucine-rich repeat glycoproteins of the extracellular matrixd. *Matrix Biol* 1998; 17: 1-19
92. Hohenester E, Maurer P, Timpl R. Crystal structure of a pair of follistatin-like and EF-hand calcium-binding domains in BM-40. *EMBO J* 1997; 16: 3778 - 3786
93. Holtzer H. In: Mauro A, Shafiq SA, Milhorat AT, editors. Regeneration of striated muscle, and myogenesis; proceedings of the international conference convened by muscular dystrophy associations of america at the institute for muscle disease; March 28-29, 1969; New York. Amsterdam: Excerpta Medica; 1969
94. Honardoust D, Varkey M, Marcoux Y, Shankowsky HA, Tredget EE. Reduced decorin, fibromodulin, and transforming growth factor- $\beta$ 3 in deep dermis leads to hypertrophic scarring. *J Burn Care Res* 2012; 33: 218-227
95. Horiuchi K, Amizuka N, Takeshita S, takamatsu H, Katsuura M, Ozawa H, Toyama Y, Bonewald LF, Kudo A. Identification and characterization of a novel protein, periostin with restricted expression to periosteum and periodontal ligament and increased expression by transforming growth factor  $\beta$ . *J Bone Miner Res* 1999; 14: 1239-1249
96. Hsia HC, Schwarzbauer JE. Meet the tenascins: multifunctional and mysterious. *JBC* 2005; 280: 26641-26644
97. Hunter W. On the structure and diseases of articulating cartilages. *Philo Trans Roy Soc.* 1743; 42B: 514-521.

98. Hunzelmann N, Hafner M, Anders S, Krieg T, Nischt R. BM-40 (osteonectin, SPARC) is expressed both in the epidermal and in the dermal compartment of adult human skin. *J Invest Dermatol* 1998; 110: 122-126
99. Hunziker EB, Rosenberg LC. Repair of partial-thickness defects in articular cartilage: cell recruitment from the synovial membrane. *J Bone Joint Surg Am* 1996; 78: 721-733
100. Ikeda-Isogai M, Ohtsuka T, Baba K, Nonaka N, Nakamura M. Calcified tissue formation of subcutaneously transplanted mouse dental pulp. *Acta Histochem* 2012; 114: 55-61
101. Iruela-Arispe ML, Lane TF, Redmond D, Reilly M, Bolender RP, Kavanagh TJ, Sage EH. Expression of SPARC during development of the chicken chorioallantoic membrane: evidence for regulated proteolysis in vivo. *Mol Biol Cell* 1995; 6: 327-343
102. Ishida O, Tanaka Y, Morimoto I, Takigawa M, Eto S. Chondrocytes are regulated by cellular adhesion through CD44 and hyaluronic acid pathway. *J Bone Miner Res* 1997; 12: 1657-1663
103. Jacobsson I, Lindgarde F, Manthorpe R. The commonest rheumatic complaints over six weeks duration in a twelve-month period in a defined Swedish population. Prevalences and relationships. *Scand J Rheum* 1989; 18:353-360
104. Janeway CA Jr, Travers P, Walport M, et al., Immunobiology: The immune system in health and disease. 5th edition. New York: Garland Science; 2001. The complement system and innate immunity. Available from: <http://www.ncbi.nlm.nih.gov/books/NBK27100/>
105. Janeway JR CA, Medzhitov R. Innate immune recognition. *Annu Rev Immunol* 2002; 20: 197-216
106. Jarvinen TAH, Jozsa L, Kannus P, Jarvinen TLN, Kvist M, Hurme T, Isola J, Kalimo H, Jarvinen M. Mechanical loading regulates tenascin-C expression in the osteotendinous junction. *J Cell Sci* 1999; 112: 3157-3166
107. Jiang D, Liang J, Fan J, Yu S, Chen S, Luo Y, Prestwich GD, Mascarenhas MM, Garg HG, Quinn DA, Homer RJ, Goldstein DR, Bucala R, Lee PJ, Medzhitov R, Noble PW. Regulation of lung injury and repair by Toll-like receptors and hyaluronan. *Nat Med* 2005; 11: 1173-1179
108. Jones FS, Jones PL. The tenascin family of ECM glycoproteins: Structure, function and regulation during embryonic development and tissue remodelling. *Dev Dyn* 2000; 218: 235-259
109. Jorgensen LH, Petersson SJ, Sellathurai J, Andersen DC, Thayssen S, Sant DJ, Jensen CH, Schroder HD. Secreted protein acidic and rich in cysteine (SPARC) in human skeletal muscle. *J Histochem Cytochem* 2009; 57: 29-39
110. Jundt G, Berghäuser KH, Termine JD, Schulz A. Osteonectin-a differentiation marker of bone cells. *Cell Tissue Res* 1987; 248: 409-415
111. Kaarteenaho-Wiik R, Lakari E, Soini Y, Pollanen R, Kinnula VL, Paakko P. Tenascin expression and distribution in pleural inflammatory and fibrotic disease. *J Histochem Cytochem* 2000; 48: 1257-1268

112. Kadi F, Charifi N, Dennis C, Lexell J, Andersen JL, Schjerling P, Olsen S, Kjaer M. The behaviour of satellite cells in response to exercise: what have we learned from human studies?. *Pflugers Arch* 2005; 451: 319-327
113. Kasper DL, Fauci AS, Longo DL, Braunwald E, Hauser SL, Jameson JL, editors. *Harrison's principles of internal medicine*. 16th ed. New York: McGraw-Hill Medical Publishing Division; 2005: Page 2600
114. Kaufmann B, Muller S, Hanisch FG, Hartmann U, Paulsson M, Maurer P, Zaucke F. Structural variability of BM-40/SPARC/osteonectin glycosylation: implications for collagen affinity. *Glycobiology* 2004; 14: 609-619
115. Kelm RJ, Swords NA, Orfeo T, Mann KG. Osteonectin in matrix remodeling. A plasminogen-osteonectin-collagen complex. *J- Biol. Chem* 1994; 269: 30147 - 30153
116. Kevorkian L, Young DA, Darrah C, Donell ST, Shepstone L, Porter S, Brockband SM, Edward DR, Parker AE, Clark IM. Expression profiling of metalloproteinases and their inhibitzors in cartilage. *Arthritis Rheum* 2004; 50: 131-141
117. Kielty CM, Kwan APL, Holmes DF, Schor SL, Grant ME. Type X collagen a product of hypertrophic chondrocytes. *Biochem J* 1985; 27: 545-554
118. Kii I, Nishiyama T, Li M, Matsumoto K, Saito M, Amizuka N, Kudo A. Incorporation of tenascin-C into the extracellular matrix by periostin underlies an extracellular meshwork architecture. *J Biol Chem* 2010; 285: 2028-2039
119. Kimura Y, Madhavan M, Call MK, Santiago W, Tsonis PA, Lambris JD, Del Rio-Tsonis K. Expression of complement 3 and complement 5 in newt limb and lens regeneration. *J Immunol* 2003; 170: 2331-2339
120. Kojima T, Freitas PH, Ubaidus S, Suzuki A, Li M, Yoshizawa M, Oda K, Maeda T, Kudo A, Saito C, Amizuka N. Histochemical examinations on cortical bone regeneration induced by thermoplastic bioresorbable plates applied to bone defects of rat calvariae. *Biomed Res* 2007; 28: 219-229
121. Kragl M, Knapp D, Nacu E, Khattak S, Maden M, Epperlein HH, Tanaka EM. Cells keep a memory of their tissue origin during axolotl limb regeneration. *Nature* 2009; 460: 60-65
122. Krützfeld J, Rajewsky N, Braich R, Kallanthottathil GR, Tuschl T, Manoharan M, Stoffel M. Silencing of microRNAs *in vivo* with 'antagomirs'. *Nature* 2005; 438: 685-689
123. Kruzynska-Frejtag A, Wang J, Maeda M, Rogers R, Krug E, Hoffman S, Markwald RR, Conway SJ. Periostin is expressed within the developing teeth at the sites of epithelial-mesenchymal interaction. *Dev Dyn* 2004; 229: 857-868
124. Lajeunesse D, Hilal G, Pelletier JP, Martel-Pelletier J. Subchondral bone morphological and biochemical alterations in osteoarthritis. *Osteoarthritis cartilage* 1999; 7: 321-322
125. Lallier TE, Miner QW Jr, Sonnier J, Spencer A. A simple cell motility assay demonstrates differential motility of human periodontal ligament fibroblasts, gingival fibroblasts, and pre-osteoblasts. *Cell Tissue Res* 2007; 328: 339-354



126. Lane TF, Iruela-Arispe ML, Johnson RS, Sage EH. SPARC is source of copper-binding peptides that stimulates angiogenesis. *J Cell Biol* 1994; 125: 929-943
127. Lane TF, Sage EH. The biology of SPARC, a protein that modulates cell-matrix interactions. *FASEB J* 1994; 8: 163-173
128. Lark MW, Bayne EK, Lohmander LS. Aggrecan degradation in osteoarthritis and rheumatoid arthritis. *Acta Orthop Scand Suppl* 1995; 266: 92-97
129. Lawrence JS, Bremner JM, Bier F. Osteoarthritis: prevalence in the population and relationship between symptoms and X-ray changes. *Annals of the Rheumatic Diseases* 1996; 55: 356-362
130. Ledda-Columbano GM, Coni P, Simbula G, Zedda I, Columbano A. Compensatory regeneration, mitogen-induced liver growth, and multistage chemical carcinogenesis. *Environ Health Perspect* 1993; 101: 163-168
131. Leung YF, Cavalieri D. Fundamentals of cDNA microarray data analysis. *TRENDS in Genetics* 2003; 19: 649-659
132. Li J, Feng ZC, Yeung FS, Wong MR, Oakie A, Fellows GF, Goodyer CG, Hess DA, Wang R. Aldehyde dehydrogenase 1 activity in the developing human pancreas modulates retinoic acid signaling in mediating islet differentiation and survival. *Diabetologia* 2014; 57: 754- 64
133. Li Y, Li J, Zhu J, Sun B, Branca M, Tang Y, Foster W, Xiao X, Huard J. Decorin gene transfer promotes muscle cell differentiation and muscle regeneration. *Mol Ther* 2007; 15: 1616-1622
134. Lindahl A, Brittberg M, Peterson L. Cartilage repair with chondrocytes: clinical and cellular aspects. *Novartis Found Symp* 2003, 175-186
135. Litvin J, Selim AH, Montgomery MO, Lehmann K, Rico MC, Devlin H, Bednarik DP, Safadi FF. Expression and function of periostin-isoforms in bone. *J Cell biochem* 2004; 92: 1044-1061
136. Lohmander LS, Ostenberg A, England M, Roos H. High prevalence of knee osteoarthritis, pain and functional limitations in female soccer players twelve years after anterior cruciate ligament injury. *Arthritis Rheum* 2004; 50: 3145-3152
137. Lu P, Zhang GR, Cai YZ, Heng BC, Ren H, Wang LL, Ji J, Zou XH, Ouyang HW. Lentiviral-encoded shRNA silencing of proteoglycan decorin enhances tendon repair and regeneration within a rat model. *Cell Transplant* 2013; 22: 1507-1517
138. Mackie EJ, Tatarczuch L, Mirams M. The skeleton: a multi-functional complex organ. The growth plate chondrocyte and endochondral ossification. *J Endocrinol* 2011; 211: 109-121
139. Mackie EJ, Thesleff I, Chiquet-Ehrismann R. Tenascin is associated with chondrogenic and osteogenic differentiation in vivo and promote chondrogenesis in vitro. *J Cell Biol* 1987; 105: 2569-2579
140. Mackie EJ, Tucker RP. The tenascin-C knockout revisited. *J Cell Sci* 1999; 112: 3847-3853
141. Maden M. Vitamin A and pattern formation in the regenerating limb. *Nature* 1982; 295: 672-675

142. Maden M. The effect of vitamin A on limb regeneration in *Rana temporaria*. Dev Biol 1983; 99: 409-416
143. Madhavan M, Haynes TL, Frisch NC, Call MK, Minich CM, Tsonis PA, Del Rio-Tsonis K. The role of PAX-6 in lens regeneration. Proc Natl Acad Sci USA 2006; 103: 14848-14853
144. Maki N, Suetsugu-Maki R, Sano S, Nakamura K, Nishimura O, Tarui H, Del Rio-Tsonis K, Ohsumi K, Agata K, Tsonis PA. Oocyte-type linker histone B4 is required for transdifferentiation of somatic cells in vivo. FASEB J 2010; 3462-3467
145. Manek NJ, Lane NE. Osteoarthritis: current concepts in diagnosis and management. Am Fam Physician 2000; 61: 1795-1804
146. Mansell JP, Bailey AJ. Abnormal collagenous bone collagen metabolism in osteoarthritis. J Clin Invest 1998; 101: 1596-1603
147. Martini, Frederich H. Anatomy & Physiology. Jurong: Pearson Education Inc, Prentice Hall; 2005
148. Matsiko A, Levingstone TJ, O'Brien FJ. Advanced strategies for articular cartilage defect repair. Materials 2013; 6: 637-668
149. Matsumoto M, Chiba K, Nojiri K, Ishikawa M, Toyama Y, Nishikawa Y. Extraforaminal entrapment of the fifth lumbar spinal nerve by osteophytes of the lumbosacral spine: anatomic study and a report of four cases. Spine 2002; 27: E169-173
150. Matthews BF. Composition of articular cartilage in osteoarthritis. Br Med J 1953; 2: 660-661
151. McGann CJ, Odelberg SJ, Keating MT. Mammalian myotube dedifferentiation induced by newt regeneration extract. PNAS 2001; 98: 13699-13704
152. Meachim G and Collins D. Cell counts of normal and osteoarthritic articular cartilage in relation to the uptake of sulphate ( $^{35}\text{SO}_4$ ) *in vitro*. Ann Rheum Dis 1962; 21: 45-50
153. Mecham JS. *Notophthalmus viridescens*. Catalogue of american amphibians and reptiles. 1967; 53: 1-4
154. Mercer SE, Odelberg SJ, Simon HG. A dynamic spatiotemporal extracellular matrix facilitates epicardial-mediated vertebrate heart regeneration. Dev Biol 2013; 382: 456-469
155. Metsäranta M, Young MF, Sandberg M, Termine J, Vuorio E. Localization of osteonectin expression in human fetal skeletal tissues by *in-situ* hybridization. Calcified Tissue International 1989; 45: 146-152
156. Midwood KS, Williams LV, Schwarzbauer JE. Tissue repair and the dynamics of the extracellular matrix. IJBCB 2004; 36: 1031-1037
157. Midwood KS, Orend G. The role of tenascin-C in tissue injury and tumorigenesis. J Cell Commun Signal 2009; 3: 287-310
158. Mitashov VI, Arsanto JP, Markitantova YV, Thouveny Y. Remodeling processes during neural retinal regeneration in adult urodeles: an immunohistochemical survey. Int J Dev Biol 1995; 39: 993-1003

159. Mitchell PG, Magna HA, Reeves LM, Lopresti-Morrow LL, Yocum SA, Rosner PJ, Geoghegan KF, Hambor JE. Clonign, expression, and type II collagenolytic activity of matrix metalloproteinase-13 from human osteoarthritic cartilage. *J Clin Invest* 1996; 97: 761-768
160. Morrison JI, Loof S, He P, Simon A. Salamander limb regeneration involves the activation of a multipotent skeletal muscle satellite cell population. *J Cell Biol* 2006; 172: 433-440
161. Müller U, Vogel P, Alber G, Schaub GA. The innate immune system of mammals and insects. *Contrib Microbiol* 2008; 15: 21-44
162. Muneoka K, Holler-Dinsmore G, Bryant SV. Intrinsic control of regenerative loss in xenopus laevis limbs. *J Exp Zool* 1986; 240: 47-54
163. Murphy LI, Fischer D, Chiquet-Ehrismann R, Mackie EJ. Tenascin-C induced stimulation of chondrogenesis is dependent on the presence of the C-terminal fibrinogen-like globular domain. *FEBS Lett* 2000; 480: 189-192
164. Nagpal S, Patel S, Asano AT, Johnson AT, Duvic M, Chandraratna RA. Tazarotene-induced gene 1 (TIG1), a novel retinoic acid receptor-responsive gene in skin. *J Invest Dermatol* 1996; 106: 269-274
165. Nakamura S, Kamihagi K, Satakeda H, Katayama M, Pan H, Okamoto H, Noshiro M, Takahashi K, Yoshihara Y, Shimmei M, Okada Y, Kato Y. Enhancement of SPARC (osteonectin) synthesis in arthritic cartilage. *Arthritis Rheum* 1996; 39: 539-551
166. Nakamura-Ishizu A, Okuno Y, Omatsu Y, Okabe K, Morimoto J, Uede T, Nagasawa T, Suda T, Kubota Y. Extracellular matrix protein tenascin-C is required in the bone marrow microenvironment primed for hematopoietic regeneration. *Blood* 2012; 119: 5429-5437
167. Nakazawa T, Nakajima A, Seki N, Okawa A, Kato M, Moriya H, Amizuka N, Einhorn TA, Yamazaki M. Gene expression of periostin in the early stage of fracture healing detected by cDNA microarray analysis. *J Orthop Res* 2004; 22: 520-525.
168. Nakoshi Y, Hasegawa M, Akeda K, Iino T, Sudo A, Yoshida T, Uchida A. Distribution and role of tenascin-C in human osteoarthritic cartilage. *J Orthop Sci* 2010; 15: 666-673
169. Nishiyama T, Kii I, Kashima TG, Kikuchi Y, Ohazama A, Shimazaki M, Fukuyama M, Kudo A. Delayed re-epithelization in periostin-deficient mice during cutaneous wound healing. *PLoS ONE* 2011; 6: e18410
170. Norose K, Clark JI, Syed NA, Basu A, Heber-Katz E, Sage EH, Howe CC. SPARC deficiency leads to early-onset cataractogenesis. *Invest Ophthalmol Vis Sci* 1998; 39: 2674-2680
171. Nuttall ME, Singh V, Thomas-Porch C, Frazier T, Gimble JM. Adipocytes and the regulation of bone remodeling: a balancing act. *Calcif Tissue Int* 2014; 46: 146-152
172. Odelberg SJ. Cellular plasticity in vertebrate regeneration. *Anat Rec B New Anat* 2005; 287: 25-35

173. Ogita M, Rached MT, Dworakowski E, Bilezikian JP, Kousteni S. Differentiation and proliferation of periosteal osteoblast progenitors are differentially regulated by estrogens and intermittent parathyroid hormone administration. *Endocrinology* 2008; 149: 5713-5723.
174. Ohnishi S, Okabe K, Obata H, Otani K, Ishikane S, Ogino H. Involvement of tazarotene-induced gene 1 in proliferation and differentiation of human adipose tissue-derived mesenchymal stem cells. *Cell Prolif* 2009; 42: 309-316
175. Ohta MT, Sakai Y, Saga Y, Aizawa S, Saito M. Suppression of hematopoietic activity in tenascin-C deficient mice. *Blood* 1998; 91: 4074-4083
176. Onda H, Goldhamer DJ, Tassava RA. An extracellular matrix molecule of newt and axolotl regenerating limb blastemas and embryonic limb buds: immunological relationship of MT1 antigen with tenascin. *Development* 1990; 108: 657-668
177. Onda H, Poulin ML, Tassava RA, Chiu IM. Characterization of a newt tenascin cDNA and localization of tenascin mRNA during newt limb regeneration by in situ hybridization. *Dev Biol* 1991; 148: 219-232
178. Orlando B, Giacomelli L, Ricci M, Barone A, Covani U. Leader genes in osteogenesis: a theoretical study. *Arch Oral Biol* 2013; 58: 42-49
179. Otsuka K, Yao KL, Wasi S, Tung PS, Aubin JE, Sodek J, Termine JD. Biosynthesis of osteonectin by fetal porcine calvarial cells in vitro. *J Biol Chem* 1984; 259: 9805-9812
180. Padial-Molina M, Volk SL, Rios HF. Periostin increases migration and proliferation of human periodontal ligament fibroblasts challenged by tumor necrosis factor- $\alpha$  and porphyromonas gingivalis lipopolysaccharides. *J Periodontal Res* 2013
181. Park SW, Chen SW, Kim M, et al., Human heat shock protein 27-overexpressing mice are protected against acute kidney injury after hepatic ischemia and perfusion. *Am J Physiol Renal Physiol* 2009; 297: F885-F894
182. Patel L, Sun W, Glasson SS, Morris EA, Flannery CR, Chockalingam PS. Tenascin-C induces inflammatory mediators and matrix degradation in osteoarthritic cartilage. *BMC Musculoskeletal Disord* 2011; 12: 164
183. Pearson CA, Pearson D, Shibahara S, Hofsteenge J, Chiquet-Ehrismann R. Tenascin: cDNA cloning and induction by TGF- $\beta$ . *EMBO J.* 1988; 7: 2977 - 2981
184. Pecorino LT, Entwistle A, Brockes JP. Activation of a single retinoic acid receptor isoform mediates proximodistal respecification. *Curr Biol* 1996; 6: 563-569
185. Petranks JW. Salamanders of the United States and Canada. Smithsonian Institution Press. 1998. Washington and London.
186. Pietsch P. Partial characterization of source of origin of regenerating limb blastema cells in *Ambystoma* larvae using selective inhibitor of DNA synthesis phleomycin. *Anat Rec* 1969; 163: 320
187. Pietsch P. Differentiation in regeneration. I. The development of muscle and cartilage following deplantation of regenerating limb blastema of *Ambystoma* larvae. *Dev. Biol* 1961; 3: 255-264

- 
188. Reboul P, Pelletier JP, Tardif G, Cloutier JM, Martel.Pelletier J. The new collagenase, collagenase-3, is expressed and synthesized by human chondrocytes but not by synoviocytes. A role in osteoarthritis. *J Clin Invest* 1996; 97: 2011-2019
  189. Reed CC, Iozzo RV. The role of decorin in collagen fibrillogenesis and skin homeostasis. *Glycoconi J* 2003; 19: 249-255
  190. Riemland S. *Notophthalmus viridescens*. (online) animal diversity web. Retrieved from [http://animaldiversity.ummz.umich.edu/accounts/Notophthalmus\\_viridescens/](http://animaldiversity.ummz.umich.edu/accounts/Notophthalmus_viridescens/). 2000
  191. Rio DC, Ares MJ, Hannon GJ, Nilsen TW. Polyacrylamide gel electrophoresis of RNA. *Cold Spring Harb Protoc* 2010
  192. Rios H, Koushik SV, Wang H, Wang J, Zhou HM, Lindsley A, Rogers R, Chen Z, Maeda M, Kruzynska-Frejtag A, Feng JQ, Conway SJ. Periostin null mice exhibit dwarfism, incisor enamel defects, and an early-onset periodontal disease-like phenotype. *Moll Cell Biol* 2005; 25: 11131-11144
  193. Riss J, Khanna C, Koo SJ, Chandramouli GVR, Yang HH, Hu Y, Kleiner DE, Rosenwald A, Schaefer CF, Ben-Sasson SA, Yang L, Powell J, Kane DW, Star RA, Aprelikova O, Bauer K, Vaselli JR, Maranchie JK, Kohn KW, Buetow KH, Linehan WM, Weinstein JN, Lee MP, Klausner RD, Barrett JC. Cancers as wound that do not heal: Differences and similarities between renal regeneration/repair and renal cell carcinoma. *Cancer Res* 2006; 66: 7216-7224
  194. Robling AG, Niziolek PJ, Baldridge LA, Condon KW, Allen MR, Alam I, Mantila SM, Gluhak-Heinrich J, Bellido TM, Harris SE, Turner CH. Mechanical stimulation of bone in vivo reduces osteocyte expression of sost/sclerostin. *JBC* 2008; 283: 5866-5875
  195. Roe AW, Grayson KL. Terrestrial movements and habitat use of juvenile and emigrating adult Eastern red-spotted newts, *Notophthalmus viridescens*. *J Herpetol* 2008, 42: 22 - 30
  196. Ross CA. Vitamin A. In: Coates PM, Betz JM, Blackman MR, et al., eds. *Encyclopedia of dietary supplements*. 2nd ed. London and New York: Informa Healthcare; 2010: 778-791
  197. Rothwell AG and Bentley G. Chondrocyte multiplication in osteoarthritic articular cartilage. *J Bone Joint Surg Brit* 1973; 55: 588-594
  198. Sage H, Johnson C, Bornstein P. Characterization of a novel serum albumin-binding glycoprotein secreted by endothelial cells in culture. *J Biol Chem* 1984; 259: 3993 - 4007
  199. Sage H, Pritzl P, Bornstein P. Secretory phenotypes of endothelial cells in culture: comparison of aortic, venous, capillary, and corneal endothelium. *Arteriosclerosis* 1981; 1: 427-422
  200. Sage H, Vernon RB, Funk SE, Everitt EA, Angelo J. SPARC, a secreted protein associated with cellular proliferation, inhibits cell spreading in vitro and exhibits Ca<sup>2+</sup>-dependent binding to the extracellular matrix. *J Cell Biol* 1989; 109: 341-356

201. Salmon CR, Silverio KG, Giorgetti AP, Sallum EA, Casati MZ, et al., Gene expression analysis in microdissected samples from decalcified tissues. *Am J Sur Pathol Part B*; 2012
202. Salter DM. Tenascin increase cartilage and synovium from arthritic knees. *Br J Rheumatol* 1993; 32: 780-786
203. Samuels J, Krasnokutsky S, Abramson SB. Osteoarthritis: a tale of three tissues. *Bull NYU Hosp Jt Dis* 2008; 66: 244-250
204. Sandel LJ, Aigner T. Articular cartilage and changes in arthritis an introduction: cell biology of osteoarthritis. *Arthritis Res* 2001; 3: 107-113
205. Sasaki T, Gohring W, Mann K, et al., Limited cleavage of extracellular matrix protein BM-40 by matrix metalloproteinases increases its affinity for collagens. *J Biol Chem* 1997; 272: 9237-9243
206. Sasaki T, Hohenester E, Gohring W, Timpl R. Crystal structure and mapping by site-directed mutagenesis of the collagen-binding epitope of an activated form of BM-40/SPARC/osteonectin. *IMBO J* 1998; 17: 1625-1634
207. Schäfer M, Werner S. Cancer as an overhealing wound: an old hypothesis revisited. *Nat Rev Moll Cell Biol* 2008; 9: 628-638
208. Schena M, Shalon D, Davis RW, Brown PO. Quantitative monitoring of gene expression patterns with a complementary DNA microarray. *Science* 1995; 270: 467-470
209. Shafritz TA, Rosenberg LC, Yannas IV. Specific effects of glycosaminoglycans in an analog of extracellular matrix that delays wound contraction and induces regeneration. *Wound Repair Regen* 1994; 2: 270-276
210. Shao YY, Wang L, Hicks DG, Ballock RT. Analysis of gene expression in mineralized skeletal tissues by laser capture microdissection and RT-PCR. *Lab Invest* 2006; 86: 1089-1095
211. Sharma L, Berenbaum F. Osteoarthritis: a companion to rheumatology. Elsevier health sciences 2007.print
212. Shutoh M, Oue N, Aung PP, Noguchi T, Kuraoka K, Nakayama H, Kawahara K, Yasui W. DNA methylation of genes linked with retinoid signaling in gastric carcinoma: expression of the retinoid acid receptor beta, cellular retinol-binding protein 1, and tazarotene-induced gene 1 genes is associated with DNA methylation. *Cancer* 2005; 104: 1609-1619
213. Slemenda C, Brandt KD, Heilman DK, et al., Quadriceps weakness and osteoarthritis of the knee. *Ann Intern Med.* 1997; 127: 97–104.
214. Steen TP. Origin and differentiative capacities of cells in the blastema of the regenerating salamander limb. *Am Zool* 1970; 10: 119-132
215. Steinert AF, Ghivizzani SC, Rethwilm A, Tuan RS, Evans CH, Nöth U. Major biological obstacles for persistent cell-based regeneration of articular cartilage. *Arthritis Res Ther* 2007; 9: 213
216. Stockwell RA. The interrelationship of cell density and cartilage thickness in mammalian articular cartilage. *J Anat* 1971; 109: 411-421

217. Stocum DL. Regenerative biology and medicine. San Diego, 2006. Online
218. Stocum DL. The urodele limb regeneration blastema: a self-organizing system. I. Morphogenesis and differentiation of autografted whole and fractional blastemas. *Dev Biol* 1968; 18: 457-480
219. Stoker NG, Epker BN. Age changes in endosteal bone remodeling and balance in the rabbit. *J Dent Res* 1971; 50: 1570-1574
220. Stoop R, Buma P, van der Kraan PM, Hollander AP, Bilinghurst RC, Meijers THM, Poole AR, van den Berg WB. Type II collagen degradation in articular cartilage fibrillation after anterior cruciate ligament transection in rats. *Osteoarthritis Cartilage* 2001; 4: 308-315
221. Summerton J, Morpholino antisense oligomers: the case for an RNase H-independent structural type. *Biochim Biophys Acta* 1999; 1489: 141-158
222. Summerton J, Weller d, Morpholino antisense oligomers: design, preparation, and properties. *Antisense Nucleic Acid Drug Dev* 1997; 7: 187-195
223. Takahashi M. Ecological divergence of the easter newt, *Notophthalmus viridescens*. PhD dissertation, 2009, The University of Memphis, Tennessee
224. Takahashi MK, Parris MJ. Life cycle polyphenism as a factor affecting ecological divergence within *Notophthalmus viridescens*. *Oecologia* 2008, 158: 23 - 24
225. Takeshita S, Kikuno R, Tezuka K, Amann E. Osteoblast-specific factor 2: cloning of a putative bone adhesion protein with homology with the insect protein fasciclin I. *Biochem J* 1993; 294: 271-278
226. Tanaka, EM and Reddien PW. The cellular basis for animal regeneration. *Dev Cell* 2011; 21: 172-185
227. Termine JD, Kleinman HK, Whitson SW, Conn KM, McGarvey ML, Martin GR. Osteonectin, a bone-specific protein linking mineral to collagen. *Cell* 1981; 26: 99-105
228. Tompkins R. Genie control of axolotl metamorphosis. *Amer Zool* 1978; 18: 313-319
229. Troeberg L, Nagase H. Proteases involved in cartilage matrix degradation in osteoarthritis. *Biochim Biophys Acta* 2012; 1824:133-145
230. van der Kraan PM, van den Berg WB. Osteophytes: relevance and biology. *Osteoarthr Cartil* 2007; 15: 237-244
231. Veje K, Hyllested-Wiinge JL, Ostergaard K. Topographic and zonal distribution of tenascin in human articular cartilage from femoral heads: normal versus mild and severe osteoarthritis. *Osteoarthritis Cartilage* 2003; 11: 217-227
232. Venn M, Maroudas M. Chemical composition and swelling of normal and osteoarthritic femoral head cartilage. I. Chemical composition. *Ann Rheum Dis* 1977; 36: 121-129
233. Wang D, Oparil S, Feng JA, Li P, Perry G, Chen LB, Dai M, John SW, Chen YF. Effects of pressure overload on extracellular matrix expression in the heart of the atrial natriuretic peptide-null mouse. *Hypertension* 2003; 42: 88-95

- 
234. Weiss C, Rosenberg L, Helet AJ. An ultrastructural study of normal young adult human articular cartilage. *J Bone Joint Surg Am* 1968; 50: 663-674
  235. Wen W, Chau E, Jackson-Boeters L, Elliott C, Daley TD, Hamilton DW. TGF-ss1 and FAK regulate periostin expression in PDL fibroblasts. *J Dent Res* 2010; 89: 1439-1443
  236. Witman N, Heigwer J, Thaler B, Lui WO, Morrison JI. miR-128 regulates non-myocytes hyperplasia, deposition of extracellular matrix and islet1 expression during newt cardiac regeneration. *Dev Biol* 2013; 383: 253-263
  237. Wu CC, Tsai F, Shyu R, Tsai Y, Wang C, Jiang S. G protein-coupled receptor kinase 5 mediates Tazarotene-induced gene 1-induced growth suppression of human colon cancer cells. *BMC Cancer* 2011; 11: 175
  238. Yang D, Buchholz F, Huang Z, Goga A, Chen CY, Brodsky FM, Bishop JM. Short RNA duplexes produced by hydrolysis with *Escherichia coli* RNase III mediate effective RNA interference in mammalian cells. *PNAS* 2002; 99: 9942-9947
  239. Yokoyama H. Initiation of limb regeneration: The critical steps for regenerative capacity. *Develop Growth Differ* 2008; 50: 13-22
  240. Yoshida N, Yoshida K, Hosoya A, Saito M, Yokoi T, Okiji T, Amizuka N, Ozawa H. Association of TIMP-2 with extracellular matrix exposed to mechanical stress and its co-distribution with periostin during mouse mandible development. *Cell Tissue Res* 2007; 330: 133-145
  241. Zelzer E, McLean W, Ng YS, Fukai N, Reginato AM, Lovejoy S, D' Amore PA, Olsen BR. Skeletal defects in VEGF (120/120) mice reveal multiple roles for VEGF in skeletogenesis. *Development* 2002; 129: 1893-1904
  242. Zhang J, Liu L, Pfeifer GP. Methylation of the retinoid response gene TIG1 in prostate cancer correlates with methylation of the retinoic acid receptor beta gene. *Oncogene* 2004; 23: 2241-2249
  243. Zhang C, Tan CK, McFarlane C, Sharma M, Tan NS, Kambadur R. Myostatin-null mice exhibit delayed skin wound healing through the blockade of transforming growth factor- $\beta$  signaling by decorin. *Am J Physiol Cell Physiol* 2012; 302: C1213-C1225
  244. Zhang M, Li H, Ma H, Qin J. A simple microfluidic strategy for cell migration assay in an in vitro wound-healing model. *Wound Repair Regen* 2013; 21: 897-903
  245. Zhang Y, Jordan JM. Epidemiology of osteoarthritis. *Clin Geriatr Med* 2010; 26: 355-369
  246. Zhu S, Barbe MF, Liu C, Hadjiargyrou M, Popoff SN, Rani S, Safadi FF, Litvin J. Periostin-like-factor in osteogenesis. *J Cell Physiol* 2009; 218: 584-592



## 9 Appendix

### 9.1 List of figures

FIGURE 1: STAGES OF LIMB REGENERATION IN AN ADULT NEWT ( <i>NOTOPHTHALMUS VIRIDESCENS</i> )	2
FIGURE 2: THE ADULT RED SPOTTED NEWT ( <i>NOTOPHTHALMUS VIRIDESCENS VIRIDESCENS</i> )	4
FIGURE 3: HEALTHY NEWT KNEE JOINT.	6
FIGURE 4: STRUCTURAL ORGANIZATION OF ARTICULAR CARTILAGE	7
FIGURE 5: ANATOMY OF AN ADULT HUMAN LONG BONE	9
FIGURE 6: ILLUSTRATION OF LONG BONE DEVELOPMENT BY ENDOCHONDRAL OSSIFICATION	10
FIGURE 7: COLLAGENASE- AND SURGICALLY-INDUCED KNEE JOINT DEFECT IN NEWT	13
FIGURE 8: CLASSIFICATION OF 88 DIFFERENTIALLY DEREGULATED GENES FROM THE CDNA MICROARRAY OF REGENERATING NEWT KNEE JOINT.	15
FIGURE 9: MODULAR STRUCTURE OF HUMAN SPARC.	16
FIGURE 10: MOLECULAR STRUCTURE OF TN-C.	19
FIGURE 11: ESIRNA GENERATION USING BLOCK-IT RNAI TOPO TRANSCRIPTION KIT AND RNASE III	46
FIGURE 12: PRIMARY AMPLIFICATION PRODUCTS OF NEWT TN-C (LANE A) AND LACZ (LANE B)	48
FIGURE 13: SECONDARY AMPLIFICATION PRODUCATS OF NEWT TN-C (LANE A, B) AND LACZ (LANE C, D).	49
FIGURE 14: POLYACRYLAMIDE GEL ELECTROPHORESIS OF (I) TN-C AND (J) LACZ ESIRNA SHOWED RNA BANDS OF 21 BP.	50
FIGURE 15: THE PROCESS OF THE NEWT CHONDROCYTES MIGRATION IN THE SCRAPE MOTILITY ASSAY	53
FIGURE 16: RELATIVE QUANTIFICATION OF TN-C DURING NEWT KNEE JOINT REGENERATION AFTER COLLAGENASE AND SURGICALLY-INDUCED OA	55
FIGURE 17: RELATIVE QUANTIFICATION OF SPARC DURING NEWT KNEE JOINT REGENERATION AFTER COLLAGENASE AND SURGICALLY-INDUCED OA	56
FIGURE 18: RELATIVE QUANTIFICATION OF POSTN DURING NEWT KNEE JOINT REGENERATION AFTER COLLAGENASE AND SURGICALLY-INDUCED OA	57
FIGURE 19: RELATIVE QUANTIFICATION OF DCN DURING NEWT KNEE JOINT REGENERATION AFTER COLLAGENASE- AND SURGICALLY-INDUCED OA.	58
FIGURE 20: RELATIVE QUANTIFICATION OF CFB DURING NEWT KNEE JOINT REGENERATION AFTER COLLAGENASE AND SURGICALLY-INDUCED OA	59
FIGURE 21: RELATIVE QUANTIFICATION OF TLR2 DURING NEWT KNEE JOINT REGENERATION AFTER COLLAGENASE AND SURGICALLY-INDUCED OA	60
FIGURE 22: RELATIVE QUANTIFICATION OF RARRES1 DURING NEWT KNEE JOINT REGENERATION AFTER COLLAGENASE AND SURGICALLY-INDUCED OA	61
FIGURE 23: TN-C EXPRESSION AND PHYSIOLOGICAL APPEARANCE OF A HEALTHY NEWT KNEE JOINT.	62
FIGURE 24: VALIDATION OF TN-C EXPRESSION IN HEALTHY NEWT KNEE JOINT USING NEWT- SPECIFIC ANTIBODY, MT-1	63
FIGURE 25: TN-C EXPRESSION AND PHYSIOLOGICAL APPEARANCE OF A NEWT KNEE JOINT 10 DAYS AFTER (A), COLLAGENASE INJECTION AND (B) BUFFER INJECTION.	64
FIGURE 26: TN-C EXPRESSION AND PHYSIOLOGICAL APPEARANCE OF A NEWT KNEE JOINT 20 DAYS AFTER (A) COLLAGENASE- AND (B) BUFFER INJECTION	66
FIGURE 27: TN-C EXPRESSION AND PHYSIOLOGICAL APPEARANCE OF A NEWT KNEE JOINT 40 DAYS AFTER (A) COLLAGENASE- AND (B) BUFFER-INJECTION	67
FIGURE 28: TN-C EXPRESSION AND PHYSIOLOGICAL APPEARANCE OF A NEWT KNEE JOINT 10 DAYS AFTER (A) SURGERY AND (B) SHAM SURGERY TREATMENT	69
FIGURE 29: TN-C EXPRESSION AND PHYSIOLOGICAL APPEARANCE OF A NEWT KNEE JOINT 20 DAYS AFTER (A) SURGERY OR (B) SHAM SURGERY TREATMENT.	70
FIGURE 30: TN-C EXPRESSION AND PHYSIOLOGICAL APPEARANCE OF A NEWT KNEE JOINT 40 DAYS AFTER (A) SURGERY OR (B) SHAM SURGERY TREATMENT	71

FIGURE 31: RELATIVE QUANTIFICATION OF TN-C IN DIFFERENT NEWT CHONDROCYTE POPULATIONS, NEWT A1 CELLS, AND NEWT B1H1 CELLS .....	74
FIGURE 32: FIRST EXPERIMENT OF TN-C KNOCKDOWN IN PRIMARY NEWT CHONDROCYTES. ....	75
FIGURE 33: SECOND EXPERIMENT OF TN-C KNOCKDOWN IN PRIMARY NEWT CHONDROCYTES. ...	76
FIGURE 34: THE EFFECT OF TN-C KNOCKDOWN TO THE ADHESIVE CAPACITY OF THE PRIMARY NEWT CHONDROCYTES. ....	77
FIGURE 35: THE EFFECT OF TN-C KNOCKDOWN IN THE MOTILITY CAPACITY OF THE PRIMARY NEWT CHONDROCYTES. ....	78
FIGURE 36: SPARC EXPRESSION IN TN-C-KNOCKDOWN PRIMARY NEWT CHONDROCYTES .....	79
FIGURE 37: DCN EXPRESSION IN TN-C KNOCKDOWN PRIMARY NEWT CHONDROCYTES. ....	79
FIGURE 38: SPARC EXPRESSION IN HUMAN BONE FROM AN RA PATIENT .....	81
FIGURE 39: SPARC EXPRESSION IN A HEALTHY NEWT KNEE JOINT. IHC STAINING AGAINST (A), (B), (C) SPARC AND AGAINST (D) GOAT POLYCLONAL IgG (ISOTYPE CONTROL). ....	82
FIGURE 40: SPARC EXPRESSION IN THE 20-DAY POST-SURGICALLY-INDUCED KNEE JOINT DEFECT. IHC STAINING OF (A), (B), (C), (D) SURGICALLY-TREATED AND (E), (F), (G) SHAM OPERATED KNEE JOINT AGAINST SPARC. ....	84
FIGURE 41: SPARC EXPRESSION IN A 40-DAY POST-SURGICAL INFLECTED NEWT KNEE JOINT DEFECT. IHC STAINING FOR SPARC IN (A), (B) SURGICALLY-TREATED AND (C), (D) SHAM OPERATED NEWT KNEE JOINTS. ....	85

## 9.2 List of tables

TABLE 1: LIST OF CHEMICALS AND MATERIALS .....	25
TABLE 2: LIST OF MEDIA AND SOLUTIONS .....	27
TABLE 3: LIST OF ENZYMES .....	29
TABLE 4: LIST OF PRIMARY ANTIBODIES .....	29
TABLE 5: LIST OF ISOTYPE CONTROL ANTIBODIES .....	30
TABLE 6: LIST OF SECONDARY ANTIBODIES .....	30
TABLE 7: LIST OF MOLECULAR BIOLOGICAL KITS .....	30
TABLE 8: LIST OF REAL-TIME PCR PRIMERS .....	31
TABLE 9: LIST OF PRIMER TO GENERATE ESIRNA TENASCIN-C .....	32
TABLE 10: SOFTWARES .....	33
TABLE 11: LIST OF INSTRUMENTS .....	33
TABLE 12: LIST OF ORGANS AND TISSUES .....	34
TABLE 13: LIST OF CELLS AND CELL LINES .....	36
TABLE 14: SUMMARY OF TN-C SPATIAL EXPRESSION FROM COLLAGENASE AND SURGERY MODEL . ....	73
TABLE 15: RELATIVE QUANTIFICATION ( $\Delta\Delta C_T$ ) OF ALL CANDIDATE GENES FROM CDNA MICROARRAY, INNATE IMMUNE SYSTEM AND VITAMIN A BIOSYNTHESIS PATHWAY DURING NEWT KNEE JOINT REGENERATION AFTER COLLAGENASE- AND SURGICALLY-INDUCED OA. ....	125

## 9.3 List of abbreviations

ac	articular cartilage
acr	articular cartilage rest
BME	basal medium eagle
bv	blood vessel
C coll day 10	control knee joint collagenase model day 10
C coll day 20	control knee joint collagenase model day 20
C coll day 40	control knee joint collagenase model day 40

---

C surgery day 10	control knee joint surgery model day 10
C surgery day 20	control knee joint surgery model day 20
C surgery day 40	control knee joint surgery model day 40
calc	calcified zone of articular cartilage
CFB	complement factor B
coll	collagenase
Coll D10	collagenase model day 10
Coll D40	collagenase model day 40
CRYGB	gamma $\beta$ crystalline
Ct	cycle threshold
da	defect area
DCN	decorin
ddH <sub>2</sub> O	double-distillated H <sub>2</sub> O
der	dermis
dsDNA	double-stranded DNA
dsRNA	double-stranded RNA
dz	deep zone of articular cartilage
end	endosteum
esiRNA	endoribonuclease small interfering RNA
fm	femur
HEPES	N-2-hydroxyethylpiperazine-N-2-ethane sulfonic acid
hr	hour
IHC	immunohistochemistry
ISH	in-situ hybridization
ITS	insulin transferin selenium
min	minute
ms	muscle
MyD88	myeloid differentiation primary response gene 88
nac	newly formed articular cartilage
nb	newly formed bone
ns	not significant
OA	osteoarthritis
oac	old articular cartilage
ob	osteoblasts
OLFML3	olfactomedin-like 3
OP	surgery
OP day 20	surgery model day 20

---

OP day 40	surgery model day 40
OP day10	surgery model day 10
os	osteocytes
osd	osteoid
PBS	phosphate buffer saline
PCR	polymerase chain reaction
POSTN	periostin
prs	periosteum
RARRES1	retinoic acid receptor responder 1
RAR- $\alpha$	retinoic acid receptor- $\alpha$
RAR- $\beta$	retinoic acid receptor- $\beta$
RAR- $\delta$	retinoic acid receptor- $\delta$
RETSAT	retinol saturase
RT	room temperature
RXR	retinoid X receptor
rz	remodelling zone
sb	subchondral bone
sec	second
siRNA	small interference RNA
SPARC	secreted protein acidic and rich in cysteine
ssRNA	single-stranded RNA
T col day 40	treated knee joint collagenase model day 40
T coll day 10	treated knee joint collagenase model day 10
T coll day 20	treated knee joint collagenase model day 20
T surgery day 10	treated knee joint surgery model day 10
T surgery day 20	treated knee joint surgery model day 20
T surgery day 40	treated knee joint surgery model day 40
tb	tibia
TLR2	toll-like receptor 2
TLR5	toll-like receptor 5
TMSB4	thymosin $\beta$ 4
TN-C	tenascin-C
ut	undifferentiated tissue

## 9.4 Result of relative quantification of candidate genes with real-time PCR

Table 15: Relative quantification ( $\Delta\Delta C_t$ ) of all candidate genes from cDNA microarray, innate immune system and vitamin A biosynthesis pathway during newt knee joint regeneration after collagenase- and surgically-induced OA. Artificial knee joint damage was induced in the red-spotted newts (*Notophthalmus viridescens*) using collagenase and surgery treatment. 10, 40 days after collagenase and 10, 20, 40 days after surgery treatment, the regenerating and the control knee joint were isolated from each 2 pool (pool A) and 3 pool animals (pool B). After isolation of total mRNA from these knee joints, the cDNA was synthesized for relative quantification using real-time PCR. Afterwards,  $\Delta\Delta C_t$  was calculated for each candidate genes. The result of the calculation and the standard deviation were presented in this table. Heat-shock protein 27 (HSP-27), complement factor B (complement factor B), periostin (POSTN), thymosin  $\beta 4$  (TMSB4), decorin (DCN), tenascin-C (TN-C), gamma B crystalline (CRYGB), secreted protein acidic and rich in cysteine (SPARC), olfactomedin-like (OLFML3), retinol saturase (RETSAT), retinoid X receptor (RXR), retinoic acid receptor  $\alpha$  (RAR- $\alpha$ ), retinoic acid receptor  $\beta$  (RAR- $\beta$ ), retinoic acid receptor  $\delta$  (RAR- $\delta$ ), myeloid differentiation primary response gene 88 (MyD88), toll-like receptor 2 (TLR2), toll-like receptor 5 (TLR5), and retinoic acid receptor responder -1 (RARRES1).

Candidate genes	Collagenase model				Surgery model					
	Day 10		Day 40		Day 10		Day 20		Day 40	
	Pool A	Pool B	Pool A	Pool B	Pool A	Pool B	Pool A	Pool B	Pool A	Pool B
CFB	4.5 $\pm 0.35$	3.2 $\pm 0.41$	0.8 $\pm 0.04$	4.9 $\pm 0.20$	11.8 $\pm 1.01$	4.5 $\pm 0.32$	4.4 $\pm 0.06$	23.6 $\pm 2.94$	5.2 $\pm 0.57$	2.7 $\pm 0.65$
POSTN	2.8 $\pm 0.15$	1.3 $\pm 0.11$	1.7 $\pm 0.09$	4.9 $\pm 0.16$	2.3 $\pm 0.16$	3.3 $\pm 0.04$	3.9 $\pm 0.26$	8.9 $\pm 1.26$	1.3 0.18	1.0 $\pm 0.02$
TMSB4	2.7 $\pm 0.02$	1.3 $\pm 0.21$	1.2 $\pm 0.07$	1.3 $\pm 0.04$	0.5 $\pm 0.04$	0.4 $\pm 0.04$	0.5 $\pm 0.01$	0.4 $\pm 0.04$	1.5 $\pm 0.19$	0.4 $\pm 0.02$
DCN	8.6 $\pm 0.38$	0.4 $\pm 0.05$	2.4 $\pm 0.06$	1.7 $\pm 0.15$	1.2 $\pm 0.06$	1.8 $\pm 0.27$	2.1 $\pm 0.03$	1.4 $\pm 0.06$	2.0 $\pm 0.09$	1.0 $\pm 0.05$
TN-C	22.4 $\pm 0.60$	3.5 $\pm 0.06$	3.8 $\pm 0.13$	12.2 $\pm 0.50$	15.6 $\pm 0.79$	12.3 $\pm 1.89$	10.1 $\pm 0.26$	33.8 $\pm 7.85$	1.1 $\pm 0.10$	0.9 $\pm 0.04$
CRYGB	1.5 $\pm 0.04$	1.0 $\pm 0.06$	1.7 $\pm 0.12$	0.7 $\pm 0.01$	6.7 $\pm 1.9$	2.5 $\pm 0.05$	1.1 $\pm 0.02$	1.6 $\pm 0.10$	0.9 $\pm 0.07$	1.0 $\pm 0.02$
SPARC	2.1 $\pm 0.05$	1.4 $\pm 0.13$	1.7 $\pm 0.06$	2.6 $\pm 0.08$	1.4 $\pm 0.08$	2.5 $\pm 0.09$	3.4 $\pm 0.12$	2.4 $\pm 0.16$	1.7 $\pm 0.07$	1.1 $\pm 0.03$

Candidate genes	Collagenase model				Surgery model					
	Day 10		Day 40		Day 10		Day 20		Day 40	
	Pool A	Pool B	Pool A	Pool B	Pool A	Pool B	Pool A	Pool B	Pool A	Pool B
OLFML3	3.8 ±0.20	1.7 ±0.07	1.1 ±0.03	4.4 ±1.00	3.7 ±0.32	2.2 ±0.11	5.0 ±0.15	4.1 ±0.06	3.0 ±0.27	1.0 ±0.02
Retsat	1.8 ±0.08	0.4 ±0.02	1.2 ±0.03	1.4 ±0.16	1.4 ±0.06	0.7 ±0.11	1.0 ±0.07	0.9 ±0.18	1.8 ±0.19	0.5 ±0.05
RXR	4.6 ±0.37	0.6 ±0.08	1.1 ±0.02	0.6 ±0.02	1.6 ±0.12	2.6 ±0.20	1.2 ±0.07	1.5 ±0.08	1.4 ±0.10	1.0 ±0.08
RAR-α	2.8 ±0.21	0.6 ±0.10	1.1 ±0.14	0.8 ±0.04	1.1 ±0.16	1.9 ±0.12	0.8 ±0.08	1.8 ±0.17	1.6 ±0.14	1.3 ±0.20
RAR-β	0.9 ±16	0.4 ±1.26	1.1 ±0.21	1.4 ±0.30	1.0 ±0.19	1.4 ±0.32	0.9 ±0.24	2.5 ±0.21	1.2 ±0.21	0.6 ±0.25
RAR-δ	3.6 ±0.41	0.9 ±0.11	1.4 ±0.16	0.8 ±0.10	2.1 ±0.26	2.4 ±0.35	1.1 ±0.03	2.1 ±0.22	1.4 ±0.13	1.3 ±0.09
RARRES 1	4.6 ±0.86	1.7 ±0.11	1.9 ±0.13	1.7 ±0.19	2.7 ±0.29	1.0 ±0.72	1.0 ±0.14	3.7 ±0.27	1.2 ±0.24	0.6 ±0.24
MyD88	1.6 ±0.10	0.6 ±0.01	1.4 ±0.12	0.8 ±0.02	1.8 ±0.58	1.8 ±0.21	1.2 ±0.11	1.3 ±0.06	1.1 ±0.12	0.6 ±0.01
TLR2	1.8 ±0.14	2.0 ±0.16	1.4 ±0.03	1.9 ±0.09	8.9 ±1.42	6.6 ±2.76	0.6 ±0.08	2.1 ±0.54	0.7 ±0.14	0.5 ±0.09
TLR5	1.4 ±0.42	0.8 ±0.06	0.3 ±0.19	1.3 ±0.25	8.1 ±3.99	1.5 ±0.50	0.3 ±0.14	1.8 ±0.26	0.6 ±0.07	1.6 ±0.56

## **Erklärung**

Ich habe die vorgelegte Dissertation selbständig und ohne unerlaubte fremde Hilfe und nur mit den Hilfen angefertigt, die ich in der Dissertation angegeben habe. Alle Textstellen, die wörtlich oder sinngemäß aus veröffentlichten Schriften entnommen sind, und alle Angaben, die auf mündlichen Auskünften beruhen, sind als solche kenntlich gemacht. Bei den von mir durchgeführten und in der Dissertation erwähnten Untersuchungen habe ich die Grundsätze guter wissenschaftlicher Praxis, wie sie in der „Satzung der Justus-Liebig-Universität Gießen zur Sicherung guter wissenschaftlicher Praxis“ niedergelegt sind, eingehalten.

Bad Nauheim, 27.04.2014

Sony Adhi Susanto

Danke.... Thank you..... Terima kasih.....

Meinen tiefsten und herzlichsten Dank möchte ich auf diesem Weg allen Personen die mich durch ihre geistige oder geistliche Unterstützung, Motivation und Hilfe bei dieser Arbeit geholfen haben, zum Ausdruck bringen

Meinen Herrn Jesus Christus sowie meiner Frau mit meinem Sohn, meine Familie in Indonesien, die mir Kraft und Motivation gaben, diese Arbeit zu erledigen. Auch meine verstorbene Tochter Rafka Liora Susanto✝, ich liebe und vermisse dich...

Prof. Dr. Robert Matthias Dinser✝, leider schon verstorben, für die die Motivation und Betreuung meiner Arbeit. Deine Begeisterung und deine Totalität in jeder Arbeit dass du begonnen hast inspirieren mich....

Frau Dr. Sigrid Schuler, für Ihre finanzielle Förderung und Ihre Begeisterung in unsere Forschungsprojekte, Herrn Prof. Dr. Ulf Müller-Ladner, für die Betreuung und sorgfältige Korrektur meiner Doktorarbeit , Dr. phil. nat. Christiane Schönfeld, Dr. rer. nat. Elena Neumann, Dr. rer. nat. Grit Krumbholz, für die Betreuung und sorgfältige Korrektur meiner Doktorarbeit

Meinen gesamten Kollegen im Labor und in der Klinik, für die Unterstützung während der Anfertigung meiner Promotionsarbeit, besonders Carina Schreiyäck für die Unterstützung während der Anfertigung, sowie Dr. med. Matthias Geyer, Dr. rer. nat. Thilo Borchardt und Dr. rer. nat. Mario Looso für die wissenschaftliche Molch-Datei

Herrn Prof. Dr. rer. nat. Adriaan Dorresteyn, Herrn Prof. Dr. rer. nat. Reinhard Dammann und Herrn Prof. Dr. med. Uwe Lange für Begutachtung meiner Doktorarbeit.

Herr Frank Milshack für die Verwaltung meiner Unterlagen während meiner Promotionsarbeit in der Kerckhoff-Klinik

Frau Jessie Noermattias von Indonesische Mineralölunternehmen (Pertamina) für die Korrektur der Englische Grammatik meiner Doktorarbeit

Dr. Bernhard Dörr von der Katholischen Krankenhausseelsorge für die geistliche Kraft und Druckangebot meiner Doktorarbeit

Meine Freunde in der Indonesischen Katholischen Gemeinde für das Gebet und die geistliche Kraft während meiner Anfertigung der Doktorarbeit